OUKA
The University of Osaka
Institutional Knowledge Archive

Title	Studies on 1-Dimensional Polymer Nanostructures with Functional Surfaces Prepared by Single Particle Nano-Fabrication Technique
Author(s)	Asano, Atsushi
Citation	大阪大学, 2013, 博士論文
Version Type	VoR
URL	https://hdl.handle.net/11094/27555
rights	
Note	

The University of Osaka Institutional Knowledge Archive : OUKA

https://ir.library.osaka-u.ac.jp/

The University of Osaka

工学 18371

Doctoral Dissertation

Studies on 1-Dimensional Polymer Nanostructures with Functional Surfaces Prepared by Single Particle Nano-Fabrication Technique

Atsushi Asano

January 2013

Graduate School of Engineering,
Osaka University

Studies on 1-Dimensional Polymer Nanostructures with Functional Surfaces Prepared by Single Particle Nano-Fabrication Technique

(一次元高分子ナノ構造体の単一粒子反応を利用した形成と機能化に関する研究)

Atsushi Asano

Contents

General Introduction

1. Introduction

Swift heavy ion can achieve ultra-high density energy deposition, which promotes various chemical effects in materials. The cylindrical energy deposition area along the trajectory is called as "ion track". In polymeric materials, the primary effects of radiation are dictated by the balance between main-chain scissions and cross-linking. The efficiency of these reactions has been statistically and quantitatively discussed, and very sophisticated statistical formulations have been successfully applied for analysis[1-6]. These formulations are, however, based on a homogeneous spatial distribution of energy deposited by the radiation, and reactive intermediates of swift heavy ions have been revealed to yield an exceptionally non-homogenous release of kinetic energies of incident particles in the form of ion tracks. Crosslinking reactions in the limited space along an ion trajectory result in a fabrication of 1 dimensional nano-structure (nanowire), and the formation of such nanowires by exposure of thin films of crosslinking type polymers for radiation to swift heavy ion has been reported; single particle nano-fabrication technique (SPNT) [7-11].

The direct observation and application of an ion track in medium have much attracted in materials science. The uses of chemical reactions in an ion track have also been the prime choice for nuclear etching[12-16] and cancer radiotherapy[17], resulting in highly dense damage in materials. The solid-state nuclear track detector used as radiation detection expands and visualizes the damage in the polymer material caused by the single particle reaction as an ion track. Young reports the observation of the nuclear division track in a lithium fluoride crystal by etching and expanding the track with an acid solution[18]. Price and Walker et al. show that corrosion progressed along the ion trajectory in mica by chemical etching[19]. At the present, CR-39, polycarbonate type polymer material indicated the high sensitivity to a charged particle is developed and utilizes for detection of the cosmic ray[20-21].

The energy deposition of charged particle to the medium is often discussed by using track model. In the ion track, half the energy is deposited in the "core" region, which has a radius r_c, the other half is deposited in the "penumbra," region, which has a radius r_p. The radius r_c is determined by the Bohr adiabatic condition, and the radius r_p is determined by the penetration of secondary electrons. The target area is excited into a non-homogeneous field of chemical reactions, known as the chemical core of the ion track. The specific properties of ion beams have been characterized by the linear energy transfer (LET), given by the energy deposition of an incident particle per unit length. The LET of swift heavy ion is one of the factors determining the radial sizes of the nanowires. J. L. Magee et al. have been suggested coaxial energy distribution of an ion track, which has core and penumbra region, as follows.

$$\rho_c = \frac{LET}{2}\left[\pi r_c^2\right]^{-1} + \frac{LET}{2}\left[2\pi r_c^2 \ln\left(\frac{e^{1/2} r_p}{r_c}\right)\right]^{-1} ; r \le r_c$$

$$\rho_p(r) = \frac{LET}{2}\left[2\pi r^2 \ln\left(\frac{e^{1/2} r_p}{r_c}\right)\right]^{-1} ; r_c < r \le r_p$$

Here, ρ_c and ρ_p are the deposited energy density in the core and penumbra areas, and e is an exponential factor. At the center core of the ion track, the deposited energy density is greater than in the outer penumbra region. It is expected that the distribution of cross-linking points in an ion track will reflect the radial energy density, and that the number of cross-linking points in the core will be much larger than in the penumbra. The radial margins of the nanowires therefore lie in the penumbra area, where cross-linking occurs by energy deposition from secondary electrons.

It is expected that the polymers form a gel in this region, with one crosslinking point per polymer chain at the outer radial boundary. The deposited energy density (ρ_p) at r is therefore adopted as the critical energy density of gelation for polymers.

Therefore, the average sizes of the nanowires were well interpreted by the theoretical model, considering the energy distribution in an ion track, efficiency of cross-linking reaction (G values (number of reactions per 100 eV of absorbed dose): $G(x)$), molecular weight of the target polymers[22].

$$r'^2 = \frac{LET \cdot G(x) mk}{400 \rho \pi A}\left[\ln\left(\frac{e^{1/2} r_p}{r_c}\right)\right]^{-1}$$

where ρ is the density of polymers m and k are the mass of monomer unit and the degree of polymerization, respectively, and A is the Avogadro's number. Thus, the radial sizes of nanowires can be easily controlled by changing LET of ion beam and molecular weight of polymer.

Ion-beam irradiation of films based on polymeric materials has been shown to cause cross-linking reactions, leading to the formation of a polymer gel containing 1D nanostructure. A single ion particle can fabricate one nanostructure along its trajectory. The non-cross-linked polymer can be removed by an appropriate solvent, utilizing the difference in solubility. Due to its flexibility, the fabricated nanowires are no longer standing and are knocked down on the substrate, observed as 2D images by using atomic force microscope (AFM) or scanning electron microscope (SEM). The length, number density, and radius of the nanowires can be controlled by changing several parameters for the irradiated ion and the film based on target polymers. Especially, the cross-section of the nanowire is entirely dependent on the LET of incident ions and molecular weight of target polymers.

This article is composed in three chapters, and discussed about the fabrication and functionalization of the nano-structures based on bio-macromolecules and synthetic polymers by using single ion reaction.

In the chapter 1, formation of nm-sized bio-macromolecular nanowires based on the proteins is demonstrates. The size controllability of the protein nanowires is discussed in film length, fluence and deposited energy density of charged particle, and the efficiency of the crosslinking reaction of the proteins. The inner structure and characteristics of protein nanowires are also evaluated. There are many functional materials

damaged and decomposed by radiation, and cannot be formed the nanowires by SPNT. Therefore, fabrication of functional nanowires is performed by using the mixture film based on functional materials and cross-linking type polymer for radiation. Size control of nanowires and improvement of cross-linking efficiencies is performed by using chemical modification of polymer materials and γ ray irradiation in chapter 2. On the other hand, fabrication of functional nanowires is demonstrated by using post-modification of the surface nanowires. Polystyrene derivative which has reactive groups is utilized in the fabrication of 1D-nanostructures by SPNT. After fabrication, reactive moieties on the surface of nanowires quantitatively are modified via chemical reactions, leading to the fabrication of 1D-protein nanowires and 2D-protein arrays in chapter 3

2. Fabrication Control of Nanowires in the SPNT

2-1. Length Control

In fabrication process of nanowires by the SPNT, the cross-linking reactions are promoted along the ion track. The observed nanowires after development are visualized the trajectory of the incident particle in polymer film. The length of nanowires is reflected the thickness of the target polymer film as shown in figure i2-1. Therefore, the SPNT can achieve the fabrication of any length of nanowires with uniformity in large area, if the target film can be formed and the fabricated nanowires indicate the sufficient mechanical strength. Seki and Watanabe reports the fabrication of long nanowires (> 10 μm) based on negative type photo-resist: SU8 with the ultra-high aspect ratio (~ 800).

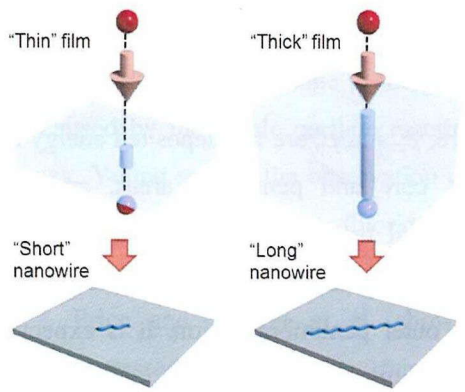

Figure i2-1. The length control of nanowires in the SPNT; the length of nanowire is reflected the film thickness.

2-2. Number Density Control

The most distinctive feature of the SPNT is a fabrication method of nanowire by utilizing the single particle reaction. Single particle can produce one nanostructure unless trajectories of particles overlap one another. Due to correspond the number of incident particles and nanostructures, the number density of nanowires can be controlled by the radiation dose as shown in figure i2-2.

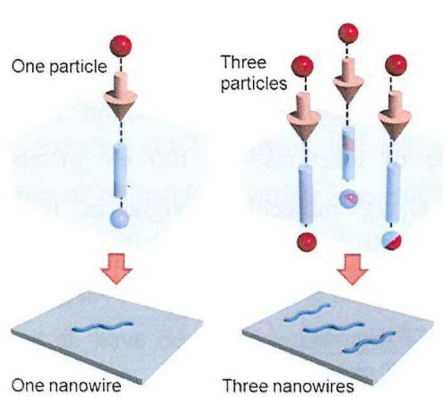

Figure i2-2. The number density control of nanowires in the SPNT; the number density of nanowires is reflected the radiation dose.

2-3. Size Control

In the ion track, the energy is deposited in the core and penumbra regions. Figure i2-3(a) shows the correlation between energy density and the distance from the center of the ion track. In core region, energy distribution is uniform. On the other hand, in penumbra region, energy density is decreased with increasing the distance from the center of the ion track. On the development process, the nanowire is knocked down on the substrate. The interaction between nanowire and surface of the substrate triggered the change of the shape of confirmed nanostructure. Assuming that the nanowire cross-section is a simple ellipse, the radius r is defined as follows.

$$r = \sqrt{r_1 \times r_2}$$

Here, the values, r_1 and r_2, is defined as the half-width and half-height at half-maximum of the cross-sectional profile from the AFM measurement.

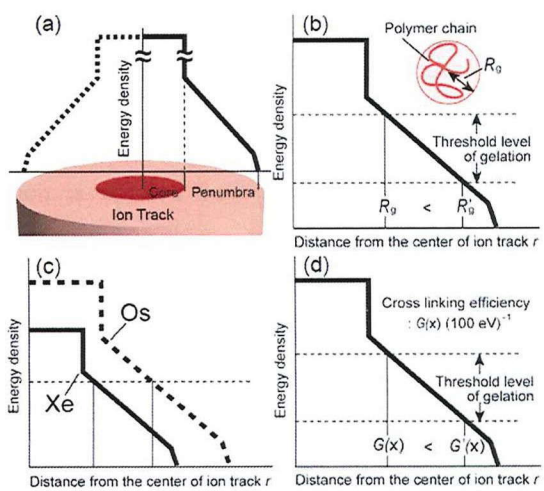

Figure i1-3. (a) The correlation between energy density and the distance from the center of the ion track. The factors affect the radius of nanowires; (b) molecular weight, (c) linear energy transfer of incident ion, and (d) cross-linking efficiency of polymer materials.

The size (radius) of nanowires formed by the SPNT is quantitatively affected by the molecular weight, cross-linking efficiency of polymer molecules and the value of linear energy transfer (LET) of incident ion.

In face of fabrication from the polymer materials with different molecular weights, the number of cross-linking points required for gelling changes with molecular weights of polymer chains. Therefore, the threshold value of gelling is decreased as the molecular weight is increasing in figure i2-3(b).

The radius of nanowires can also be changed by selecting the values of linear energy transfer (LET). The higher-LET ion beam maintains elevated energy densities to a greater radial distance compared to the lower-LET ion beam as shown in figure i2-3(c).

The sensitivity to radiation changes with polymer materials. The cross-linking efficiency: G(x) is the one of the factors to evaluate the sensitivity for radiation. G(x) indicates the efficiency of crosslinking reactions induced by irradiation (number of reactions per 100 eV energy absorbed). The polymer cross-linking reactions at the boundary of nanowires appears to be the principal factor determining the size of the final nanowires. The threshold value of gelling is decreased as the cross-linking efficiency of polymer material is increasing in figure i2-3(d).

3. Accelerators

A particle accelerator is a device to accelerate charged particles by using the electromagnetic fields. Accelerators can be classified as

electrostatic and oscillating field accelerators. Electrostatic accelerators use static electric fields to accelerate particles. On the other hand, oscillating field accelerators use radio frequency electromagnetic fields.

3-1. Electrostatic Particle Accelerators

The charged particles are accelerated by using a static high voltage potential. The acceleration energy is regulated by the applied voltage, but the electrostatic accelerator is the only device generating the continuous beam. There are two methods to achieve the high voltage as Cockcroft–Walton and Van de Graaf generator.

Cockcroft–Walton generator

In 1932, Cockcroft and Walton used for the first transmutation experiments with artificially accelerated particles (proton). Figure i3-1(a) shows the system generating the high voltage and overview of acceleration device. The Cockcroft–Walton generator consists of the voltage multiplier ladder network of capacitors and diodes. This generator is a voltage multiplier that converts electrical power from a low voltage to a higher DC voltage. The peak in the acceleration voltage is depended on the dielectric strength voltage, and generally shows the value around 1 MeV in the atmosphere.

Van de Graaf generator

The idea for generating high-voltage by transporting and accumulating the charge with insulated belt and rotating disk existed in the 17th century or even before. In 1929, Van de Graaff utilized this system and developed the high voltage generator. This generator consists of an insulated belt and a hollow metal sphere anchored by the insulated materials as shown in figure i3-1(b). The belt is passed the charges from the corona discharges on the grounded electrode. The charges are transported and discharged to the metal sphere. The charges are accumulated on the surface of the metal sphere until the capacitance is filled. The difference of potential is approximately equal to the sphere's radius multiplied by the electric field where corona discharges begin to form within the surrounding gas.

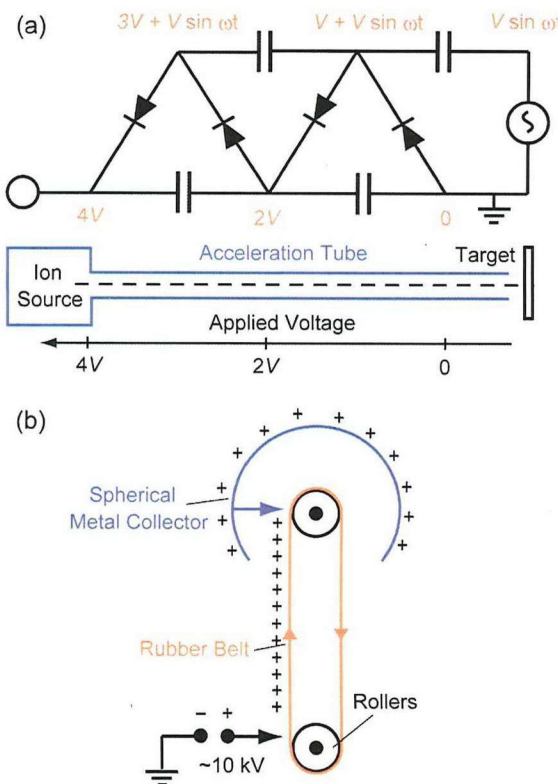

Figure i3-1. (a)Cockcroft–Walton type and (b)Van de Graaf type generator achieving the high voltage utilized in the electrostatic particle accelerators

3-2. Oscillating Field Particle Accelerators

Due to the limitation of the applied voltage between electrodes from the various practical problems, there is an acceleration voltage ceiling

of the electrostatic particle accelerators. In order to accelerate particles to higher energies, oscillating field is used. In oscillating field particle accelerators, the electrodes can be arranged to accelerate particles in a line (linear particle accelerator) or circle (cyclotron).

Linear particle accelerators

A linear particle accelerator (linac) is a type of particle accelerator that greatly increases the velocity of charged particles by applying the oscillating electric potentials along a linear beamline as shown in figure i3-2(a). Linac is capable of accelerating heavy ions to energies exceeding those available in ring-type accelerator (cyclotron), which are limited by the strength of the magnetic fields required to maintain the ions on a curved path.

Cyclotrons

The cyclotron is one of the earliest types of particle accelerators, and is still used as the first stage of some large multi-stage particle accelerators. Cyclotron accelerates the charged particle using a high frequency alternating voltage which is applied between two electrodes called "dee" as shown in figure i3-2(b). A static magnetic field B is applied in perpendicular direction to the electrode plane resulting particles to penetrate the accelerating voltage many times at the same phase. In order to accelerate the particles, the voltage frequency is needed to match the particle's cyclotron resonance frequency. This frequency is given by centripetal force and magnetic Lorentz force. The particles increase their kinetic energy only when re-circulating through the gap between the electrodes.

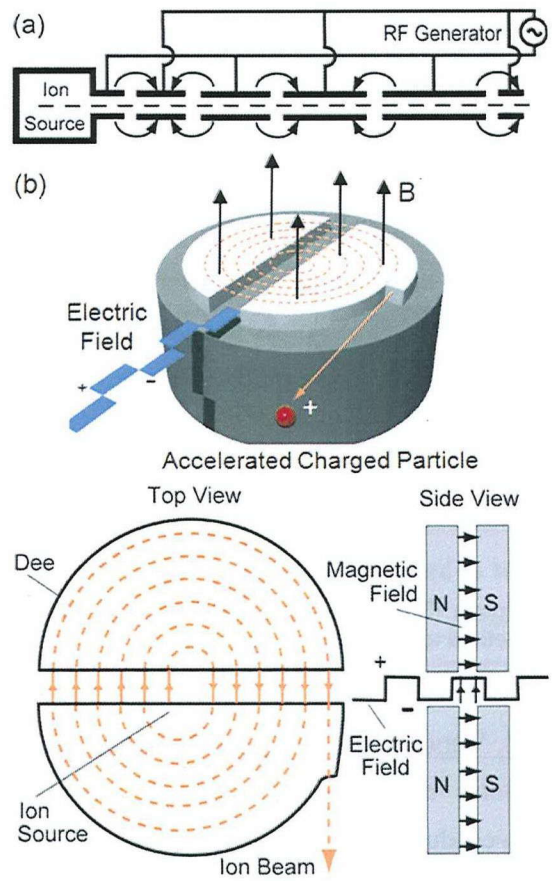

Figure i3-2. Illustration of the line and circle type oscillating field particle accelerators; (a) Linear particle accelerator (linac) and (b) cyclotron

3. Other Synthesis Methods of Nanowires

3-1. Template-Assisted Method

The template-assisted synthesis of nanowires is a conceptually simple and intuitive way to fabricate nanostructures. Many kind of materials; metal, organic materials, and bio-macromolecules are fabricated the nanowires by using this methods. These templates contain very small cylindrical pores or voids within the host material, and the empty spaces are filled with the chosen material, which adopts the pore morphology, to form

nanowires as shown in figure i3-1. There are many methods (chemical, electrochemical[23-24], and vapor deposition[25]) filling the templates with the materials. This method can easily control the radius and length of nanowire by changing the pore size and the thickness of the template film.

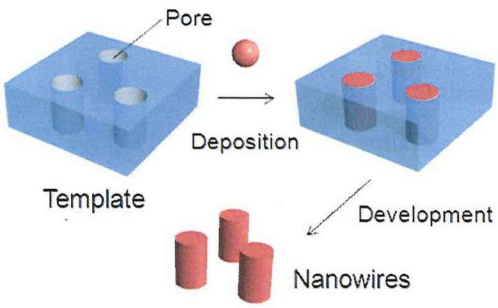

Figure i3-1. Illustration of the template-assisted method to fabricate the nanowires.

3-2. Vapor-Liquid-Solid (VLS) Method

Some of the recent successfully synthesized semiconductor nanowires are based on the vapor-liquid-solid (VLS) mechanism of anisotropic crystal growth[26-28]. This mechanism is first proposed for the growth of single crystal silicon. The growth mechanism of semiconductor nanowires begins the absorption of source material from the gas phase into a liquid droplet of catalyst. The nucleation generates a solid precipitate of the source material. This seed serves as a preferred site for further deposition of material at the interface of the liquid droplet, promoting the elongation of the seed into a nanowire as shown in figure i3-2.

Due to the liquid droplet catalyzes the incorporation of material from the gas source to the growing crystal, the deposit grows anisotropically.

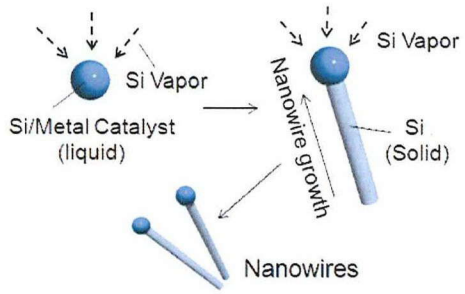

Figure i3-2. Illustration of the vapor-liquid-solid (VLS) method to fabricate the anisotoropic semiconductor nanowires.

3-3. Electro-Spinning Method

The electro-spinning method is driven by the electrical forces on charges inside a polymeric liquid. In electro-spinning, the force is generated by the interaction of an applied electric field with the electrical charge carried by the spinning tip. When the free charges in the liquid polymer, which are generally ions, move in response to the electric field, they quickly transfer a force to the polymer liquid. Finally, the elongation of the fiber resulting from an applied force leads to the formation of uniform fibers with nanometer-scale diameters as shown in figure i3-3. The nanowires fabricated by using this method are utilized in medical, material[29] and catalyst science[30].

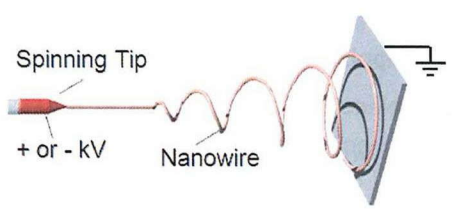

Figure i3-3. Illustration of the electro-spinning method method to fabricate the nanowires from the polymer solution.

3-4. Self-Assembling Method

A number of synthetic and bio-macromolecular

molecules indicated the self-assemble ability has been reported. These self-assembling molecules adopt the fixed aggregation form under the specific conditions; concentration, temperature, and pH, as shown in figure i3-4. In the case of small semiconductor molecules, there is great interest of fabrication of 1D-nanowires by using π-π interactions between planar aromatic molecules because the aggregation theoretically resulting the high mobilities in electronic devices[31].

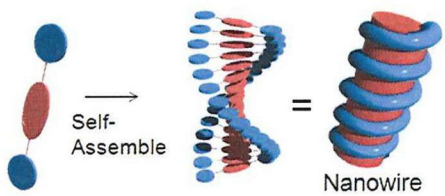

Figure i3-4. Illustration of the self-assembling method (VLS) method to fabricate the nanowires.

4. Click Chemistry

4-1. Concept

In 2001, Kolb, Finn and Sharpless suggested a new concept, click chemistry, for organic chemistry[32].

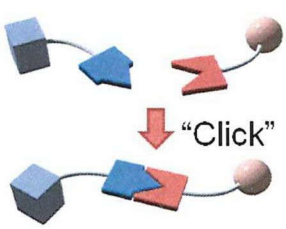

Figure i4-1. Illustration of the concept of click chemistry

Sharpless defined the concept of click chemistry as "The reaction must be modular, wide in scope, give very high yields, generate only inoffensive byproducts that can be removed by nonchromatographic methods, and bestereospecific (but not necessarily enantioselective). The required process characteristics include simple reaction conditions (ideally, the process should be insensitive to oxygen and water), readily available starting materials and reagents, the use of no solvent or a solvent that is benign (such as water) or easily removed, and simple product isolation. Purification - if required - must be by nonchromatographic methods, such as crystallization or distillation, and the product must be stable under physiological conditions." Therefore, the name of 'Click' was coined to show not the specific reaction, but the principle demanded by the fields of modern chemistry in particular, drug discovery.

4-2. Click Reactions

Azide - Alkyne Cycloaddition

The most popular click reaction is the copper(I) catalyzed 1,3-dipolar azide-alkyne cycloaddition. First, Huisgen performed azide-alkyne cycloaddition at high temperatures resulting in the formation of both 1,4- and 1,5-substituted 1,2,3-triazoles conflicting with both the required simple reaction conditions and stereospecificity as shown in figure i4-2(a)[33-34]. Mock et al. demonstrated that the azide-alkyne cycloaddition is catalyzed by encapsulation of amine functionalized reagents with cucurbituril yielding only the 1,4-substituted-1,2,3-triazole[35]. The major condition of the azide–alkyne cycloaddition is reported in 2002[32]. Sharpless and Meldal reported the use of copper(I) catalysts for the 1,3-dipolar cycloaddition of azides and alkynes. The use of a copper(I) catalyst results in the formation of the

1,4-substituted 1,2,3-triazole and it accelerates the reaction allowing cycloadditions as shown in figure i4-2.

Recently, Bertozzi reported the copper free click chemistry by using strained cyclooctyne in 2007[36]. This type of reaction allowed the reaction to proceed quickly and without live cell toxicity by eliminating a cytotoxic copper catalyst.

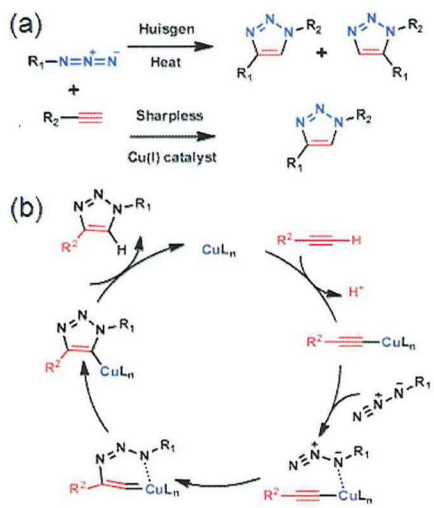

Figure i4-2. The reaction mechanism of a copper(I) catalyzed cycloaddition.

Thiol-Ene Reaction

The hydrothiolation between thiol and ene is one of the old-established reaction in the field of polymer synthesis[37]. Due to the recognition of its click characteristics, thiol-ene reaction has been widely used. This reaction can proceed under a variety of conditions via radical mediated pathway as shown in figure i4-3a. A wide range of thiols and enes can be employed, and these reactions are generally extremely rapid even at ambient temperature and pressure.

Generally, the thiol-ene reaction has been conducted under radical conditions, often photochemically induced. Under such conditions it proceeds via a typical chain process with initiation, propagation and termination steps as shown in figure i4-3b[38-40]

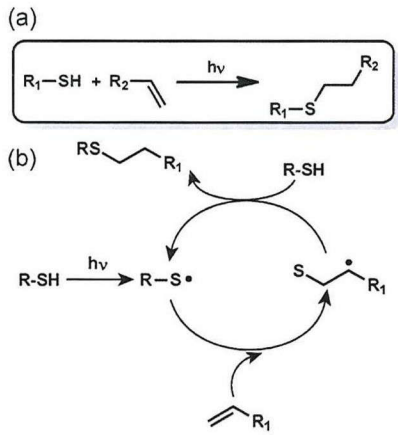

Figure i4-3. (a) The click reaction of thiol-ene chemistry induced by the photo-irradiation. (b) Reaction mechanism of the thiol- ene click reaction.

Tetrazine-*Trans*-Cyclooctene Reaction

The Diels-Alder reaction between tetrazine and *trans*-cyclooctene is the new type click reaction as shown in figure i4-4[41].

Fox reported this reaction that proceeds with unusually fast reaction rates without need for catalysis: the cycloaddition of *s*-tetrazine and *trans*-cyclooctene derivatives. The reactions tolerate a broad range of functionality and proceed in high yield in organic solvents, water, cell media, or cell lysate. The rate of the ligation between *trans*-cyclooctene and 3,6-di-(2-pyridyl)-*s*-tetrazine is very rapid ($k_2 \sim 2000\ Ms^{-1}$). This fast reactivity enables protein modification at low concentration.

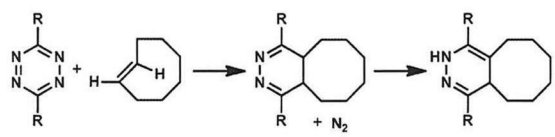

Figure i4-4. Diels-Alder reaction between tetrazine and *trans*-cyclooctene.

References

1. Saito, O. *J. Phys. Soc. Jpn.* **1958**, *13*, 1451-1464.

2. Saito, O. *J. Phys. Soc. Jpn.* **1959**, *14*, 798-806.
3. Inokuti, M. *J. Chem. Phys.* **1960**, *33*, 1607-1615.
4. Inokuti, M. *J. Chem. Phys.* **1963**, *38*, 2999-3005.
5. Zhang, Y. F.; Ge, X. W.; Sun, J. Z. *Radiat. Phys. Chem.* **1990**, *35*, 163-166.
6. Olejniczak, K.; Rosiak, J.; Charlesby, A. *Radiat. Phys. Chem.* **1991**, *37*, 499-504.
7. Seki, S.; Maeda, K.; Tagawa, S.; Kudoh, H.; Sugimoto, M.; Morita, Y.; Shibata, H. *Adv. Mater.* **2001**, *13*, 1663-1665.
8. Tsukuda, S.; Seki, S.; Tagawa, S.; Sugimoto, M.; Idesaki, A.; Tanaka, S.; Ohshima, A. *J. Phys. Chem. B* **2004**, *108*, 3407-3409.
9. Seki, S.; Tsukuda, S.; Maeda, K.; Matsui, Y.; Saeki, A.; Tagawa, S. *Phys. Rev. B* **2004**, *70*, 144203-8.
10. Seki, S.; Tsukuda, S.; Maeda, K.; Tagawa, S.; Shibata, H.; Sugimoto, M.; Jimbo, K.; Hashitomi, I.; Kohyama, A. *Macromolecules* **2005**, *38*, 10164-10170.
11. Watanabe, S.; Asano, A.; Seki, S.; Sugimoto, M.; Yoshikawa, M.; Tagawa, S.; Tsukuda, S.; Tanaka, S. *Radiat. Phys. Chem.* **2009**, *78*, 1071-1075.
12. Price, P. B.; Walker, R. M. *Nature* **1962**, *196*, 732-734.
13. Spohr, R. *Ion Tracks and Microtechnology: Principle and Applications*; Vieweg: Braunschweig, 1990.
14. Peng, L.; Apel, P.; Maekawa, Y.; Yoshida, M. *Nucl. Instrum. Methods B* **2000**, *168*, 527-532.
15. Apel, P. *Radiat. Meas.* **2001**, *34*, 559-566.
16. Fink, D. *Fundamentals of Ion-Irradiated Polymers*; Springer: Berlin, 2004.
17. Wilson, R. R. *Radiology* **1946**, *47*, 487-491.
18. Young, D.A. *Nature* **1985**, *182*, 375
19. Price, P. B.; Walker, R. M. *J. Appl. Phys.* **1962**, *33*, 3409.
20. S'eguin, F. H.; DeCiantis, J. L., Frenje, J. A.; Kurebayashi, S.; Li, C. K.; Rygg, J. R., Chen, C.; Berube, V.; Schwartz, B. E.; Petrasso, R. D.; Smalyuk, V. A.; Marshall, F. J.; Knauer, J. P.; Delettrez, J. A.; McKenty, P. W.; Meyerhofer, D. D.; Roberts, S.; Sang-ster, T. C.; Mikaelian, K.; Park, H. S. *Review of Scientific Instruments* **2004**, *75*, 3520
21. Kinoshita, K.; Price, P.B., *Phys. Rev. D* **1981**, *24*, 1707–1717.
22. Peng, L.; Apel, P.; Maekawa, Y.; Yoshida, M. *Nucl. Instrum.Methods Phys. Res., Sect. B* **2000**, *168*, 527–532.
23. Piraux, L.; George, I. M.; Despres, J. F.; Leroy, C.; Ferain, E.; Legras, R.; Ounadjela, K.; Fert, A. *Appl. Phys. Lett.*, **1994**, *65*, 2484-2486.
24. Routkevitch, D.; Bigioni, T.; Moskovits, M.; and Xu, J. M. *J. Phys. Chem.*, **1996**, *100*, 14073-14047
25. Cheng, G. S.; Zhang, L. D.; Chen, S. H.; Li, Y.; Li, L.; Zhu, X. G.; Zhu, Y.; Fei, G. T.; Mao, Y. Q. *J. Mater. Res.* **2000**, 15, 347-350.
26. Wagner, R. S.; Ellis, W. C. *Appl. Phys. Lett.* **1964**, *4*, 89-91.
27. Gudiksen, M. S.; Lauhon, L. J.; Wang, J.; Smith, D.; Lieber, C. M., *Nature* **2002** ,*415*, 617-620.
28. Wu, Y.; Fan, R.; Yang, P. *Nano Lett.* **2002**, *2*, 83-86.
29. Matthews J. A.; Wnek G. E.; Simpson D. G.; Bowlin G. L. Biomacromolecules. **2002**, 3, 232-8
30. Li, D.; Xia. Y. *Adv. Mater.* **2004**, *16*, 1151-1170.
31. Curtis, M. D.; Cao, J.; Kampf, J. W. *J. Am. Chem. Soc.* **2004**, *126*, 4318-4328.
32. Kolb, H. C.; Finn, M. G.; Sharpless, K. B., *Angew. Chem. Int. Ed.* **2001**, *40*, 2004-2021.
33. Huisgen, R. *Angew. Chem. Int. Ed. Engl.* **1963**, *2*, 565-598.
34. Huisgen, R. *Angew. Chem. Int. Ed. Engl.* **1963**, *2*, 633-645.
35. Mock, W. L.; Irra, T. A.; Wepsiec J. P.; Manimaran, T. L. *J. Org. Chem.* **1983**, *48*, 3619.
36. Baskin, J. M.; Prescher, J. A.; Laughlin, S. T.; Agard, N. J.; Chang, P. V.; Miller, I. A.; Lo, A.; Codelli, J. A.; Bertozzi, C. R. Proc. *Natl. Acad. Sci. U. S. A.*, **2007**, *104*, 16793-16797.
37. Posner, T.*Ber. Dtsch. Chem. Ges.*, **1905**, *38*, 646-657.
38. Campos, L. M.; Killops, K. L.; Sakai, R.; Paulusse, J. M. J.; Damiron, D.; Drockenmuller, E.; Messmore, B. W.; Hawker, C. J. *Macromolecules*, **2008**, 41, 7063-7070.
39. Campos, L. M.; Meinel, I.; Guino, R. G.; Schierhorn, M.; Gupta, N.; Stucky, G. D.; Hawker, C. J. *Adv. Mater.*, **2008**, *20*, 3728-3733.
40. Jonkheijm, P.; Weinrich, D.; Kohn, M.; Engelkamp, H.; Christianen, P. C. M.; Kuhlmann, J.; Mann, J. C.; Nusse, D.; Schroeder, H.; Wacker, R.; Breinbauer, R.; Niemeyer, C. M.; Waldmann, H. *Angew. Chem., Int. Ed.*, **2008**, *47*, 4421-4424.
41. Blackman, M. L.; Royzen, M; Fox, J. M. *J. Am. Chem. Soc.*, **2008**, *130*, 13518-13519.

Chapter 1 Fabrication of Bio-Macromolecular Nanowires

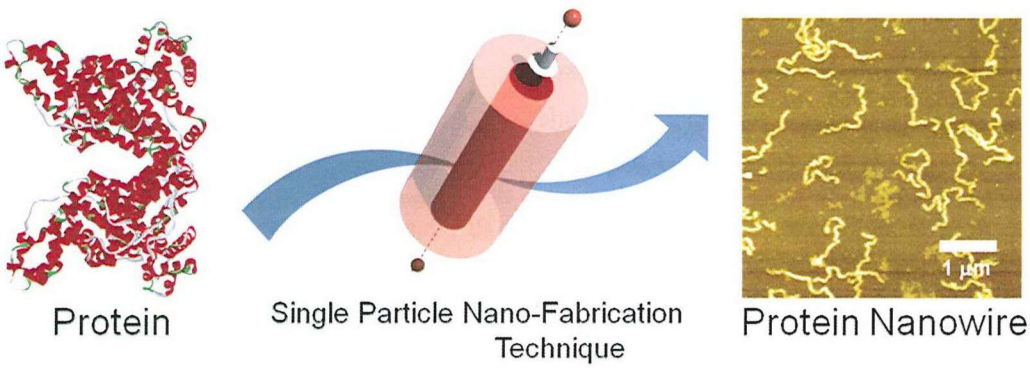

1-1 Introduction

The MeV-order high energy charged particles release non-homogeneously their kinetic energy to the materials, and induce reactive intermediates (ion radicals, neutral radicals, etc.) distributed cylindrically along the particle trajectories, which is called as charged particle tracks[1, 2]. Because of effective and high-density formation of neutral radical species, their recombination reactions within an ion track produce highly-efficient cross-linking of polymer backbones, resulting in 1-D nano-structured polymer gels with fairly controlled sizes. Unlikely to the case of focused beam of charged particles used commonly as a probe of nanofabrication, no dispersion of "a" particle secures intrinsically the nm-scaled area of released energy and cross-linking reactions, leading to the potentials of "a" high energy charged particle as a tool to fabricate polymeric materials with ultra-high aspect ratio. Direct formation of 1-dimensional nanostructures based on the cross-linking reactions in the thin films of several kinds of synthetic polymers is succeeded by irradiation of high energy charged particles, single particle nano-fabrication technique: SPNT[1]. The uses of chemical reactions in an ion track have also been the prime choice for nuclear etching[12-16] and cancer radiotherapy,[17] resulting in highly dense damage in materials. In contrast to these conservative applications of ion tracks, a variety of one-dimensional functional materials have been developed directly by SPNT. MeV-order high energy charged particles non-homogeneously induce reactive intermediates (ion radicals, neutral radicals, etc.) in polymeric materials along the particle trajectories, referred to as ion tracks. When such radical species are generated in radiation cross-linking type polymers, chemical reactions within the ion track can produce 1D-nanostructures. SPNT can thus be used to fabricate nanowires with controlled sizes.[7,10]

Bio-macromolecules, especially proteins, show many valuable properties, but poor physical stability and difficulty in modification have prevented their direct use in material science. H. Yan *et al.* reported the array of proteins by using DNA templates. S. Burazerovic *et al.* and D. Men *et al.* reported the fabrication of 1D-nanostructure based on proteins by using avidin-biotin interactions or self-assemble of amyloid. These formation methodologies demand the complicated chemical and biological techniques.

Based on the concept of high energy deposition leading to nano-fabrication, this chapter demonstrates the formation of nm-sized bio-macromolecular nanowires based on the proteins. The size controllability of the protein nanowires is discussed in film length, fluence and deposited energy density of charged particle, and the efficiency of the crosslinking reaction of the proteins. The inner and outer structure of fabricated protein nanowires is evaluated by hydrolysis of nanowires triggered by the enzyme and chemical modification.

1-2 Fabrication of Protein Nanowires

Swift heavy ion irradiation of synthetic polymers is shown to cause crosslinking reactions leading to the formation of a polymer gel containing 1d-nanostructures. This section describes the direct formation of bio-macromolecular nanowires based on the

protein by ion beam irradiation, single particle nano-fabrication technique: SPNT. The fabrication of nanowires composed of albumins and avidin are successfully confirmed by AFM measurements. Albumin indicates high cross-linking efficiency for radiation. This technique demonstrates the feasibility of fabrication of nano-structures based on various proteins.

Experimental

Human serum albumin (HSA), bovine serum albumin, and ovalbumin from egg were purchased from Sigma Aldrich Chemical Co. and of the best commercial quality available and used without further purification unless otherwise noted. Avidin from chicken egg white was purchased from Calzyme Lab, Inc. All the proteins were dissolved 5-10wt% in distilled water, and spin-coated or drop-casted on Si or glass substrate. The thickness of the films was confirmed by a Dektak 150 surface profiler.

The films of the proteins were irradiated by 450 MeV Xe and 490 MeV Os ion beams from cyclotron accelerator at Japan Atomic Energy Agency, Takasaki Advanced Radiation Research Institute. The number of incident particles was controlled from 1×10^8 to 1×10^9 cm^{-2} to prevent over lapping of the particle trajectories. The irradiated films were developed directly immersing into phosphate buffered saline (PBS) at pH 7.4 to 9.0 for 5 min.

The sizes and shapes of the nanostructure formed along particle trajectories were observed using a SPI-4000 atomic force microscope (AFM) from Seiko Instruments Inc.

Fabrication of Protein Nanowres

Ion irradiation without overlapping ion tracks triggered cross-linking reactions in the target materials, giving a 1D-nanostructure in the thin film. In the case of cross-linking type polymers for radiation, high energy deposition induces the gelation, and the undamaged area can be removed by development with an appropriate solvent. This technique can be used to prepare isolated nanowires on the substrate.

Direct formation of nanowires based on the protein was performed by using the same procedure in the case of fabrication of nanowirres based on synthetic polymers. First, the nanowires based on the human serum albumin were confirmed by the AFM measurement. Figure 1-2-1(b) indicated the development process of nanowires with PBS at pH 7.4. As the non-cross-linking proteins are removed by PBS, the protein nanowires were isolated on the substrate. SPNT could also form the nanowires based on bovine serum albumin (BSA), ovalbumin (OVA), and avidin as shown in figure 1-2-2.

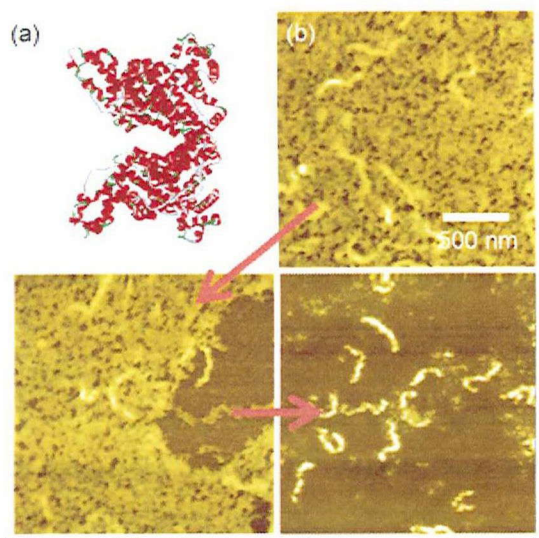

Figure 1-2-1. Development process of protein naowires based on HAS.

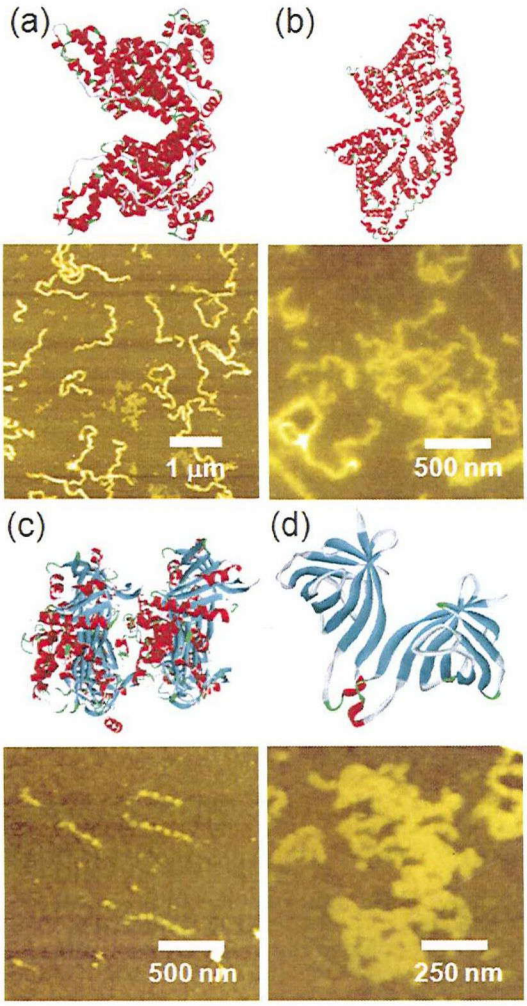

Figure 1-2-2. AFM micrographs of nanowires based on (a) human serum albumin: HAS (PDB ID: 1ao6), (b) bovine serum albumin: BSA (PDB ID: 3v03), (c) ovalbumin: OVA (PDB ID: 1ova), and (d) avidin (PDB ID: 1avd).

Bilayer Nanowires Based on Protein and Polymer

The adhesion of nanowires to substrates is an important feature in view of the practical application of the present technique to nano-material fabrication requiring precise controllability in the special arrangement of devices. It should be noted that the bottom-side terminal of the nanowire fabricated by SPNT is tightly connected to the substrate. Therefore, the nanwoires could be confirmed on the substrate after development.

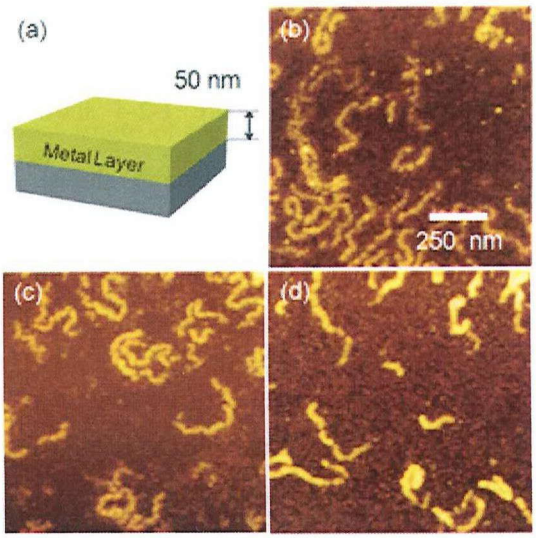

Figure 1-2-3. (a)Metal deposited substrate of 50 nm thickness. AFM micrographs of nanowires based on HSA prepared by exposing films to a 450 MeV $^{129}Xe^{25+}$ at 3.0 × 10^8 ions cm^{-2} on (b) Au, (c) Al, and (d) Ti substrates

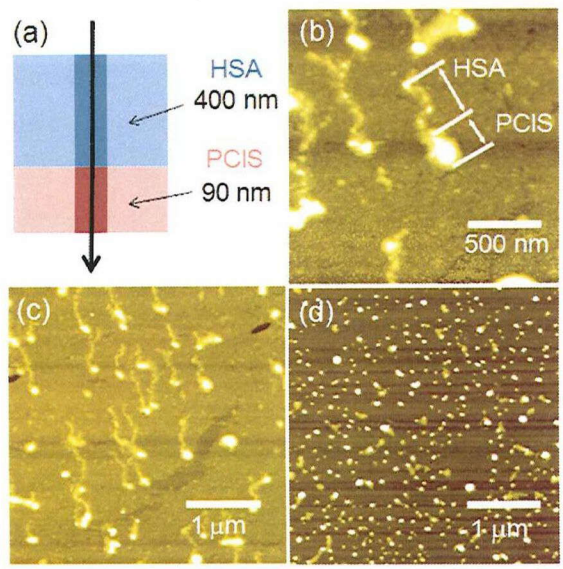

Figure 1-2-4. (a)Multi-layer film based on HSA and synthetic polymer. AFM micrographs of nanowires based on (b) HSA and poly(4-chlorostyrene), (d) poly(4-chlorostyrene) prepared by exposing films to 470 MeV $^{192}Os^{30+}$ particles at an ion influence of (b)1.0×10^8, (d)1.0×10^9 ions cm^{-2}.

Nano-fabrication by SPNT is promoted along the trajectory of an ion in the film. Protein nanowires could be fabricated not only on the glass and Si substrates, but also on the metal; Au, Al, Ti

substrates as shown in Figure 1-2-3.

The use of two-layer films was examined as a potential to connect the protein and synthetic polymer nanowires. Figure 1-2-4 shows AFM images of the two-layer (HSA/poly(4-chlorostyrene)) film, which was developed sequentially in PBS (to remove HSA) and then toluene (to remove poly(4-chlorostyrene)) after exposure to the ion beam. The resultant nanowires were composed of a 400 nm segment of HSA and 90 nm segment of poly(4-chlorostyrene), reflecting the thicknesses of each of the original films.

Cross-Linking Efficiency of Proteins

It is expected that the polymers form a gel in this region, with one crosslinking point per polymer chain at the outer radial boundary. The deposited energy density (ρ_p) at r is therefore adopted as the critical energy density of gelation for polymers. Therefore, the average sizes of the nanowires were well interpreted by the theoretical model, considering the energy distribution in an ion track, efficiency of cross-linking reaction (G values (number of reactions per 100 eV of absorbed dose): $G(x)$), molecular weight of the target polymers

$$r'^2 = \frac{LET \cdot G(x) mk}{400 \rho \pi A} \left[\ln\left(\frac{e^{1/2} r_p}{r_c} \right) \right]^{-1} \quad (1)$$

where ρ is the density of polymers m and k are the mass of monomer unit and the degree of polymerization, respectively, and A is the Avogadro's number. Thus, the radial sizes of nanowires can be easily controlled by changing LET of ion beam and molecular weight of polymer.

The cross-linking efficiencies of nanowires based on the protein were evaluated by using equation (1). Table 3-5-1 showed the values of radius of naowire and cross-linking efficiency. Especially, HSA indicated the high cross-linking efficiency comparable to the value of poly(4-bromostyrene).

Table 3-5-1. The values of cross-sectional radius of nanowires and cross-linking efficiency based on the proteins fabricated by the SPNT.

	HSA	BSA	OVA	Avidin
Molecular weight (kDa)	66	45	68	68
Radius r (nm)	15 ± 0.5	12 ± 1.1	8.1 ± 0.9	14 ± 1.5
$G(x)$	1.4[a]	1.2[a]	0.7[b]	1.1[a]

a: Development was carried out with PBS at pH 8.0. b: Development was carried out with water.

1-3 Size Control of Protein Nanowires

This section describes the fabrication of protein nanowires by irradiation to the films based on the plasma proteins. High energy charged particles penetrating into polymer materials cause non-homogeneous crosslinking along the irradiated particle trajectories, giving 1d-nanowires. Sizes (length and radius) and number density control of protein nanowires are demonstrated by changing

the film thickness and energy and fluence of ions.

Experimental

Human serum albumin (HSA) was purchased from Sigma Aldrich Chemical Co. HAS was dissolved 5-20wt% in distilled water, and spin-coated or drop-casted on Si substrate. The thickness of the films was confirmed by a Dektak 150 surface profiler.

The films of the proteins were irradiated by 320 MeV $^{102}Ru^{18+}$, 450 MeV $^{129}Xe^{25+}$, and 490 MeV $^{192}Os^{30+}$ ion beams from cyclotron accelerator at Japan Atomic Energy Agency, Takasaki Advanced Radiation Research Institute. The number of incident particles was controlled from 3×10^7 to 5×10^9 cm^{-2} to prevent over lapping of the particle trajectories. The irradiated films were developed directly immersing into phosphate buffered saline (PBS) at pH 7.4 for 5 min to 12 h.

The sizes and shapes of the nanostructure formed along particle trajectories were observed using a SPI-4000 atomic force microscope (AFM) from Seiko Instruments Inc.

Size Control of Protein Nanowires

The size control of protein nanowires is one of the important factors to demonstrate the processabilities of proteins in SPNT. As the irradiated ions penetrate through the polymer film, the length of the nanowires can be precisely controlled by changing the film thickness within the range of penetration length of the ions. Nanowires based on HSA fabricated by 490 MeV Os particles were observed by AFM measurement as shown in figure 1-3-1. The images of the nanowires showed the uniform length of the HSA nanowires reflecting the initial thickness of the target protein film (250 – 1200 nm).

HSA nanowires with a high aspect ratio could be fabricated from drop-casted films. The maximum length of the HSA nanowire reached 8 μm in length, though the fragmentation of the nanowires during the development process was confirmed.

After the development procedure, HSA nanowires remain adhered to the substrate and the nanowires remain isolated from each other. This indicates that one end of the wire is tightly connected to the substrate by chemical bonds. Therefore, the number density of HSA nanowires could be controlled by the fluence of irradiated ions. Figure 1-3-3 indicated the good agreement of the number density of HSA nanowires with the ion fluence.

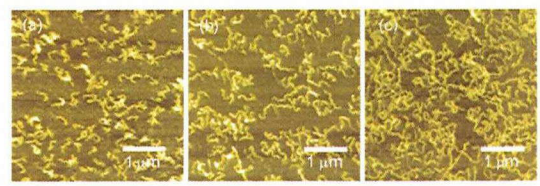

Figure 1-3-1. AFM micrographs of nanowires based on HSA prepared by exposing films of (a)250, (b)560, and (c)1200 nm thickness to 480 MeV $^{192}Os^{30+}$ particles at 1.0×10^9 ions cm^{-2}.

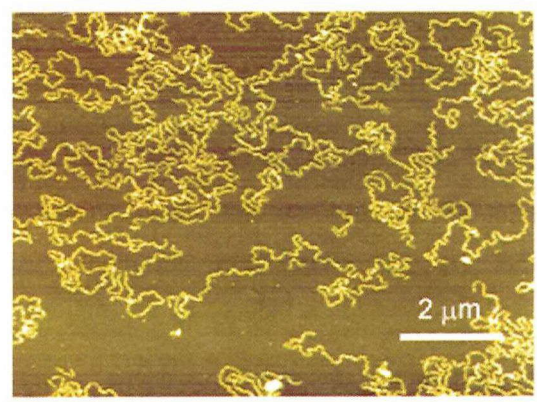

Figure 1-3-2. AFM micrographs of nanowires based on HSA prepared by exposing drop-casted film to 480 MeV $^{192}Os^{30+}$ particles at of 3.0×10^7 cm^{-2}

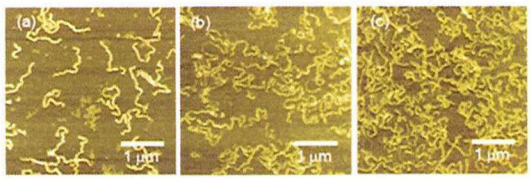

Figure 1-3-3. AFM micrographs of nanowires based on HSA prepared by exposing films of 1200 nm thickness to 480 MeV $^{192}Os^{30+}$ particles at of (a)1.0×10^{8}, (b)3.0×10^{8}, and (c) 5.0×10^{8} ions cm^{-2}

The radius of HSA nanowires could be changed by selecting the values of linear energy transfer (LET: energy deposition rate of incident particles per unit length) of swift heavy ions. High LET ion such as 480 MeV $^{192}Os^{30+}$ gave thick nanowires (r = 15 nm) compared with low LET ion, as 450 MeV $^{129}Xe^{25+}$ (r = 12 nm) and 320 MeV $^{102}Ru^{18+}$ (r = 11 nm) (Figure 1-3-4).

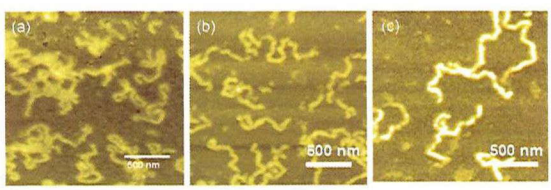

Figure 1-3-4. AFM micrographs of nanowires based on Human Serum Albumin prepared by exposing films to a (a)320 MeV $^{102}Ru^{18+}$, (b)450 MeV $^{129}Xe^{25+}$, (c)480 MeV $^{192}Os^{30+}$

1-4 Evaluation of the Inner Structure and the Function of Protein Nanowire

Section 1-3 described the fabrication and size control of protein nanowires by high energy particle irradiation to the films based on proteins. SPNT is the fabrication technique using cross-linking reactions induced by the high energy deposition. The cross-links in the nanowires are considered as "damage" of target polymers. In this section, evaluation of the inner structure of protein nanowires is demonstrated by utilizing the enzymatic hydrolysis reaction of trypsin. The preservation of function of the protein nanowires is also confirmed by using bio-macromolecular interactions.

Experimental

General. Human serum albumin (HSA) was purchased from Sigma Aldrich Chemical Co. Tripsin was purchased from Wako Chemical Co. Avidin from chicken egg white was purchased from Calzyme Lab, Inc. Biotin *N*-hydroxysuccinimide ester were prepared by methods described in the literature. All other reagents and solvents were purchased from Tokyo Kasei Kogyo Co. and Wako Chemical Co. and used without further purification.

HAS was dissolved 5-20wt% in distilled water, and spin-coated or drop-casted on Si substrate. The thickness of the films was confirmed by a Dektak 150 surface profiler. The films of the proteins were irradiated by 490 MeV $^{192}Os^{30+}$ ion beam from cyclotron accelerator at Japan Atomic Energy Agency, Takasaki Advanced Radiation Research Institute. The number of incident particles was controlled from 3×10^{7} to 5×10^{9} cm^{-2} to prevent over lapping of the particle trajectories. The irradiated films were developed directly immersing into phosphate buffered saline (PBS) at pH 7.4 for 5 min to 12 h.

The sizes and shapes of the nanostructure formed along particle trajectories were observed using a SPI-4000 atomic force microscope (AFM) from Seiko Instruments Inc.

Hydrolysis of protein nanowires

HSA nanowirs with a length of 710 nm were fabricated on Si substrates (0.5×0.5 cm^{2}). After development with PBS at pH 7.4 for 5 min,

hydrolysis of HSA nanowires were carried out by immersing in 0.5 w/v% trypsin - 1 mM EDTA·4Na aqueous solution at 37°C for 3 and 20 min, respectively. Hydrolysis processes were confirmed by AFM measurement in each time.

Surface modification of HSA nanowires by using NHS-biotin

HSA nanowirs with a length of 650 nm were fabricated on Si substrates (0.5 × 0.5 cm^2). After development with PBS at pH 7.4 for 5 min, biotinylation of HSA nanowires were carried out by immersing in DMF solution of *N*-hydroxysuccinimide-biotin (1 mM) at room temperature and carefully washed with distilled water to eliminate the organic solvent. Finally, biotinylated nanowires were immersed in an avidin solution (10 μM) in pH7.4 PBS for 30 min. Modification processes were confirmed by AFM measurement in each step.

Surface modification of avidin nanowires by using dibiotinyl linker

Avidin nanowirs were fabricated from the thin film based on the HSA and avidin on Si substrates (0.5 × 0.5 cm^2). After development with PBS at pH 7.4 for 3 min, substrates were immersed in a PBS solution of dibiotinyl linker (10 μM) by using DMSO as co-solvent for 30 min and carefully washed with distilled water. Linker modified substrates were immersed in an avidin solution (10 μM) in pH 7.4 PBS for 30 min. Modification procedures were repeated three times in order to promoted the avidin-biotin interactions.

Hydrolysis of Protein Nanowires

Hydrolysis of HSA nanowires was carried out in order to evaluation of inner structure of protein nanowires fabricated by SPNT. Trypsin is one of the serine proteases, cleaving peptide chains mainly at the carboxyl side of the amino acids; lysine or arginine as shown in figure 1-4-1a. The fragmentation of nanowires was confirmed by AFM measurement after immersing trypsin solution for 3 min (Figure 1-4-1b-ii). Finally, after 20 min, the HSA nanowires were completely decomposed and no nano-structures were confirmed as shown in figure 1-4-1b-iii.

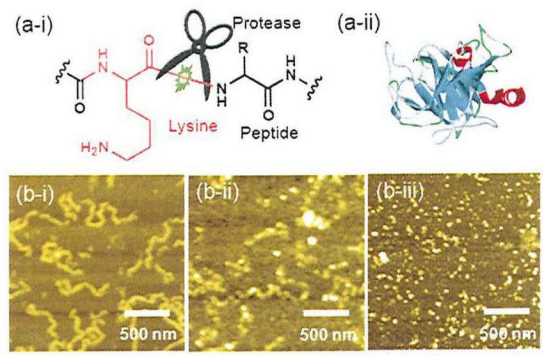

Figure 1-4-1. (a) Hydrolysis system and structure of tripsyn. Trypsin cleaves the amide bond of the lysine or arginine. (b) AFM micrographs of nanowires based on HSA prepared by exposing films to 450 MeV $^{129}Xe^{25+}$ particles at 3.0×10^8 ions cm^{-2}. AFM micrographs of the hydrolysis process of nanowires with immersing into 0.5 w/v% trypsin - 1 mM EDTA·4Na aqueous solution at 37°C for (b-ii) 5 and (b-iii) 20 min, respectively. $^{192}Os^{30+}$

The radius of HSA nanowires in the hydrolysis process were evaluated as 13± 0.2 nm (before hydrolysis) and 8± 4 nm (after 3 min) from the cross-sectional profile. Assuming the hydrolysis process was promoted in constant pace, apparent turnover rate of trypsin was calculated as 0.9 s^{-1}. This calculated value is extremely low compared with the reported value as 96 s^{-1} by Seydoux *et al.* These results indicate HSA nanowires retain the specific sequence of peptide structures, but conformation of protein in the naowires were damaged and collapsed.

Surface Modification of HSA Nanowires by Using NHS-Biotin

There are many amino groups derived from basic amino acid; lysine or arginine on the surface of the protein. Therefore, protein naowires also have the amino groups on the surface of nanowires. On the other hand, it is well-known that the *N*-hydroxyimide ester compounds are reactive with an amino group. Introducing the biotin to the surface of nanowires and modification of avidin were performed (Figure 1-4-2).

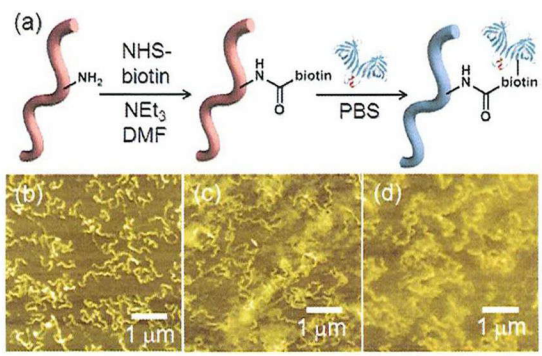

Figure 1-4-2. Schemes for surface modification of nanowires composed of protein. (a) AFM micrograph of nanowires based on HSA fabricated by exposing films of 650 nm thickness to a 470 MeV $^{192}Os^{30+}$ beam at 5.0×10^{8} ions cm^{-2}. (b) AFM micrographs of biotinylated nanowires. The surface is modified by the reaction between amine groups of HSA and NHS-biotin. (c) AFM micrograph of nanowires modified by avidin.

Amino groups on the surface of nanowires were reacted with biotin *N*-hydroxysuccinimide ester. Biotinylated nanowires were interacted with avidin. AFM micrographs of modification process were shown as figure 1-4-2b and c, respectively. The radius of nanowires were estimated to 14 nm (before modification), 10 nm (after biotinylation), and 16 nm (after modification of avidin), respectively. Due to denaturation of protein in the nanowires induced by organic solvent, decrease of the radius was confirmed in biotinilation process. But, significant increase of the radius was confirmed after modification of avidin. These results indicate that the introducing the avidin to the surface of nanowires are successfully promoted. Moreover, it is demonstrated the surface of HSA nanowires can be utilized as the reactive scaffold.

Surface Modification of HSA Nanowires by Using NHS-Biotin

The surface of a nanowire is to be found in the threshold region for the gelation of target materials where one crosslink is induced per a polymer chain in average. Proteins on the surfaces of nanowires have minimum amounts of cross-links. Therefore, it is expected that the surface of a nanowire preserves the functions of proteins.

In order to demonstrate the preservation of the function of protein nanowires, the function of avidin nanowires was evaluated by using dibitynyl linker. When the activity of avidin on the surface of nanowires is preserved, increasing of the radius is expected by interaction between dibiotynyl linker mediated nanowires and avidin. Due to low mechanical strength, fragmentation of avidine nanowires was often confirmed. This fragmentation of nanowires was improved by fabrication of nanowires from the mixture of HSA and avidin film. Figure 1-4-3a and b show the AFM images of avidin-HSA nanowires before and after modification of avidin, respectively. The radii of the nanowires were evaluated to be 15 nm and 14 to 20 nm, respectively from the cross-sectional profiles. This result indicates that the surface of the nanowire is modified avidin by the avidin-biotin interaction, and the function of avidin is partly preserved.

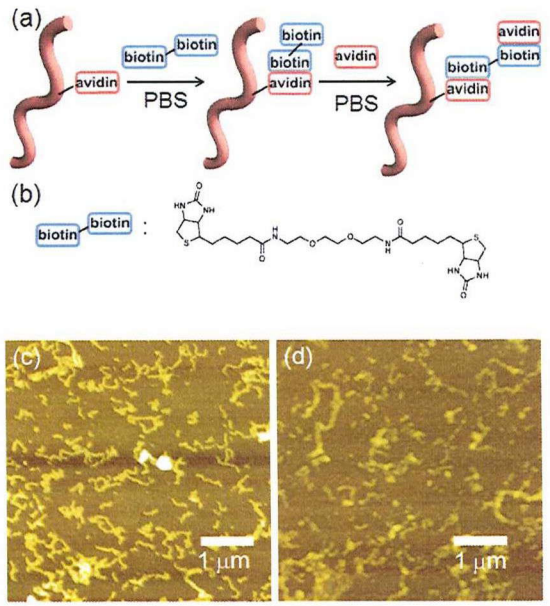

Figure 1-4-3. Schemes for surface modification of nanowires composed of protein. (a)AFM micrograph of nanowires based on HSA and Avidin.fabricated by irradiation of 470 MeV $^{192}Os^{30+}$ particles at 3.0×10^{8} ions cm^{-2}.(b)AFM micrograph of modified nanowires. The surface is modified by dibiotinyl linker and avidin in three times. (c)Chemical structure of dibiotinyl linker.

1-4 Summary

Human serum albumin (HSA) was successfully utilized in the fabrication of 1D-nanostructures by SPNT without using complicated chemically synthetic or biological procedures. The protein nanowires were also confirmed from the film based on bovine serum albumin (BSA), ovalbumin (OVA), and avidin. These results indicated that the SPNT is the effective technique for fabrication of bio-compartible nanostructures based on protein. HSA nanowires could be fabricated not only on the Si substrate but also on the various metal substrates (Au, Al, and Ti). Moreover, the use of two-layer films was examined as a potential to connect the protein and synthetic polymer nanowires.

Especially, HSA showed the high cross-linking efficiency, which is comparable with cross-linking type synthetic polymers for radiation. Due to high cross-linking efficiency of HSA, the length, number density, and radius of HSA nanowires can be controlled by the initial film thickness, the number of incident particles, and linear energy transfer, respectively. In length control of nanowires, the maximum length of nanowire reached 8 μm. The successful size control of protein nanowires was demonstrated that HSA was appropriate material for SPNT.

Section 1-4 was discussed about the inner structure and surface functionality of protein nanowires by using hydrolysis reaction or surface modification. Hydrolysis of HSA nanowires by trypsin triggered the fragmentation of nanowires, and finally, nanowires were completely decomposed. These results indicated HSA nanowires retained the specific sequence of peptide structures. It was demonstrated that fabrication of protein nanowires by SPNT. On the other hand, the functionality of amino groups derived from the basic amino acids on the surface of HSA nanowires was preserved, and amino groups reacted with the *N*-hydroxyimide ester compounds leading to the modification of nanowires with avidin.

Hydrolysis of protein nanowires also indicated the conformation of protein in the naowires were damaged and collapsed. But, preservation of the function of protein nanowires was demonstrated by surface modification of avidin-HSA nanowires with dibiotinyl linker and avidin. These results indicated that the proteins on the surface of nanowires have minimum amounts of cross-links.

References

1. Saito, O. *J. Phys. Soc. Jpn.* **1958**, *13*, 1451-1464.
2. Saito, O. *J. Phys. Soc. Jpn.* **1959**, *14*, 798-806.
3. Inokuti, M. *J. Chem. Phys.* **1960**, *33*, 1607-1615.
4. Inokuti, M. *J. Chem. Phys.* **1963**, *38*, 2999-3005.
5. Zhang, Y. F.; Ge, X. W.; Sun, J. Z. *Radiat. Phys. Chem.* **1990**, *35*, 163-166.
6. Olejniczak, K.; Rosiak, J.; Charlesby, A. *Radiat. Phys. Chem.* **1991**, *37*, 499-504.
7. Seki, S.; Maeda, K.; Tagawa, S.; Kudoh, H.; Sugimoto, M.; Morita, Y.; Shibata, H. *Adv. Mater.* **2001**, *13*, 1663-1665.
8. Tsukuda, S.; Seki, S.; Tagawa, S.; Sugimoto, M.; Idesaki, A.; Tanaka, S.; Ohshima, A. *J. Phys. Chem. B* **2004**, *108*, 3407-3409.
9. Seki, S.; Tsukuda, S.; Maeda, K.; Matsui, Y.; Saeki, A.; Tagawa, S. *Phys. Rev. B* **2004**, *70*, 144203-8.
10. Seki, S.; Tsukuda, S.; Maeda, K.; Tagawa, S.; Shibata, H.; Sugimoto, M.; Jimbo, K.; Hashitomi, I.; Kohyama, A. *Macromolecules* **2005**, *38*, 10164-10170.
11. Watanabe, S.; Asano, A.; Seki, S.; Sugimoto, M.; Yoshikawa, M.; Tagawa, S.; Tsukuda, S.; Tanaka, S. *Radiat. Phys. Chem.* **2009**, *78*, 1071-1075.
12. Price, P. B.; Walker, R. M. *Nature* **1962**, *196*, 732-734.
13. Spohr, R. *Ion Tracks and Microtechnology: Principle and Applications*; Vieweg: Braunschweig, 1990.
14. Peng, L.; Apel, P.; Maekawa, Y.; Yoshida, M. *Nucl. Instrum. Methods B* **2000**, *168*, 527-532.
15. Apel, P. *Radiat. Meas.* **2001**, *34*, 559-566.
16. Fink, D. *Fundamentals of Ion-Irradiated Polymers*; Springer: Berlin, 2004.
17. Wilson, R. R. *Radiology* **1946**, *47*, 487-491.
18. Malkoch, M.; Thibault, R. J.; Drockenmuller, E.; Messerschmidt, M.; Voit, B.; Russell, T. P.; Hawker, C. J. *J. Am. Chem. Soc.* **2005**, *127*, 14942-14949.
19. O'Reilly, R. K.; Joralemon, M. J.; Hawker, C. J.; Wooley, K. L. *Chem. Eur. J.* **2006**, *12*, 6776-6786.
20. Huisgen, R. *Angew. Chem. Int. Ed. Engl.* **1963**, *2*, 565-598.
21. Huisgen, R. *Angew. Chem. Int. Ed. Engl.* **1963**, *2*, 633-645.
22. Rostovtsev, V. V.; Green, L. G.; Fokin, V. V.; Sharpless, K. B. *Angew. Chem. Int. Ed.* **2002**, *41*, 2596-2599.
23. Tornoe, C. W.; Christensen, C.; Meldal, M. *J. Org. Chem.* **2002**, *67*, 3057-3064.
24. Kolb, H. C.; Finn, M. G.; Sharpless, K. B., *Angew. Chem. Int. Ed.* **2001**, *40*, 2004-2021.
25. van Steenis, D. J. V. C.; David, O. R. P.; van Strijdonck, G. P. F.; van Maarseveen, J. H.; Reek, J. N. H. *Chem. Commun.* **2005**, 4333-4335.
26. Zhu, Y.; Huang, Y.; Meng, W.-D.; Li, H.; Qing, F.-L., *Polymer* **2006**, *47*, 6272-6279.
27. Detz, R. J.; Heras, S. A.; de Gelder, R.; van Leeuwen, P. W. N. M.; Hiemstra, H.; Reek, J. N. H.; van Maarseveen, J. H. *Org. Lett.* **2006**, *8*, 3227-3230.
28. Whittaker, M. R.; Urbani, C. N.; Monteiro, M. J. *J. Am. Chem. Soc.* **2006**, *128*, 11360-11361.
29. Rozkiewicz, D. I.; Janacuteczewski, D.; Verboom, W.; Ravoo, B. J.; Reinhoudt, D. N. *Angew. Chem. Int. Ed.* **2006**, *45*, 5292-5296.
30. Li, H.; Cheng, F; Duft, A. M.; Adronov, A. *J. Am. Chem. Soc.* **2005**, *127*, 14518-14524
31. Seki, S.; Watanabe, S.; Sugimoto, M.; Tagawa, S.; Tsukuda, S. *J. Photopolym. Sci. Technol.* **2008**. *21*, 541-543.
32. Fleischmann, S.; Komber, H.; Voit, B. *Macromolecules* **2008**, *41*, 5255-5264.
33. Tang, C.; Bang, J.; Stein, G. E.; Fredrickson, G. H.; Hawker, C. J.; Kramer, E. J.; Sprung, M.; Wang, J. *Macromolecules* **2008**, *41*, 4328-4339.
34. Tercjak, A.; Gutierrez, J.; Peponi, L.; Rueda, L.; Mondragon, I. *Macromolecules* **2009**, *42*, 3386-3390.
35. Chan, T.-F.; Ha, C.; Phong, A.; Cai, D.; Wan, E.; Leung, L.; Kwok, P. -Y.; Xiao, M. A *Nucl. Acids Res.* **2006**. *34*. e113.
36. Li, Y.; Tsuboi, K.; Michinobu, T. *Macromolecules* **2010**, *43*, 5277-5286.
37. Burazerovic, S.; Gradinaru, J.; Pierron, J.; Ward, T. R. *Angew. Chem. Int. Ed.* **2007**, *46*, 5510-5514.
38. Men, D.; Guo, Y.-C.; Zhang, Z.-P.; Wei, H.P.; Zhou, Y.-F.; Cui, Z.-Q.; Liang, X.-S.; Li, K.; Leng, Y. You, X.-Y.; Zhang, X.-E. *Nano Lett.* **2009**, *9*, 2246-2250.
39. Scheibel, T.; Parthasarathy, R.; Sawicki, G.; Lin, X.-M.; Jaeger, H.; Lindquist, S. L. *Proc. Nat. Acad. Sci. USA* **2003**, *100*, 4527-4532.
40. Green, N. *Biochem. J.* **1963**, *89*, 585-591
41. Bayer, E. A.; de Meester, F.; Kulik, T.; Wilchek, M. *Appl. Biochem. Biotechnol.* **1995**, *53*, 1-9.
42. Rina, M.-L. L.; Lue, Y. P.; Chen, G. Y. J.; Zhu, Q.; Yao, S. Q. *J. Am. Chem. Soc.* **2002**, *124*, 8768-8769.
43. Reichel, A.; Schaible, D.; Furoukh, N. A.; Cohen, M.; Schreiber, G.; Piehler, J. *Anal. Chem.* **2007**, *79*, 8590-8600.
44. Pugliese, L.; Coda, A.; Malcovati, M.; Bolognesi, M. *J. Mol. Biol.* **1993**, *231*, 698-710.
45. Urbani, C. N.; Bell, C. A.; Lonsdale, D. E.; Whittaker, M. R.; Monteiro, M. J. *Macromolecules* **2007**, *40*, 7056-7059.
46. Ornelas, C.; Mery, D.; Cloutet, E.; Aranzaes, J. R.; Astruc, D. Cross *J. Am. Chem. Soc.* **2008**, *130*, 1495-1506.
47. Becker, J.M.; Wilchek, M.; Katchalski, E. *Proc. Nat. Acad. Sci. USA* **1971**, *68*, 2604-2607.
48. Tsuda, K.; Ishizone, T.; Hirao, A.; Nakahama, S. *Macromolecules* **1993**, *26*, 6985-6991.

Chapter 2 Direct Fabrication of Functional Nanowires

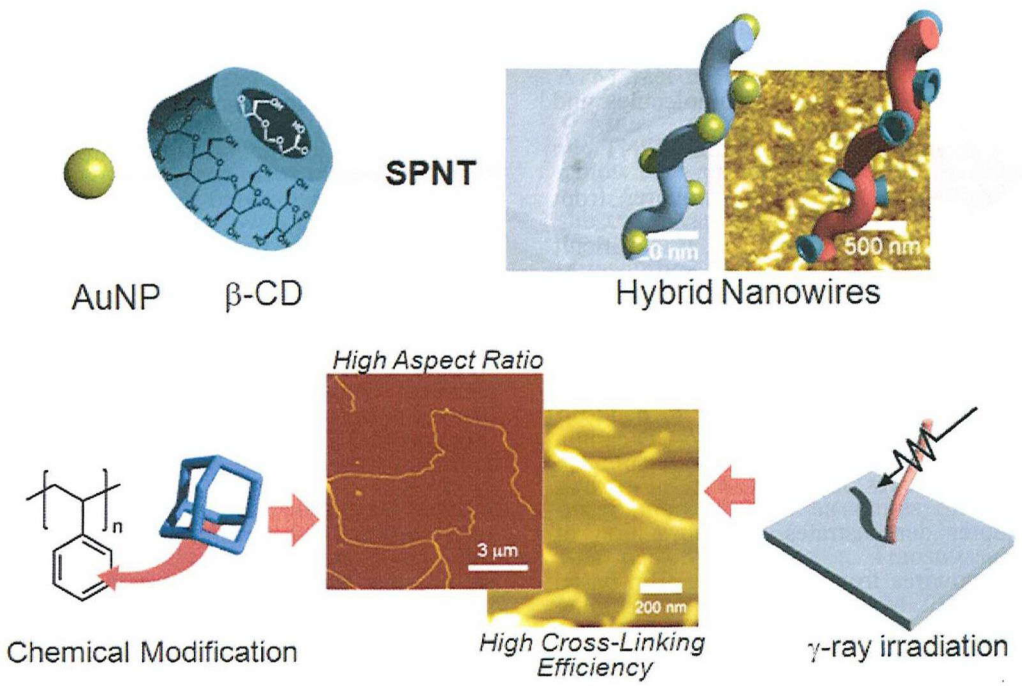

2-1 Introduction

Radiation promotes various chemical effects not only in inorganic but also in organic materials. The predominant effects of radiation on the primary structural changes in polymeric materials have been analyzed statistically, and controlled in terms of chain scission and cross-linking reaction efficiencies. Direct formation of 1-dimensional nanostructures based on the cross-linking reactions in the thin films of several kinds of synthetic polymers is succeeded by irradiation of high energy charged particles, single particle nano-fabrication technique: SPNT[1].

Chapter 1 demonstrated the direct formation of nanostructures based on bio-macromolecules and preservation of function in nanowires. SPNT can directly fabricate the functional nanowires from the polymer films with function. But, it is difficult for fabrication of nano-structures based on materials with low molecular weight and decomposition for radiation. For example, irradiation to the thin film of pristine β-CD cannot give isolated nanowires on the substrate[2]. First half of this chapter demonstrates the fabrication of functional nanowires from the mixture film based on functional materials and cross-linking type polymer for radiation.

.In Section 2-2-1, the direct formation of the poly(vinylphenol) (PHS) and Au nanoparticles hybrid nanowires, produce by single ion irradiation of the PHS films including Au nanoparticles. The observation is carried out using AFM, and inner structures of nanowires are observed by TEM.

In Section 2-2-2, nanostructures based on copolymer consisted with β-CD derivatives and acrylamide are formed by SPNT. In order to evaluate the response of nanowires to vapors of formic acid, quartz crystal microbalance (QCM) measurement is performed.

Polystyrene gives the well-controlled nano-structures in length and number density by SPNT[3,4]. However with an increase in the aspect ratio of nanowires higher than a few hundreds, fragmentation of nanowires is often observed by AFM measurement. Due to a low cross-linking efficiency of polystyrene upon irradiation, nanowires with low mechanical strength are considerably affected by the development conditions; handling, development time, and solvent. This collapse is a fatal problem for formation of nanowires from the polymer film blended with functional materials. In order to prevent the fragmentation of naowires, the polymer materials are demanded the high tolerance for various conditions. In second half of chapter, size control of nanowires and improvement of cross-linking efficiencies are demonstrated by chemical modification of polymer materials (Section 2-3-1) and γ ray irradiation (Section 2-3-2)

In Section 2-3-1, several polystyrene derivatives are polymerized from styrene monomers appended with functional groups to increase cross-linking efficiency. Precise formation of 1D-nanowires is demonstrated via the effective cross-linking reaction of the functional groups with high aspect-ratio.

In Section 2-3-2, ion beam firstly irradiates to polystyrene and polymer films in order to form nanowires. Additionally, γ ray irradiation to the same film is carried out. The effects for radial sizes of nanowires which produced by ion beam and γ ray irradiation are disccuced.

2-2-1 Fabrication of nanowires including Au nanoparticles

The heavy-ion irradiation of a poly(vinylphenol) (PHS) thin film has been shown to cause cross-linking reactions along ion tracks, yielding a nano-gel with reduced solubility in organic solvents. Wet-development affords isolated nanowires. In this section, the direct formation of the hybrid nanowires based on PHS including Au nanoparticles (PHS/Au) was demonstrated by using single particle nano-fabrication technique: SPNT. The hybrids nanowires based on PHS/Au was successfully visualized by AFM on the substrate, and the included Au particles in the single PHS nanowire were also observed clearly using TEM.

Experimental

All reagents and chemicals were purchased from Wako Pure Chemical Industries unless otherwise noted. The PHS and $HAuCl_4 \cdot 4H_2O$ were dissolved in MeOH at 5 and 0.1 wt%. This hybrid solution was spin-coated on the Si substrate. These thin films of PHS and PHS/Au hybrids were subsequently placed in a vacuum chamber and exposed to 450 MeV $^{129}Xe^{23+}$ and 490 MeV $^{192}Os^{30+}$ beams at the Takasaki Ion Accelerators for Advanced Radiation Application (TIARA) cyclotron accelerator facility of the Japan Atomic Energy Agency. After irradiation, the samples were developed using isopropylalcohol (IPA) for 1 min. The irradiated part of the film, where a polymer gel was formed, was insoluble in IPA. After development and drying procedures, the direct observation of the surface of the substrates was performed using an atomic force microscope (AFM Seiko Instruments Inc. (SII) SPI-4000). The radius and shape of cross-section of nanowire was also measured using AFM. The nanowires formed an elliptical cross-section due to sagging onto the substrate surface after development. Assuming that the nanowire cross-section is a simple ellipse, the nominal radius r is defined as follows to facilitate discussion of the distribution of deposited energy and crosslinking reactions on an ion track.

$$r = \sqrt{r_1 \times r_2} \quad (1)$$

Here, the values, r_1 and r_2, is defined as the half-width and half-height at half-maximum of the AFM trace of the cross-sections.

After wet-development procedures, the nanowires were isolated on the Si substrate. This substrate was put in the IPA solution, and then ultrasonification was carried out for 10 min. Here, the nanowires were separated from the Si substrate. This IPA solution including many nanowires was dropped on TEM grid. After drying process, this specimen was placed in TEM holder. The observation of inner structures of the nanowires was performed using a Transmission Electron Microscope (TEM: JEOL JEM-2010).

Fabrication of the hybrids nanowires based on PHS/Au

In PHS, the crosslinking reactions along the ion track result in the formation of a cross-linked nanogel (nanowire) in thin films. The non-crosslinked area can be removed by development with IPA, utilizing the change in solubility due to the gelation of PHS. The nanowires formed by ion bombardment can therefore be completely isolated on the substrate. After the wet-development procedure, the

nanowires lie prostrate on the substrate surface. Figure 2-2-1-1 show the nanowires based on PHS formed by 450 MeV Xe and 490 MeV Os ion beam irradiation with 1.1×10^9 ions/cm^2. The radii of nanowires based on PHS were 6.6 and 4.3 nm for 490 MeV Os and 450 MeV Xe, respectively. It has been reported that the radius of nanowire increased with the LET (linear energy transfer: energy deposition rate of incident particle per unit length) of the ion beam and molecular weight of polymer[5,6]. Especially, the LET of ion beam is a primary factor determining the radial sizes of the nanowires, because the deposited energy distribution in an ion track is inhomogeneous. *LET* = 10800 and 13800 eV nm^{-1} (calculated for 450 MeV Xe and 490 MeV Os ions in PHS by the Monte Carlo simulation code "SRIM 2003" [7]), ρ=1.16 g cm^{-3}, and mN=1.0×10^4 g mol^{-1}. Magee et al.[7] have suggested coaxial energy distribution of an ion track, which has core (Eq.(2)) and penumbra (Eq.(3)) regions, as follows:

$$\rho_c = \frac{LET}{2}\left[\pi r_c^2\right]^{-1} + \frac{LET}{2}\left[2\pi r_c^2 \ln\left(\frac{e^{1/2} r_p}{r_c}\right)\right]^{-1}; \quad r \le r_c \qquad (2)$$

$$\rho_p(r) = \frac{LET}{2}\left[2\pi r^2 \ln\left(\frac{e^{1/2} r_p}{r_c}\right)\right]^{-1}; \quad r_c < r \le r_p \qquad (3)$$

Here, ρ_c and ρ_p are the deposited energy density in the core and penumbra areas, and r_c and r_p are the radii of core and penumbra areas, e is an exponential factor. At the center core of the ion track, the deposited energy density is greater than in the outer penumbra region. However, the radial margins of the nanowires lie in the penumbra area, where crosslinking occurs by energy deposition from secondary electrons [9]. According to Eq. (3), the distribution of deposited energy depends on the LET of the incident ion, therefore, the higher LET beam (490 MeV Os) irradiation gives thicker nanowires than 450 MeV Xe irradiated one.

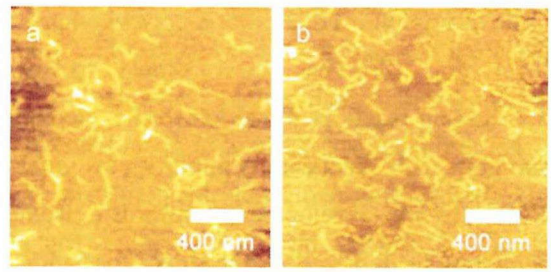

Figure 2-2-1-1. AFM micrographs of nanowires formed by 450 MeV Xe and 490 MeV Os ion beam irradiation to PHS thin films with the fluence of 1.0×10^9 ions/cm^2.

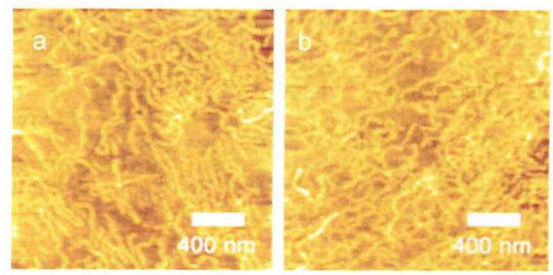

Figure 2-2-1-2. AFM micrographs of PHS/Au nanowires formed by 450 MeV Xe ion beam irradiation to hybrid thin films with the fluence of 1.0×10^{10} ions/cm^2.

The hybrid PHS film including Au nanoparticles was prepared on Si substrate. This film was also exposed to 450 MeV Xe and 490 MeV Os ion beam at ion fluence of 1.0×10^{10} ions/cm^2. After development procedure using IPA, the hybrid nanowires based on PHS including Au nanoparticles (PHS/Au) were successfully formed and isolated on the Si substrate, as shown in figure 2-2-1-2. The radii of PHS and PHS/Au nanowires were also measured using AFM trace and summarized in table 2-2-1-1.The radii of the PHS/Au nanowires were determined as 6.2 and 3.7 nm for 490 MeV Os and 450 MeV Xe ion beams by AFM measurement and calculation on the ellipse model (Eq. (1)), respectively. The radii of nanowires based on PHS/Au were smaller than that

of original nanowires for each beam. These results indicate that the including Au-nanoparticles inhibit cross-linking reaction, resulting in reduced cross-linking efficiency of the PHS/Au film compared with that of PHS. The significant decrease on cross-linking efficiency between PHS and PHS/Au influences the radial sizes.

Table 2-2-1-1. Radii of the nanowires based on PHS and PHS/Au for 450 MeV Xe and 490 MeV Os ion beams.

Ion beam	LET (eV/nm)	Radius (*r*) (nm)	
		PHS	PHS/Au
490 MeV Os	13800	6.6	6.2
450 MeV Xe	10800	4.3	3.7

TEM observation of the hybrids nanowires based on PHS/Au

In order to observe the Au nanoparticles in the PHS nanowires, the TEM observation was carried out. Figure 2-2-1-3 shows PHS/Au nanowires observed by TEM. The observed structures were large entangled structures. In preparation method of TEM specimen, the nanowires were separated from substrate during ultrasonification in IPA solution for 10 min. Then, the separated nanowires were firstly dispersed in the IPA solution. However, the nanowires were entangled with each other, and became large aggregation structures that consisted of many nanowires. As the result, the nanowires were observed as large aggregation structure as shown in figure 2-2-1-3. However, the 1–3 isolated nanowires were partially observed as shown in Figure 4. Here, Au nanoparticles were clearly observed in single PHS nanowires. The particle sizes including in the nanowires were 3.6–5.5 nm. In SPNT, cross-linking reaction is most important role for formation mechanism. Therefore, it is expected that the inner-structures of nanowires consisted of three dimensional cross-kinked network structures, and then this inner-network structures of PHS polymer functions to bind the Au nanoparticles within the nanowires.

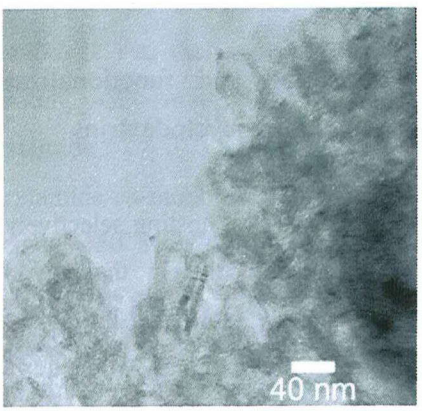

Figure 2-2-1-3. A TEM micrograph of entangled hybrid nanowires based on PHS/Au.

The hybrids nanowires based on PHS including Au nanoparticles were successfully formed by SPNT. The radii of cross-section of nanowires based on PHS and PHS/Au depended on LET. The average radial sizes of PHS/TIP hybrid nanowires also decreased compared with that of the PHS nanowires. These results indicate that the cross-linking efficiency is decreased in the hybrid films, because the including Au nanoparticles inhibit the cross-linking reaction between PHS

chains. Inner Au nanoparticles in the PHS nanowire were clearly observed by TEM, and the sizes of the Au nanoparticles were ranging from 3.6 to 5.5 nm. It is demonstrated that SPNT is also applicable to hybrid films and easily form hybridized nanowires.

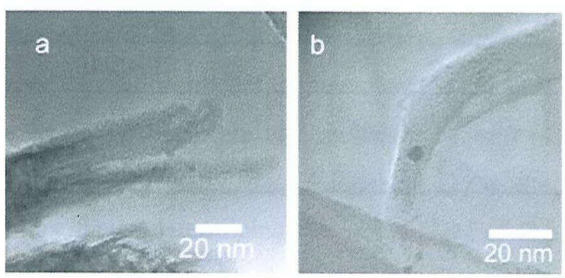

Figure 2-2-1-4. TEM micrographs of nanowires formed by 490 MeV Os ion beam irradiation to PHS included Au nano-particles thin films at the fluence of 1.0×10^{10} ions cm^{-2}.

2-2-2 Fabrication and functionalization of nanowires including cyclodextrins

Cyclodextrins (CDs), hosting selectively a wide range of guest molecules in their hydrophobic cavity, were directly fabricated into 1-dimensinal nanostructures with extremely wide surface area by single particle nanofabrication technique. The copolymers of acrylamide and mono(6-allyl)-*β*-CD were synthesized, and the crosslinking reaction of the polymer alloys with poly(4-bromostyrene) (PBrS) in SPNT gave nanowires on the quarts substrate with high number density of 5×10^9 cm^{-2}. Quartz crystal microbalance (QCM) measurement suggested 320 fold high sensitivity for formic acid vapor adsorption in the nanowire fabricated surfaces compared with that in the thin solid film of PBrS, due to the incorporation of CD units and extremely wide surface area of the nanowires.

Experimental

General.

Poly(acrylamide-*co*-mono(6-allyl)-*β*-CD) were dissolved 1wt% in water, and spin-coated on Si substrate that had been treated with KOH aqueous solution over a period of 5min. Per(6-acetyl)-*β*-CD and poly(4-bromostyrene) was dissolved 5wt% in toluene, and spin-coated on Si substrate. The thickness of the films was confirmed by a Dektak 150 surfaceprofiler. The films of the Poly(acrylamide-*co*-mono(6-allyl)-*β*-CD) and the mixture of per(6-acetyl)-β-CD and poly(4-bromostyrene) were irradiated by several kind of MeV order charged particles from cyclotron accelerator at Japan Atomic Energy Agency, Takasaki Advanced Radiation Research Institute. The number of incident particles was controlled from 1×10^9 to 5×10^9 cm^{-2} to prevent over lapping of the particle trajectories. The irradiated films were developed directly in water or toluene for 1 - 5min. The sizes and shapes of the nanostructure formed along particle trajectories were observed using a SPI-4000 atomic force microscope (AFM) from Seiko Instruments Inc. In QCM measurement, 9 MHz QCM with Au electrodes was prepared, which is utilized as a gas sensor coated with nanowires fabricated by SPNT on the surface.

Synthesis. All reagents and solvents used in the synthesis were purchased from Nacalai Tesque, Inc. or Aldrich Chemical Co. and of the best commercial quality available and used without further purification.

Mono(6-tosyl)-*β*-CD β-CD (5.0 g) was dissolved in 20 mL of dry pyridine under argon, cooled to 5°C and *p*-toluenesulfonyl chloride (1.7 g) was added. After 5h, the solvent was removed under

reduced pressure. The residue was purified by reversed pahse chromatography: Chromatorex (Fuji Silysia chemical LTD.) using a linear gradient of water/MeOH from 90:10 to 60:40. Yield: 1.8 g (33%)

Mono(6-allyl)-*β*-CD Mono(6-tosyl)-β-CD (540 mg) was dissolved in 15 mL of dry allylamine at 70°C under argon. After 5h, the solution was diluted 15 mL methanol and 100 mL acetonitrile was added. The precipitate was filtrated under reduced pressure. Yield: 380 mg (69%)

Poly(acrylamide-*co*-mono(6-allyl)-*β*-CD) Mono(6-allyl)-*β*-CD (200 mg) and acrylamide (400 mg) was dissolved in 8 mL 1:1 DMF/water solution. Ammonium persulfate (20 mg) and *N,N,N',N'*-tetramethylethylenediamine (8 μL) were added into the reaction mixture and stirred for 5h. The solution was concentrated under reduced pressure and the polymer was precipitated two times in hexane to give as a powder.

Scheme 2-2-2-1. The synthetic route of and poly(acrylamide-co-mono(6-allyl)-β-CD)

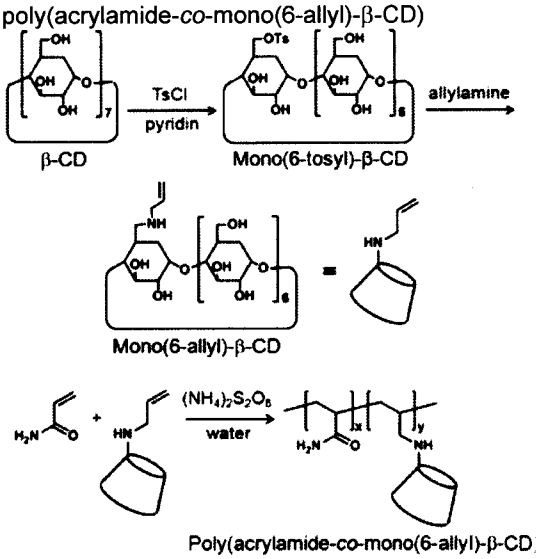

Formation of nanostructures based on cyclodextrin containing polyacrylamide

Irradiation to the thin film of pristine *β*-CD could not give isolated nanowires on the substrate, because the sufficient crosslinking reactions between the molecules had not been introduced within each ion track along the projectile ions[10]. Thus it has been indispensable for the nanowire formation incorporating with CDs to promote effective crosslinking reaction via copolymerization of monomers with CD substituents and units with high crosslinking efficiencies. Polyacrylamide is known not only as a water-soluble polymer with high radiation induced crosslinking efficiency but also used as gel electrophoresis (SDS-PAGE) or flocculating agent, etc. These properties of polyacrylamide assist the effective separation of isolated nanowires in the future handling processes. Thus the author designed poly(acrylamide-*co*-mono(6-allyl)-*β*-CD) (Scheme 2-2-2-1) as the target polymer materials incorporating CD units. The thin films of polyacrylamide and poly(acrylamide-*co*-mono(6-allyl)-*β*-CD) were irradiated by 450 MeV Xe ion beams. After the development procedure, isolated nanostructures of polyacrylamide and poly(acrylamide-*co*-mono(6-allyl)-*β*-CD) were observed on the substrate by AFM measurement as shown in Figure 2-2-2-1 and 2-2-2-2, respectively.

The thickness of the initial target film no longer reflects the length of the nanostructures based on polyacrylamide and poly(acrylamide-*co*-mono(6-allyl)-*β*-CD). These results suggest the considerable fragmentation of the nanowires occurs during the development procedure because of the low mechanical strength of cross-linked polyacrylamide. In case of fabrication of nanostructures based on poly(acrylamide-*co*-mono(6-allyl)-*β*-CD), *β*-CD

units are acting as an inhibitor for the crosslinking reaction of acrylamide [10]., leading to the fragmentation of nanostructures.

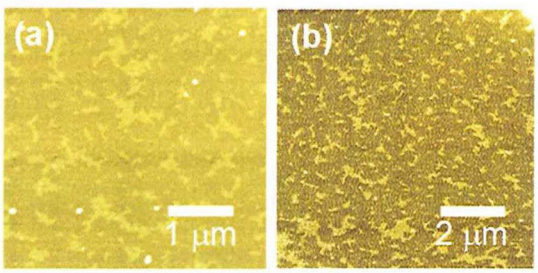

Figure 2-2-2-1. AFM micrographs of nanowires based on poly(acrylamide) produced by SPNT. Images (a) – (b) were observed in the thin films of poly(acrylamide) at 200 nm thick.

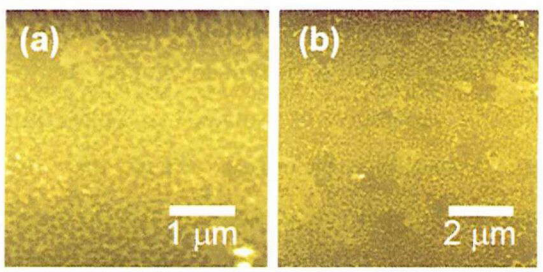

Figure 2-2-2-2. AFM micrographs of nanowires based on poly(acrylamide-*co*-mono(6-allyl)-*β*-CD) produced by SPNT. Images (a) – (b) were observed in the thin films of poly(acrylamide) at 200 nm thick.

Quartz crystal microbalance sensing by using CD containing nanowires

Quartz crystal microbalance (QCM) is a mass sensitive device being used for monitoring surface and interface processes. QCM devices modified by host molecules can be used as sensors for chemical and biochemical analysis. In order to evaluate the adsorption ability of nanostructures produced by SPNT, QCM measurement was performed. The nanostructures based on poly(acrylamide-*co*-mono(6-allyl)-*β*-CD) was unfit for QCM measurement, because that the length and number density of nanostructures could not be fairly controlled by the fragmentation reactions. Therefore, sugar nanowire based on blended polymer alloys of per(6-acetyl)-*β*-CD and poly(4-bromostyrene) (PBrS) was measured by QCM. Sugar nanowires blended with the polymer matrices can be well controlled in length and number density. This formation of nanowire was previous reported[10], and confirmed by AFM measurement as shown in Figure 2-2-2-3. The QCM plates were modified successfully by blended polymer (*β*-CD-OAc+PBrS-QCM) nanowires. To distinguish the roles of the *β*-CD derivative in the frequency response, it is essential to assess the background adsorption by nanowires based on PBrS (PBrS-QCM). Figure 2-2-2-4 shows the typical transient responses to formic acid obtained with the QCM modified by nanowires. The sensing chamber was opened 3 min after injection the gas. Each response shows that the gas sensor with the nanowires exhibits the excellent sensitivity to formic acid. The resonance frequency of the *β*-CD-OAc+PBrS-QCM and PBrS-QCM increases rapidly, reaching saturation within 50 s. The subsequent tracing is back of the frequency value when the chamber is opened. This is a typical QCM response when the QCM is introduced in a certain environment and indicates that QCM devices adsorb the gas of chemical compound. The saturated frequencies of the *β*-CD-OAc+PBrS-QCM and PBrS-QCM show 320 and 80 times higher than that observed in the QCM coated with PBrS thin film, respectively. The nanowires on the QCM plates highly expand the surface area physically adsorbed formic acid, giving the 2 orders of magnitude higher sensitivity for physical adsorption of formic acid at PBrS surfaces. Introduction of CD derivatives to the nanowires gives further rise in the sensitivity. The

trace of frequency changes observed in β-CD-OAc+PBrS-QCM shows the constant value after 2 min from opening the chamber, suggesting formic acid adsorption into the CD cavity by host-guest interaction with the high binding constant. The quick response in the trace after the gas injection also supports the dual mechanism of the adsorption of formic acids on the β-CD-OAc+PBrS-QCM nanowire surfaces.

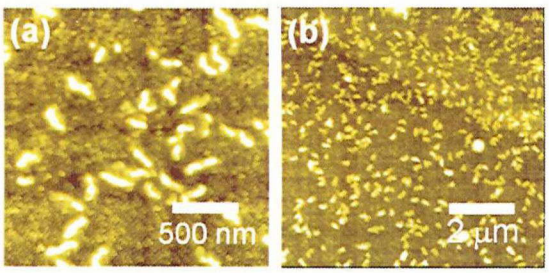

Figure 2-2-2-3. AFM micrographs of nanowires on a QCM plate surface produced by SPNT for 200 nm thick films of PBrS matrices blended with per(6-acetyl)-β-CD at 10 wt% conc. Images (a) – (b) were observed in the different scales after irradiation of 450 MeV Xe ion beams at the fluence of 3.0×10^{9} ions cm^{-2}.

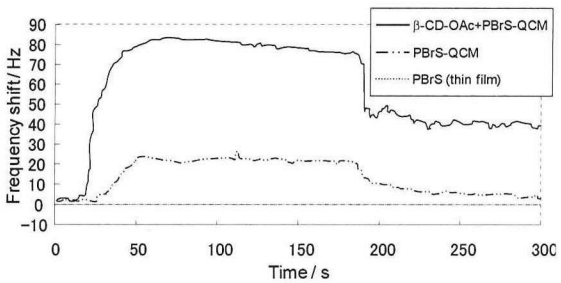

Figure 2-2-1-4. Comparison of sensor responses of QCMs with β-CD-OAc+poly(4-bromostyrene) nanowires (β-CD-OAc+PBrS-QCM), poly(4-bromostyrene) nanowires (PBrS-QCM), and thin film of poly(4-bromostyrene) to formic acid vapor at 2.5 mL in an 800 mL chamber.

2-3-1 Size control of nanowire by chemical modification of polymer materials

Polystyrene also gives the well-controlled nano-structures in length and number density by SPNT.[1] However with an increase in the aspect ratio of nanowires higher than a few hundreds, fragmentation of nanowires is often observed by atomic force microscope (AFM) measurement. Due to a low cross-linking efficiency of polystyrene upon irradiation, nanowires with low mechanical strength are considerably affected by the development conditions; handling, development time, and solvent. In this section, several polystyrene derivatives were polymerized from styrene monomers appended with functional groups to increase cross-linking efficiency. We also demonstrated precise formation of 1D-nanowires via the effective cross-linking reaction of the functional groups with high aspect-ratio reaching up to ~10^3, as well as orientation control of nanowires based on adamantane modified polystyrene derivatives.

Experimental

All reagents and solvents used in the synthesis were purchased from Wako Pure Chemical Industries or Sigma Aldrich Chemical Co. and of the best commercial quality available and used without further purification unless otherwise noted. Polystyrene (PS) and poly(styrene-*co*-4-chloromethylstyrene) (PSClS) were synthesized from styrene and 4-chloromethylstyrene by using standard nitroxide-mediated radical polymerization (NMP) [11 - 13] with *N*-*tert*-butyl-*N*-(2-methyl-1-phenylpr-o-pyl)-*o*-(1-phenylethyl)hydroxylamine at 110 °C under an atmosphere of nitrogen, respectively, as shown in scheme 2-3-1-1(a). . Poly(styrene-*co*-4-azidemethylstyrene) (PSAS) was prepared using chloromethyl groups of PSAS in the presence of sodium azide in *N*, *N*-dimethylformamide (DMF) at 50 °C for 48 h[14].

Poly(styrene-*co*-4-(adamantanyltriazolyl)styrene) (PSAdS)[16] was synthesized from poly(styrene-*co*-4-ethynylstyrene)[15] reacted with 1-adamantane azide in the presence of catalytic amount of Cu(I) in THF for 14 h as shown in scheme 2-3-1-1(b). All polystyrene derivatives were reprecipitated from 2-propanol and dried under reduced pressure. PS, PSCS and PSAS were dissolved 10 wt% in toluene, and spin-coated on Si substrate. The thickness of the films was confirmed by a Dektak 150 surface profiler. PSAdS was dissolved at 5wt% in toluene, and spin-coated or drop-casted on a Si substrate. The films of the all polystyrene derivatives were irradiated by 450 MeV Xe and 490 MeV Os ion beams from cyclotron accelerator at Japan Atomic Energy Agency, Takasaki Advanced Radiation Research Institute. The number of incident particles was controlled from 1 × 10^7 to 1 × 10^9 cm^{-2} to prevent over lapping of the particle trajectories. The irradiated films were developed directly immersing into THF or toluene for 30 min for 24 h. The sizes and shapes of the nanostructure formed along particle trajectories were observed using a SPI-4000 atomic force microscope (AFM) from Seiko Instruments Inc.

Scheme 2-3-1-1. (a)Synthesis of polystyrene derivatives by using nitroxide mediated polymerization. (b)Synthesis of adamantane modified polystyrene.

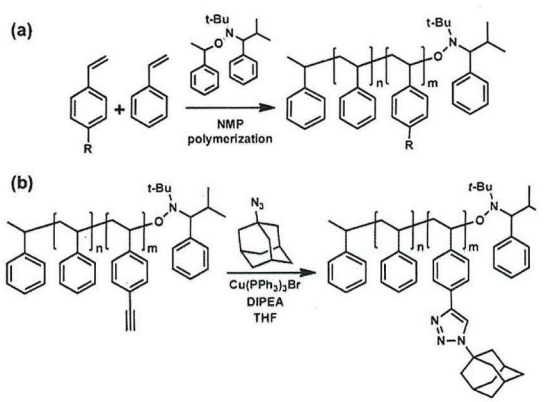

Evaluation of the cross-linking efficiencies of polystyrene derivatives

Polystyrene derivatives (figure 2-3-1-1) were synthesized by using nitroxide-mediated radical polymerization.

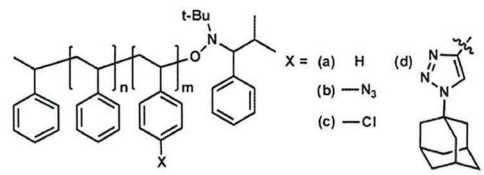

Figure 2-3-1-1. Chemical structures of polystyrene derivatives; (a) PS (M_n = 17200, PDI = 1.18), (b) PSCIS (M_n = 13900, PDI = 1.82, m = 0.37), (c) PSAS (M_n = 14500, PDI = 1.81, m = 0.35), and (d) PSAdS (M_n = 15200, PDI = 1.35, m = 0.25)

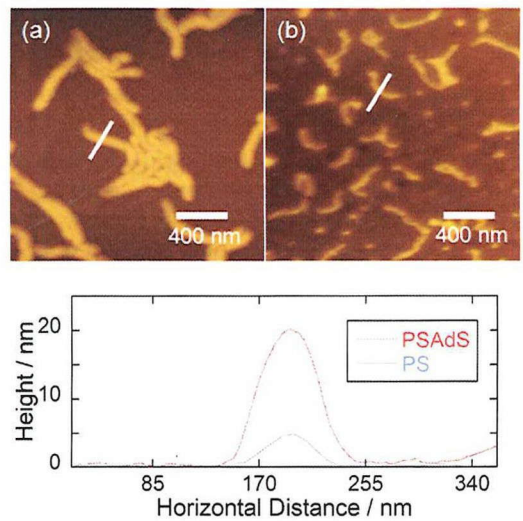

Figure 2-3-1-2. AFM micrographs of nanowires based on (a) PSAdS and (b) PS. Images (a) and (b) were observed in the films at 510 nm and 280 nm thickness after irradiation of 490 MeV $^{192}Os^{30+}$ particles at 1.0×10^9 ions cm^{-2}, respectively. (c) Cross-sectional profiles of nanowires. The profile were measured at the position indicated by lines in the corresponding AFM images.

After irradiation and development in toluene for 30 min, the surfaces of Si substrate were observed by AFM measurement under dry conditions. Figure 2-3-1-2(a) and (b) show the AFM micrographs of the nanowires based on PSAdS and PS,

respectively. Under this development condition, fragmentation of the nanowires based on PS was confirmed, giving random distribution of the nanowire length. PSAdS and other polystyrene derivatives gave the nanowires with perfectly uniform length and number density. The cross-sectional profiles of the nanowire are also greatly changed between PS and PSAdS as shown in figure 2-3-1-2(c). The cross-linking efficiency can be estimated by the semi-empirical modeling of nanowire sizes. [16] The radius of the nanowire was obtained by cross-sectional measurements, and the values are summarized in table 2-3-1-1 as well as the values of efficiency for polystyrene and polystyrene derivatives, respectively. Radiation induced cross-linking efficiency has been often characterized in terms of G-value (*G(x)*); number of crosslinks produced per absorbed energy of 100 eV by the polymer material. The values of PSCS: *G(x)* as > 4.6 $(100\ eV)^{-1}$, PSAS: *G(x)* as > 2.1 $(100\ eV)^{-1}$, and PSAdS: *G(x)* as > $(100\ eV)^{-1}$ are higher than the value of PS: *G(x)* as > 0.6 $(100\ eV)^{-1}$. PSAdS indicates the highest cross-linking efficiency. This result means the cross-linking efficiency of polystyrene is drastically changed by introducing functional groups into the styrene monomers. In particular, adamantane moieties play an important role to promote cross-linking reactions. High stability of adamantly radicals were observed upon irradiation of neat adamantane with clear EPR signals at 230 K, and the signals were postulated even at 300 ~ 400K though the signal had shown no longer hyperfine structures.[17] Especially, 1-adamantyl radical showed extremely higher stability than that of 2-adamantyl ones, leading to the polymerized products under the irradiation conditions. This is the case giving extremely higher efficiency is observed for cross-linking reactions in PSAdS, reflected as the dramatic increase in the thickness of the nanowires.

Fabrication of nanowires with high aspect ratio

The nanowires with ultra-high aspect ratio were demonstrated for the drop-casted film of PSAdS (~ 38 μm thick) as shown in figure 2-2-1-3(a). A long nanowire is clearly observed clearly on the substrate. The length of the nanowire is almost identical to the initial film thickness without fragmentation. This result indicates that the nanowires based on PSAdS have high mechanical strength by densely induced crosslinks in the nanowires via interconnection of adamantine moieties. This was also evident from the fact that fragmentation of the nanowires was not observed under the hard development conditions; with good solvents for PSAdS (THF, chloroform, and toluene) and extremely long time (~ 24h) immersing into the solvents.

With an increase in the number density of the nanowires on the substrate, the long nanowires are bundled as shown in figure 2-3-1-3(b). Figure 2-3-1-3(c) shows the cross-sectional profile of the aggregated structure. Aggregated number of nanowires in the cross-sectional profile is countable, given as configured 6 nanowires. The height of aggregated structure is almost constant, and identical to the height of single nanowire as shown in figure 2-3-1-3(c). This result clearly demonstrates the self-organization of 1D nanowires forming into 2D sheet-like structures with the help of surface interaction of the nanowires. It is also plausible that the interaction between the nanowires and the surface is even

higher than the inter-nanowire interaction, leading to the 2-D sheet-like structures without pilling up of the nanowires on the substrate.

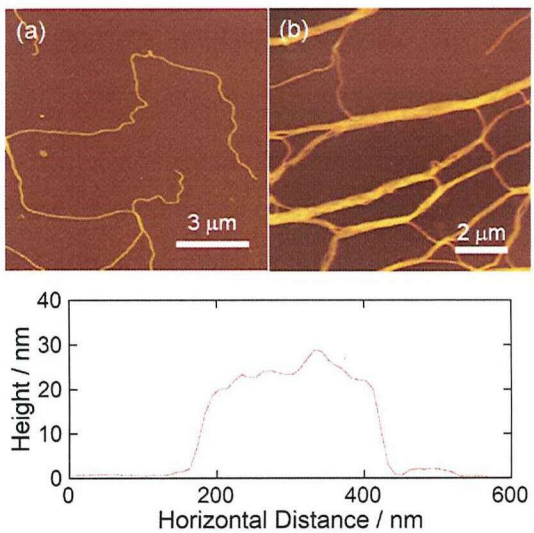

Figure 2-3-1-3. AFM micographs of (a) nanowire with high aspect-retio and (b) array of nanowires based on PSAdS. Images (a) and (b) were observed in the films of PSAdS at ~38 μm thickness after irradiation of 490 MeV $^{192}Os^{30+}$ particles at 1.0×10^{7} and 1.0×10^{8} ions cm^{-2}. (c) Cross-sectional profile of array of nanowires (b). The profile was measured at the position indicated by lines in the corresponding AFM image.
were fabricated by irradiation of 490 MeV $^{192}Os^{30+}$ particles at 1.0×10^{8} ions cm^{-2}.

It should be noted that the bottom-side terminal of the nanowire is tightly connected to the substrate. Based on the high mechanical strength and the presence of tightly connected ends on the surfaces, the orientation control of the nanowires was examined by developing the nanowires in solvent flow along one direction. The lines of the nanowire apsides are oriented clearly along the directions of solvent flows as shown in figure 2-3-1-4(a) and (b). Simple dipping processes of the substrate into solvents give highly oriented surface structures of nanowires with ultra-high aspect ratio.

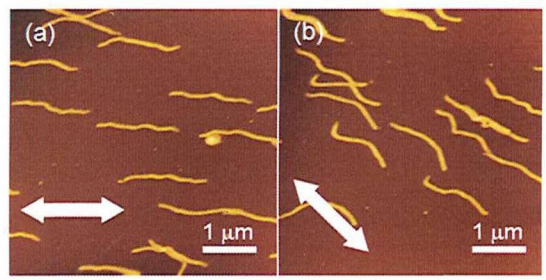

Figure 2-2-1-4. AFM micrographs of PSAdS nanowires on a Si substrate after development by slow dipping with THF. Arrows in (a) and (b) indicate the dipping directions. The nanowires were fabricated by irradiation of 490 MeV $^{192}Os^{30+}$ particles at 1.0×10^{8} ions cm^{-2}.

Table 2-3-1-1. The values of cross-linking efficiency and radius of nanowires based on polystyrene derivatives fabricated by the SPNT.

Ion beams	$G(x)$ and (r / nm)			
	PS	PSCIS	PSAS	PSAdS
450 MeV $^{129}Xe^{23+}$	–	4.6 (13.0)	2.1 (8.9)	–
490 MeV $^{192}Os^{30+}$	0.60 (4.5)	–	–	9.2 (19.6)

2-3-2 Size control of nanowire by ion beam and γ ray irradiation

The radius of nanowires fabricated by SPNT can be controlled by the linear energy transfer (LET) of the swift heavy ion. It is difficult to control the radius of nanowires precisely. When the nanowires were fabricated from the polymer materials which show low cross-linking efficiencies, it is necessary to promote the cross-linking reactions. In this

section, 450 MeV Xe ion beam firstly irradiated to polystyrene (PS) and polycarbosilane (PCS) films in order to form nanowires. Additionally, γ ray irradiation to the same film was carried out. The radial sizes of nanowires which produced by ion beam and γ ray irradiation were increased with the dose of γ ray. The change of radial sizes which depended on the dose was quantitatively measured.

Experimental

All reagents and chemicals were purchased from Wako Pure Chemical Industries unless otherwise noted. Poly(dimethylsilane) (PDMS) was synthesized by the reaction of dimethyldichlorosilane with lithium in refluxing tetrahydrofuran (THF) under an atmosphere of predried argon (Ar), or with sodium in toluene under pressurized Ar in an autoclave. Chlorosilane was purchased from Shin-Etsu Chemical and doubly distilled prior to use. The PDMS obtained was washed with toluene, THF, and methanol. The dried PDMS was placed in the autoclave and pyrolyzed at 450 °C for 6 h. The pyrolyzed product was dissolved in toluene, and the insoluble portion was separated by filtration with a 1-μm-pore-size PTFE membrane filter. PCS was fractionally precipitated from the solution by the stepwise addition of methanol, and precipitates were collected by centrifugation. The molecular weight (*Mw*) of PCS was measured by gel permeation chromatography (VP-10, Shimadzu) using THF as an eluent in a chromatograph equipped with four columns (Shodex KF-805L, Showa Denko); the measured *Mw* was 1.8×10^3 with a dispersion smaller than 1.5. PS ($M_n = 4.0 \times 10^4$, M_w/M_n = 1.04) was purchased from Aldrich Chemical Co. PCS and PS was spin-coated on Si substrates from the respective toluene solutions at 5 wt%.

The samples were subsequently placed in a vacuum chamber and exposed to 450 MeV Xe ion beams at the Takasaki Ion Accelerators for Advanced Radiation Application (TIARA) cyclotron accelerator facility of the Japan Atomic Energy Agency. The ion irradiated films were also exposed to γ ray with the dose form 22~120 kGy.

After irradiation, the samples were developed using organic solvents for 2 minutes. The irradiated part of the film, where a polymer gel was formed, was insoluble in solvents. After development and drying, the direct observation of the surface of the substrates were performed using an atomic force microscope (AFM Seiko Instruments Inc.(SII) SPI-4000).

Size control of nanowire by ion beam and γ ray irradiation

Ion irradiation at low fluence without overlapping between ion tracks produces single ion events in the target materials. Single ion bombardment can release active intermediates at high density within a limited area along the single ion track. These active intermediates form a heterogeneous spatial distribution in the ion track due to the variety of chemical reactions involved. In PCS and PS, the crosslinking reactions along the ion track result in the formation of a cross-linked nanogel (nanowire) in thin films. The non-crosslinked area can be removed by development with toluene, utilizing the change in solubility due to the gelation of PS and PCS. The nanowires formed by ion bombardment can therefore be completely isolated on the substrate. After the wet-development procedure, the nanowires lie prostrate on the substrate surface.

Figure 2-3-2-1 (a) and (b) show the nanowires based on PS and PCS formed by 450 MeV Xe beam irradiation with 1.1 x 10^9 ions/cm^2. The length of the nanowires reflects the thickness of the original film. These radii of cross-section of nanowires (r) based on PS and PCS were 5.1 and 7.2 nm, respectively. It has been reported that the radius of nanowire increased with the LET of the ion beam and molecular weight of polymer[7].

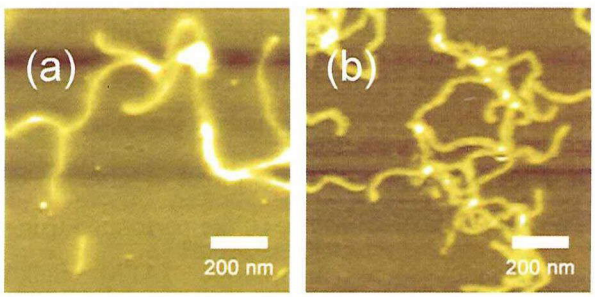

Figure 2-3-2-1. AFM micrographs of nanowires based on (a) PS and (b) PCS. These nanowires were formed by 450 MeV Xe ion beam irradiation to their thin films at 1.0 x10^9 ions/cm^2.

Especially, the LET of ion beam is a primary factor determining the radial sizes of the nanowires, because the deposited energy distribution in an ion track is inhomogeneous. Magee et al. have been suggested coaxial energy distribution of an ion track, which has core and penumbra region, as follows.[12)]

$$\rho_c = \frac{LET}{2}\left[\pi r_c^2\right]^{-1} + \frac{LET}{2}\left[2\pi r_c^2 \ln\left(\frac{e^{1/2} r_p}{r_c}\right)\right]^{-1}$$

$$; r \le r_c \qquad (2)$$

$$\rho_p(r) = \frac{LET}{2}\left[2\pi r^2 \ln\left(\frac{e^{1/2} r_p}{r_c}\right)\right]^{-1} \; ; \; r_c < r \le r_p$$

(3)

Here, ρ_c and ρ_p are the deposited energy density in the core and penumbra areas, and r_c and r_p are the radii of core and penumbra areas, e is an exponential factor. At the center core of the ion track, the deposited energy density is greater than in the outer penumbra region. It is expected that the distribution of crosslinking points in an ion track will reflect the radial energy density, and that the number of crosslinking points in the core will be much larger than in the penumbra. However, the core size suggested by theoretical considerations[2] is 0.87 nm for a 450 MeV Xe ion. In contrast, the nominal radius (r) of nanowire based on PS and PCS for this ion beam in the present experiments is 5.1 and 7.2 nm. The radial margins of the nanowires therefore lie in the penumbra area, where crosslinking occurs by energy deposition from secondary electrons.

It is expected that the polymers form a gel in this region, with one crosslinking point per polymer chain at the outer radial boundary. The deposited energy density (ρ_p) at r is therefore adopted as the critical energy density of gelation for polymers.

Therefore, the average sizes of the nanowires were well interpreted by the theoretical model, considering the energy distribution in an ion track, efficiency of cross-linking reaction (G values (number of reactions per 100 eV of absorbed dose): $G(x)$), molecular weight of the target polymers[2]

$$r'^2 = \frac{LET \cdot G(x) mk}{400 \rho \pi A}\left[\ln\left(\frac{e^{1/2} r_p}{r_c}\right)\right]^{-1}$$

(4)

where ρ is the density of polymers m and k are the mass of monomer unit and the degree of polymerization, respectively, and A is the Avogadro's number. Thus, the radial sizes of nanowires can be easily controlled by changing LET of ion beam and molecular weight of polymer.

In addition, γ ray irradiation was also useful to control their radial sizes of nanowires obtained by ion beam irradiation. The γ ray irradiation to the same films with (~171.7 kGy) was carried out after 450 MeV Xe ion beam irradiation. Figure 2-3-2-2 shows the results of additional γ irradiation with 22.4, 52.2 and 171.7 kGy, respectively. The isolated nanowires were observed on the substrate after the wet-development procedure. These radii of nanowires based on PS and PCS were larger than that of the original nanowires shown as Figure 2-3-2-1, respectively. The value of radius also increased with the dose of γ ray, as shown in Table 2-3-2-1.

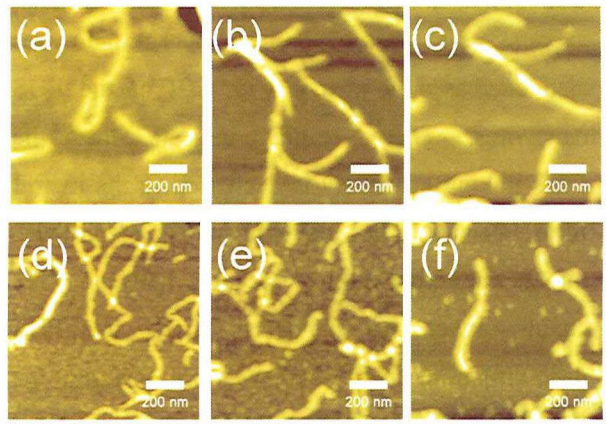

Figure 2-3-2-2. AFM micrographs of nanowires based on PS (a-c) and PCS (d-f). The nanowires were formed by 450 MeV Xe ion beam irradiation at 1.1 x 10^9 ions/cm^2, and additional γ ray irradiation with the dose of (a, d) 22.4, (b, e) 52.2, and (c, f)171.7 kGy,

These results indicate the γ ray irradiation produces homogeneous crosslinking reactions throughout films, and the cross-linking reactions between the boundary of original nanowires and around polymer chains were caused in the solid films by the γ irradiation. Therefore, the radius (r) of cross-section of nanowires was increased with an increase of the radiation dose of γ ray.

Table 2-3-2-1. The radii of PCS and PS nanowires formed by the ion beam and γ ray irradiation.

	[b]Dose [kGy]			
	0[b]	22.4[b]	52.2[b]	171.7[b]
Radius (PS) r [nm]	5.1[a]	8.6	9.1	10.2
Radius (PCS) r [nm]	7.2[a]	7.8	8.2	11.5

a: These values were radius of nanowires formed by ion beam irradiation.
b: These values were the dose of γ ray irradiation.

2-4 Summary

This chapter demonstrated the functionalization and size control of nanowires. Fabrication of functional nanowires was performed by using the mixture film based on functional materials and cross-linking type polymer for radiation. On the other hand, size control of nanowires and improvement of cross-linking efficiencies were succeeded by using chemical modification of polymer materials and γ ray irradiation.

The hybrids nanowires based on PHS including Au nanoparticles were successfully formed by SPNT. The radii of cross-section of nanowires

based on PHS and PHS/Au depended on LET. The average radial sizes of PHS/TIP hybrid nanowires also decreased compared with that of the PHS nanowires. These results indicate that the cross-linking efficiency is decreased in the hybrid films, because the including Au nanoparticles inhibit the cross-linking reaction between PHS chains. Inner Au nanoparticles in the PHS nanowire were clearly observed by TEM, and the sizes of the Au nanoparticles were ranging from 3.6 to 5.5 nm. It is demonstrated that SPNT is also applicable to hybrid films and easily form hybridized nanowires (Section 2-2-1). The crosslinking reactions in the ion tracks result in localized gelation, giving isolated β-CD nanostructures. The nanowires based on poly(acrylamide-*co*-mono(6-allyl)-β-CD) were confirmed by AFM measurement. QCM measurements demonstrated that the nanowires fabricated by SPNT highly enhance the sensitivity for formic acid adsorption. Introduction of β-CD derivatives into the nanowires also indicated not only physical adsorption of formic acid but also effective capturing of the molecule into the cavity of CDs via host-guest interactions (Section 2-2-2).

These blended techniques indicated the feasibility of SPNT to direct formation of various functional nanowires with facile procedure. But, the degradation of nanowires was often confirmed. Therefore, polymer materias were demanded the high cross-linking efficiencies leading to high tolerance against various conditions.

The introduction of functional groups and molecule into the polystyrene backbones can control the cross-linking efficiency of polystyrene derivatives upon exposure to MeV-order charged particles. Adamantane modified polystyrene: PSAdS showed dramatic increase in the cross-linking efficiency via radiation induced interconnection of adamantine moieties, providing high density crosslinks inside the nanowires, hence the higher mechanical strength than that of polystyrene based nanowires. The tough nanowires with ultra-high aspect ratio of ~750 were successfully produced in the present study, and in-plane orientation of the nanowires was also fairly controlled by the simple dipping process of the nanowires with connected ends on the substrate (Section 2-3-1). Tow step irradiation of ion beam and γ ray gives different reaction field in the polymeric materials. Ion irradiation to the PS and PCS thin films gives local crosslinking reaction along the ion path, leading to the cross-linked nanowires. On the other hand, the additional γ rays irradiation of the same film after ion irradiation produced homogeneous distribution of cross-linking points in the film. The cross-linking reactions also occurred at the boundary of the original nanowires, resulting in increase of the radial size (Section 2-3-2).

Reference

1. 1. S. Seki, K. Kanzaki, Y. Kunimi, S. Tagawa, Y. Yoshida, H. Kudoh, M. Sugimoto, T. Sasuga, T. Seguchi, H. Shibata, *Radiat. Phys. Chem.*, **50** (1997) 423.
2. S. Seki, K. Maeda, Y. Kunimi, S. Tagawa, Y. Yoshida, H. Kudoh, M. Sugimoto, Y. Morita, T. Seguchi, T. Iwai, H. Shibata, K. Asai, K. Ishigure, *J. Phys. Chem. B*, **103** (1999) 3043.
3. S. Seki, K. Maeda, S. Tagawa, H. Kudoh, M. Sugimoto, Y. Morita, H. Shibata, *Adv. Mater.*, **13** (2001) 1663.
4. S. Tsukuda, S. Seki, S. Tagawa, M. Sugimoto, A. Idesaki, S. Tanaka, A. Ohshima, *J. Phys. Chem. B*, **108** (2004) 3407.
5. S. Seki, S. Tsukuda, K. Maeda, Y. Matsui, A. Saeki, S. Tagawa, *Phys. Rev. B*, **70** (2004) 144203-1–8
6. S. Seki, S. Tsukuda, K. Maeda, S. Tagawa, H. Shibata, M. Sugimoto, K. Jimbo, I. Hashitomi, A.

Koyama, *Macromolecules*, **38** (2005), pp. 10164–10170

7. J.F. Zieglar, J.P. Biersack, U. Littmark, *Pergamon Press*, New York (2003)
8. J.L. Magee, A. Chattarjee, G.R. Freeman, John Wiley & Sons, New York (1987) p. 171 (Chapter 4)
9. S. Tsukuda, S. Seki, M. Sugimoto, S. Tagawa, *Appl. Phys. Lett.*, **87** (2005) 233119–1-3
10. Watanabe, S., Asano, A., Seki, S., Sugimoto, M., Yoshikawa, M., Seiichi, T., Tsukuda, S., Tanaka, S.-I., *Radiation Physics and Chemistry*, **78** (2009) 1071-1075.
11. C. J. Hawker, *J. Am. Chem. Soc.*, **116** (1994) 11185.
12. D. Benoit, V. Chaplinski, R. Braslau, C. J. Hawker, *J. Am. Chem. Soc.*, **121** (1999) 3904.
13. N. S. Lee, Y. Li, C. M. Ruda, K. L. Wooley, *Chem. Commun.*, **42** (2008) 5339.
14. C. N. Urbani, C. A. Bell, D. E. Lonsdale, M. R. Whittaker, M. J. Monteiro, *Macromolecules*, **40** (2007) 7056.
15. S. Fleischmann, H. Komber, B. Voit, *Macromolecules*, **41** (2008) 5255.
16. M. Malkoch, R. J. Thibault, E. Drockenmuller, M. Messerschmidt, B. Voit, T. P. Russell, C. J. Hawker, *J. Am. Chem. Soc.*, **127** (2005) 14943.
17. S. Tsukuda, S. Seki, S. Tagawa, M. Sugimoto, *Appl. Phys. Lett.*, **87** (2005) 233119-1-3.
18. R. V. Lloyd, S. DlGregorlo, L. DIMauro, D. E. Wood, *J. Phys Chem.*, **84** (1980) 2891.

Chapter 3 Fabrication and Surface Modification of the Acetylene Functionalized Nanowires

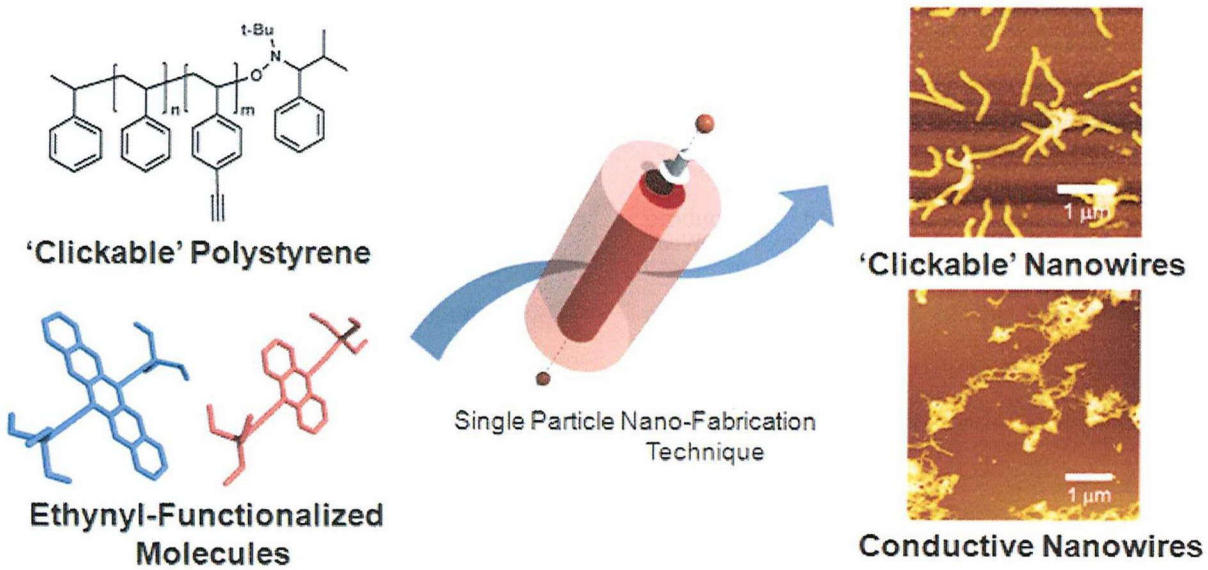

3-1 Introduction

Ion-beam irradiation promotes various chemical effects in materials. In polymeric materials, the primary effects of radiation are dictated by the balance between main chain scissions and cross-linking. The efficiency of these reactions has been statistically and quantitatively discussed[1-6] and very-sophisticated statistical formulations have been successfully applied for analysis. These formulations are however based on a homogeneous spatial distribution of energy deposited by the radiation, and reactive intermediates of high energy charged particles have been revealed to yield exceptionally non-homogenous release of kinetic energies of incident particles in the form of ion tracks. The author have successfully applied reactions in the ion track to control the spatial distribution of cross-links, yielding 1D-nanostructures; this methodology is referred to as the single particle nano-fabrication technique (SPNT).[7-11] The uses of chemical reactions in an ion track have also been the prime choice for nuclear etching[12-16] and cancer radiotherapy,[17] resulting in highly dense damage in materials. In contrast to these conservative applications of ion tracks, a variety of one-dimensional functional materials have been developed directly by SPNT. MeV-order high energy charged particles non-homogeneously induce reactive intermediates (ion radicals, neutral radicals, etc.) in polymeric materials along the particle trajectories, referred to as ion tracks. When such radical species are generated in radiation cross-linking type polymers, chemical reactions within the ion track can produce 1D-nanostructures. SPNT can thus be used to fabricate nanowires with controlled sizes.[7,10]

Polystyrene derivatives are older but interesting polymeric materials, and not only their functionalization but also their photo and radiation reactions have been vigorously investigated to date.[11,18,19] Polystyrene molecules bearing pendant groups provide numerous pathways for the relaxation of excess energies on the backbone, leading to suppression of main chain scission reactions, resulting in relatively higher effects from cross-linking reactions. The extension of conjugated electronic orbitals in pendant groups promotes extraordinary efficiency of cross-linking reactions. 4-ethynyl styrene is one of the simple structures of styrene derivatives extending the conjugated system. This monomer protected with the silyl group can be readily synthesized by Sonogashira coupling and polymerized by nitroxide-mediated radical polymerization.[18]

On the other hand, an alkyne moiety has the ability to easily introduce functionality by the formation of a strong covalent linkage. The copper(I)-catalyzed Huisgen 1,3-dipolar cycloaddition of alkyne and azide,[20-23] called the "Click reaction",[24] has recently been revealed to be an important modification technique because this reaction can result in high yields, under mild and differing conditions, and with ease of operation. A number of studies on "Click reaction" have reported in many fields including polymer chemistry,[25,26] drug discovery,[27] and materials chemistry.[28-30]

This work reports the successful fabrication of "Clickable" nanowires based on alkyne pendant polystyrene, PSES, utilizing SPNT. The alkyne moieties have two important roles: improving the cross-linking efficiency for radiation and introducing functional materials with Click reactions. Fabrication of 1D-nanowires and highly controlled 2D-arrays of bio-macromolecules can be carried out by simple surface modification and assembly of PSES nanowires.

3-2 Fabrication of acetylene functionalized nanowires.

This section describes the synthesis of the acetylene functionalized polystyrene (poly(styrene-*co*-4-ethynyl styrene): PSES) and fabrication of the nanowires based on PSES. PSES was synthesized controlling the molecular weight and dispersity by nitroxide-mediated radical polymerization. PSES gave the clear AFM image of 1D-nanostructures and indicated the extremely high cross-linking efficiency. The SPNT can be easily controlled the size (length and thickness) and number density of PSES nanowires with high mechanical strength.

Experimental

General. Nuclear magnetic resonance (NMR) spectra were collected using an NM-EXSP instrument from JEOL Ltd. with chloroform-*d* as a solvent and tetramethylsilane as an internal standard. The molecular weight distribution of the obtained polymer was measured by gel permeation chromatography (GPC) on a series of double Shodex GPC KF-805L columns using a polystyrene calibration standards. The column was eluted with tetrahydrofuran (THF). The column temperature was 40 °C.

Poly(styrene-*co*-4-ethynylstyrene) (PSES) was dissolved in toluene to an extent of 5-10 wt%, and spin-coated or drop-casted on a Si substrate. The thickness of the films was confirmed by a Dektak 150 surface profiler from Veeco Instruments Inc. Films of PSES were irradiated by several kinds of MeV order charged particles from a cyclotron accelerator at the Japan Atomic Energy Agency, Takasaki Advanced Radiation Research Institute. The number of incident particles was controlled from 1×10^7 to 8×10^8 ions cm^{-2} to prevent overlapping of the particle trajectories. The irradiated films were developed directly in THF with times from 5 min. The sizes and shapes of the nanostructures produced along particle trajectories were observed using an SPI-4000 atomic force microscope (AFM) from Seiko Instruments Inc. The loss of kinetic energy of the ions due to penetration through the polymer films was estimated using the SRIM 2000 calculation code.

Synthesis of PSES.

N-tert-Butyl-*N*-(2-methyl-1-phenylpropyl)-*O*-(1-phenylethyl)hydroxylamine were used as-received from Sigma-Aldrich Chemical Co. Styrene (99.0%, Wako), was purified by vacuum distillation and used immediately. All other reagents and solvents were purchased from Tokyo Kasei Kogyo Co. and Wako Chemical Co. and used without further purification.

4-(Trimethylsilylethinyl)benzaldehyde, 1. To a stirred mixture of 4.63 g (25.0 mmol) of 4-bromobenzaldehyde, 380 mg (2.0 mmol) of CuI, 700 mg (1.0 mmol) of bis(triphenylphosphine)palladium(II)chloride in 20 mL of THF, and 10 mL of *N,N*-diisopropylethylamine, a solution of 2.6 g (26.2 mmol) of trimethylsilylacetylene in 4 mL of THF was slowly added. The mixture was stirred for 16 hours at 50 °C and the solvent was evaporated. The obtained brown crude product was purified by column chromatography eluting with n-hexane to give **1** as a colorless liquid of 4.70 g (93%). ^{1}H NMR (270 MHz, $CDCl_3$): δ 9.98 (s, 1H), 7.80 (dm, J = 8.4 Hz, 2H), 7.59 (dm, J = 8.4 Hz, 2H), 0.26 (s, 9H).

4-(Trimethylsilyl)ethynylstyrene, 2.[48] To a stirred mixture of methyltriphenylphosphonium iodide (10.8 g, 30.0 mmol) and 75.0 mL of dried THF at -20 °C, a solution of *n*-BuLi (1.6 M in hexane, 18.3 mL, 29.2 mmol) was added dropwise over 20 min. The reaction mixture was stirred for 30 min at -20 °C, and then

slowly allowed to warm to room temperature and stirred for an additional 30 min at room temperature. The solution was cooled to -78 °C. To this solution, a solution of the **1** (5.0 g, 24 mmol) in 15.0 mL of dry THF was added dropwise over 1 h. The reaction mixture was stirred for 30 min at -20 °C, 3 h at 0 °C, and was then allowed to warm to room temperature. The reaction was quenched by adding 10.0 mL of saturated $NaHCO_3$ solution. The aqueous layer was extracted with diethyl ether (20.0 mL × 3). The combined organic layers were washed with brine, dried with anhydrous Na_2SO_4, and concentrated in vacuo. The residue was purified by column chromatography eluting with *n*-hexane and distillation to yield 3.76 g (76%) of **2** as colorless liquid. ^{1}H NMR (270 MHz, $CDCl_3$): δ 7.45 (d, J = 8.1 Hz, 2H), 7.32 (d, J = 8.3 Hz, 2H), 6.68 (dd, J = 17.5 Hz, 1H), 5.74 (d, J = 17.5 Hz, 1H), 5.28 (d, J = 11.0 Hz, 1H), 0.25 (s, 9H).

Poly[styrene-*co*-4-(trimethylsilyl)ethynylstyrene], 3. A solution of *N-tert*-Butyl-*N*-(2-methyl-1-phenylpropyl)-*O*-(1-phenylethyl)hydroxylamine (80.5 mg, 0.15 mmol), styrene (5.12 g, 48.9 mmol) and 4-(trimethylsilyl)ethynylstyrene, **2**, (3.22 g, 16.3 mmol) was degassed and heated at 125 °C under N_2. After 20 h, the solution was dissolved in THF and precipitated twice in 2-propanol to yield **3** as a white powder (2.43 g, M_n = 17,200 g/mol, PDI = 1.32). ^{1}H NMR (270 MHz, $CDCl_3$): δ 6.15-7.31 (m), 1.10-2.28 (m), 0.30 (s)

Poly(styrene-*co*-4-ethynylstyrene). Poly[styrene-*co*-4-(trimethylsilyl)ethynylstyrene] was dissolved in 20 mL anhydrous THF. To this suspension at 0 °C, tetrabutylammonium fluoride (1 M in THF, 10.5 mL) was slowly added over 20 min. The reaction mixture was stirred for 30 min at 0 °C. The solution was concentrated and precipitated twice in 2-propanol and methanol to give PSES as a white powder (1.69 g, M_n = 15,200 g/mol, PDI = 1.31). 1 NMR (270 MHz, $CDCl_3$): δ 6.15-7.41 (m), 3.02 (br s), 1.11-2.29 (m)

Scheme 1-2-4. Synthesis of ethynyl functionalized styrene monomer and PSES

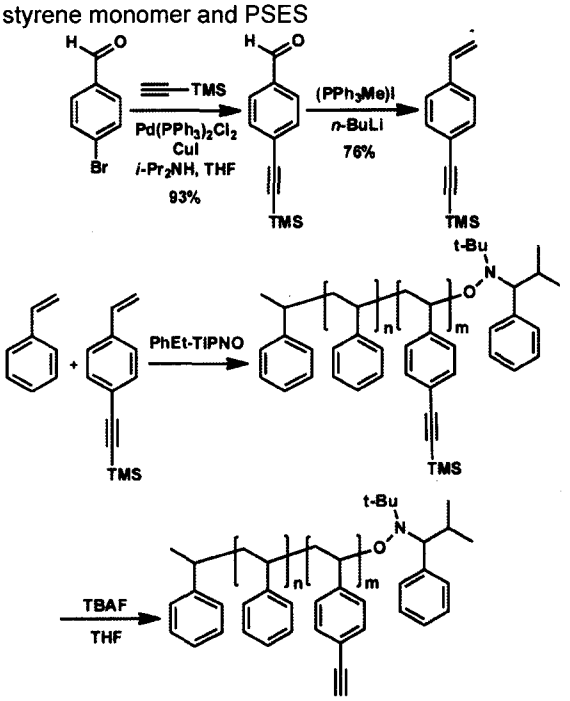

Fabrication of the PSES nanowires

Ion-beam irradiation of films based on polymeric materials has been shown to cause cross-linking reactions, leading to the formation of a polymer gel containing 1D-nanostructures. A single ion particle can fabricate one nanostructure along its trajectory (Scheme 3-2-1-i). The non-crosslinked polymer can be removed by an appropriate solvent, utilizing the difference in solubility (Scheme 3-2-1-ii). The fabricated nanowires are no longer standing, and are knocked down on the substrate, observed as 2D-images (Scheme 3-2-1-iii).

Scheme 3-2-1. Fabrication process of 1D-nanostructures by SPNT

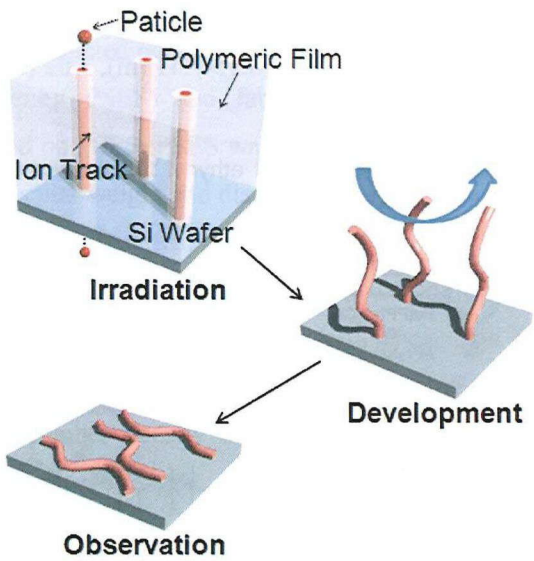

The procedure developed for isolating nanowires based on PSES and PS fabricated by the SPNT is shown in Figure 3-2-1. The sizes of the nanowires drastically changed between PSES and PS. The cross-sectional radius of PSES and PS nanowires was estimated to be 13.2 nm and 4.7 nm, respectively. The nanowire size was revealed to have good correlation with the spatial distribution of deposited energy in an ion track by a penetrating ion particle, the parameters of the target materials, and the efficiency of cross-linking reactions. Semi-empirical modeling of the PSES nanowire size gives estimates of the cross-linking efficiency of $G_{PSES}(x)$ as > 3 $(100\ eV)^{-1}$, which is a higher value compared to PS with $G_{PS}(x)$ > 0.4 $(100\ eV)^{-1}$.

Size control of PSES nanowires

The length, number density, and radius of PSES nanowires can be controlled by the initial film thickness, the number of incident particles, and linear energy transfer, respectively. Fragmentation of the nanowires during the development process, shown in Figure 3-2-1-b(iii, iv), was not observed, and thus the length of the PSES nanowires was uniform and could be controlled perfectly.

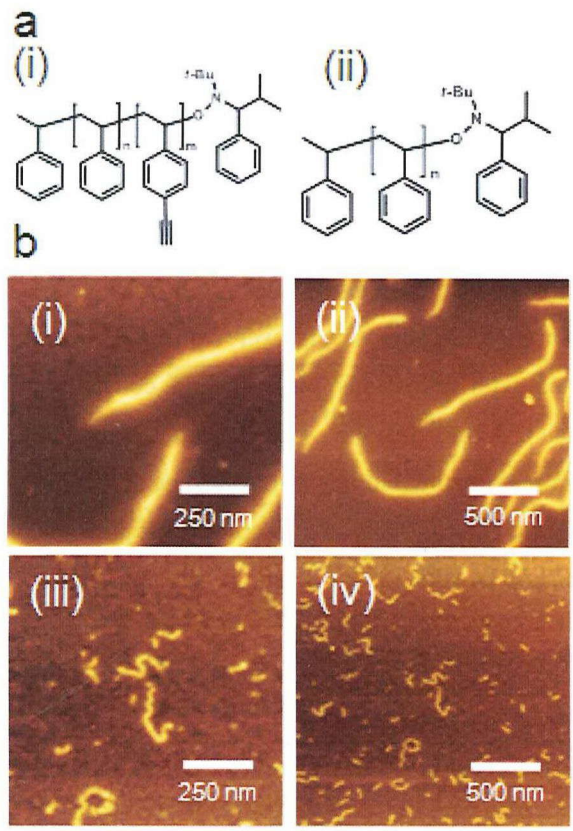

Figure 3-2-1. Chemical structures and AFM micrographs of nanowires based on (b-i,ii) PSES (M_n = 15,200 g/mol, PDI = 1.31) and (b-iii,iv) fragmentation of the nanowires based on PS (M_n = 13,200 g/mol, PDI = 1.18) fabricated by irradiation of 450 MeV $^{129}Xe^{23+}$ particles at 3.0×10^8 ions cm^{-2}. Development was carried out using THF for 5 min.

Due to the high cross-linking efficiency, PSES nanowires with a high aspect ratio could be fabricated from drop-casted films. The maximum aspect ratio of the PSES nanowire reached ~750, which is a high value compared to the case of using the negative type photo-resist SU-8 (Figure 3-2-2b).[31] The number density of PSES nanowires were also shown to be in good agreement with the ion fluence. The radius of nanowires could be changed by selecting the values of linear energy transfer (LET: energy deposition rate of

incident particles per unit length) of swift heavy ions. High LET Ion such as 470 MeV $^{192}Os^{30+}$ gave thick nanowires (r = 16 nm) compared with low LET ion, as 450 MeV $^{129}Xe^{25+}$ (r = 13 nm) and 12 MeV $^{48}Ti^{3+}$ (r = 5 nm) (Figure 3-2-3).

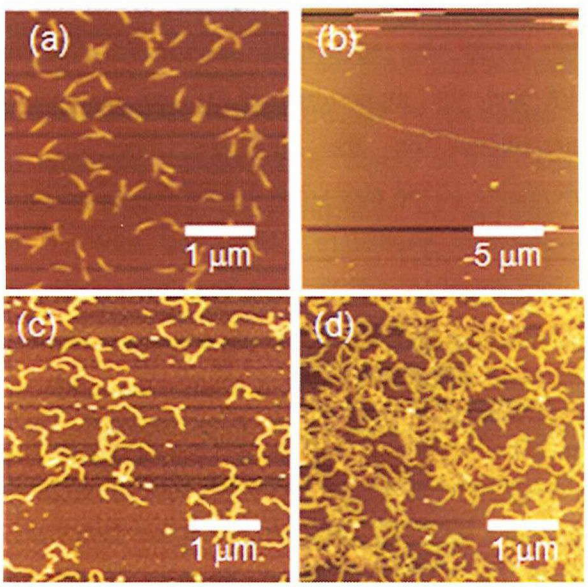

Figure 3-2-2. AFM micrographs of nanowires based on PSES prepared by exposing films of (a)200 nm and (b)22 μm thickness to 470 MeV $^{192}Os^{30+}$ particles. AFM micrographs of nanowires based on PSES prepared by exposing films of 1 μm thickness to 470 MeV $^{192}Os^{30+}$ particles at of (c) 4.0×10^{8} and (d) 8.0×10^{8} ions cm^{-2}.

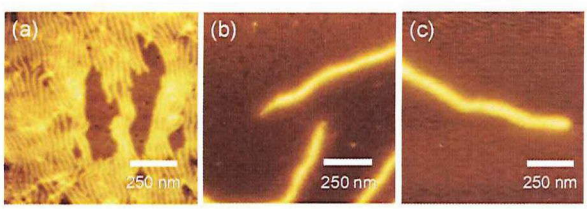

Figure 3-2-3. AFM micrographs of nanowires based on PSES prepared by exposing films to a (a)12 MeV $^{48}Ti^{3+}$; 2800 eV nm^{-1}, (b)450 MeV $^{129}Xe^{25+}$; 9200 eV nm^{-1}, and (c).470 MeV $^{192}Os^{30+}$; 11200 eV nm^{-1}particles.

3-3 Orientation and arrangement control of PSES nanowires

Manipulation of 1D-nanostructures is one of the critical steps in the development of novel functional materials and surfaces. Orientation and arrangement control approaches were reported using phase segregation,[33] liquid crystals,[34] and a stretching method.[35] The PSES nanowires could be easily arranged and the assembly controlled for flexibility and high mechanical strength. In this section demonstrates the orientation and arrangement control of PSES nanowires by using development method and solvents.

Experimental

Poly(styrene-*co*-4-ethynylstyrene) (PSES) was polymerized by nitroxide-mediated radical polymerization. PSES was dissolved in toluene to an extent of 10 wt%, and spin-coated or drop-casted on a Si substrate. The thickness of the films was confirmed by a Dektak 150 surface profiler from Veeco Instruments Inc. Films of PSES were irradiated by 470 MeV $^{192}Os^{30+}$ from a cyclotron accelerator at the Japan Atomic Energy Agency, Takasaki Advanced Radiation Research Institute. The number of incident particles was 1×10^{8} ions cm^{-2}. The irradiated films were developed directly in toluene, THF, or a mixture of toluene and THF with times from 5 min to 12 h.

The sizes and shapes of the nanostructures produced along particle trajectories were observed using an SPI-4000 atomic force microscope (AFM) from Seiko Instruments Inc and a JSM-7001F scanning electron microscope (SEM) from JEOL Ltd. The loss of kinetic energy of the ions due to penetration through the polymer films was estimated using the SRIM 2000 calculation code.

Orientation control of PSES nanowires

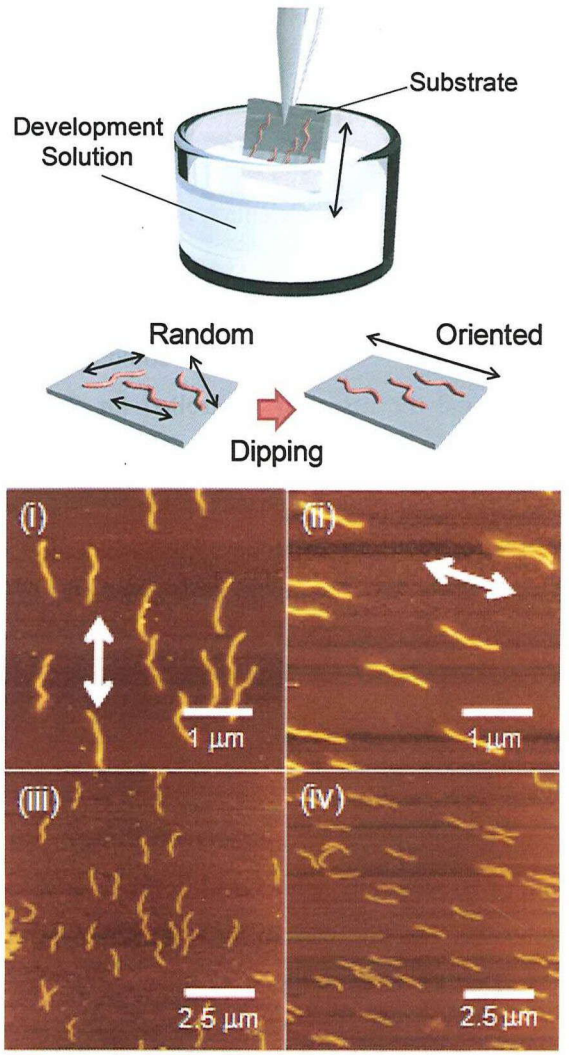

Figure 3-3-1. (a) Orientational control process of nanowires on the Si substrate. The arrows indicate the direction of raising of the substrate. (b) AFM micrographs of PSES nanowires on a Si substrate. The nanowires were fabricated by irradiation of 480 MeV $^{192}Os^{30+}$ particles at 1.0×10^{8} ions cm^{-2}. The arrows indicate thedirection of raising of the substrate: (c) upper and (d) diagonally upper directions in the development process, respectively.

The nanowires fabricated by SPNT have flexibility because they are in the form of nanosized gel induced by cross-linking reactions among the polymer chains. Thus, the arrangement of the nanowires is affected by the development conditions and length of the nanowires. In particular, the PSES nanowires show high mechanical strength, preventing the collapse of the nanostructures under harsh conditions. Fragmentation of the PSES nanowires was not observed under the various conditions used including different development solvents (THF, chloroform, and toluene) and time (~24h).

When a nanowire is produced by SPNT, the high-energy charged particle penetrates the polymer film and the mono-terminal of the nanowire is immobilized on the substrate. Therefore, the orientation of the nanowires can be controlled by the development procedure. When the substrate was slowly raised in one direction from the development solution, the nanowires were aligned along the raised direction. Figures 2c and d shows the orientation control of the nanowires corresponding to the direction of raising the substrate. This development procedure is applicable to nanowires less than 8 μm in length. On the other hand, in the case of nanowires more than 8 μm in length, the orientation control of nanowires was difficult as shown in figure 3-3-2. This is because the interactions between tnanowire and the substrate increased.

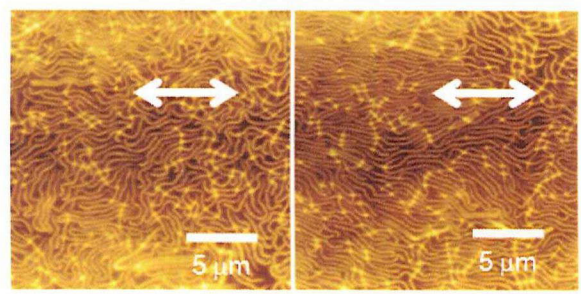

Figure 3-3-2. AFM micrographs of poly(styrene-co-4-ethynylstyrene) nanowires on a Si substrate after development by slow dipping into THF. The nanowires were fabricated by irradiation of 480 MeV $^{192}Os^{30+}$ particles at 1.0×10^{8} ions cm^{-2}. The arrows indicate the direction of raising of the substrate.

Arrangement control of PSES nanowires

The development solvents used also affect the arrangement of nanowires. The aggregation structures

of the PSES nanowires with lengths of 8 μm were changed with development solvents as shown in figures 3-3-3a-c. When the development was carried out in THF and toluene, "linear" and "sheet" structures of nanowires were confirmed, as shown in figures 3-3-3a and b, respectively. Furthermore, when the development was carried out in a mixed solvent of THF and toluene, a "net" structure of the nanowires was confirmed, as shown in Figure 3-3-3c. These results indicate that the arrangement of nanowires is controlled by competition of the interactions between nanowires and between the nanowire and substrate in each solvent.

In the case of nanowires more than 20 μm in length, the interactions between nanowires significantly increased. The nanowires were entangled with each other and formed a fabric-like structure. This "fabric" could be peeled off from the substrate with tweezers and transferred to other substrates, as shown in figure 3-3-4.

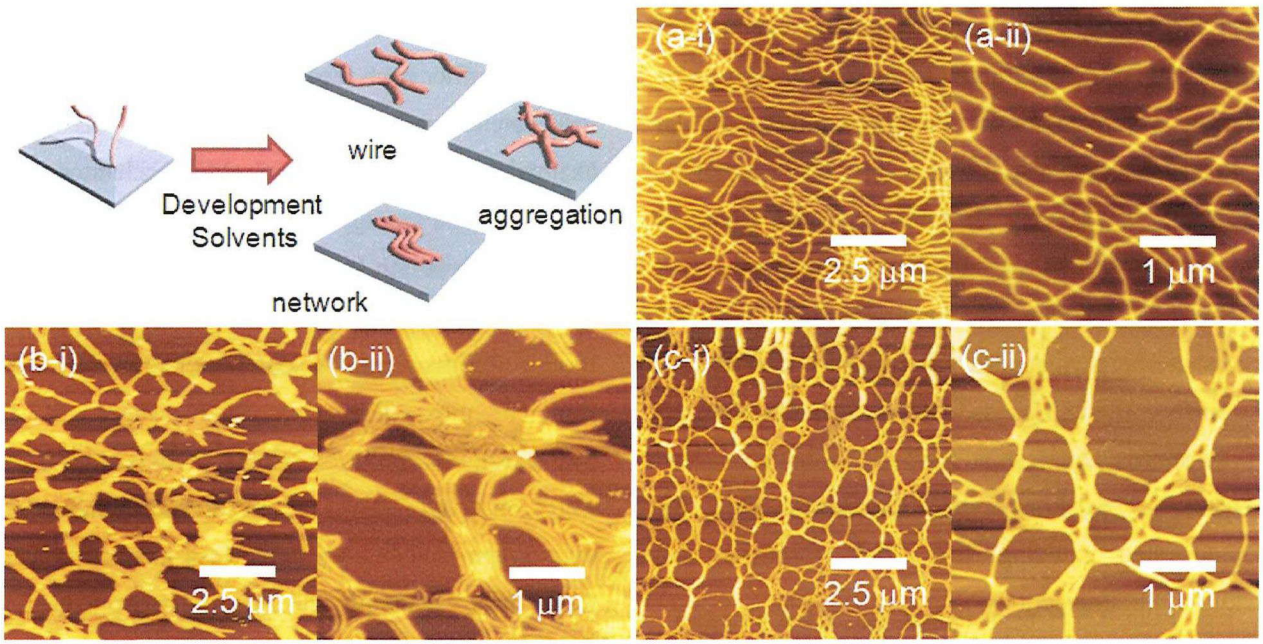

Figure 3-3-3. Aggregation control of nanowires by the development solvents. (b-d) AFM micrographs of nanowires prepared by exposing PSES films to 480 MeV $^{192}Os^{30+}$ particles at 1.0×10^{8} ions cm^{-2}. Development was carried out in (a-i,ii) THF for 5 min, (b-i,ii) toluene for 5min, and (c-i,ii) mixture solution of THF and toluene.

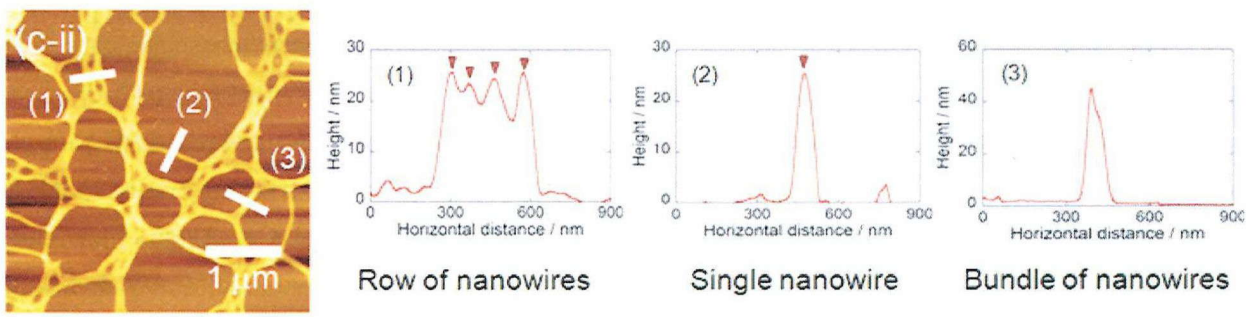

Figure 3-3-4. AFM micrographs of nanowires prepared by exposing PSES films to 480 MeV $^{192}Os^{30+}$ particles at 1.0×10^{8} ions cm^{-2}. Development was carried out in THF and toluene. Cross-sectional profiles of the nanowires on Si substrate. The profile was measured at the position indicated by lines (1) to (3) in the corresponding AFM image.

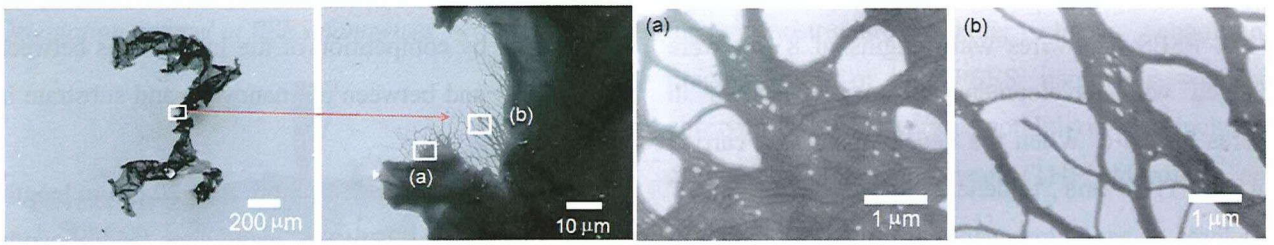

Figure 3-3-5. SEM image of the fabric of PSES nanowires produced from a film of > 20 μm thickness irradiated by 490 MeV $^{192}Os^{30+}$ particles at 1.0×10^{7} ions cm^{-2}. Development was carried out in THF for 24h.

3-4 Functionalization of PSES nanowires by using surface modification technique

PSES contains alkyne groups in its backbone, and alkyne moieties quantitatively react with the azide group via copper (I)-catalyzed 1,3-dipolar cycloaddition called Click chemistry. PSES nanowire surfaces can be modified by various kinds of functional materials using Click chemistry. This section describes the fanctionalization of nanowires by using chemical modification to alkyne groups on the surface of PSES nanowires with polymer materials. Furthermore, fabrication of 1D-nanowires and 2D-arrays based on bio-macromolecules was demonstrated utilizing the Click reactions and avidin-biotin interactions.

Experimental

General. Nuclear magnetic resonance (NMR) spectra were collected using an NM-EXSP instrument from JEOL Ltd. with chloroform-d as a solvent and tetramethylsilane as an internal standard. The molecular weight distribution of the obtained polymer was measured by gel permeation chromatography (GPC) on a series of double Shodex GPC KF-805L columns using a polystyrene calibration standards. The column was eluted with tetrahydrofuran (THF). The column temperature was 40 °C.

Poly(styrene-*co*-4-ethynylstyrene) (PSES) was dissolved in toluene to an extent of 5-10 wt%, and spin-coated or drop-casted on a Si substrate. The thickness of the films was confirmed by a Dektak 150 surface profiler from Veeco Instruments Inc. Films of PSES were irradiated by several kinds of MeV order charged particles from a cyclotron accelerator at the Japan Atomic Energy Agency, Takasaki Advanced Radiation Research Institute. The number of incident particles was controlled from 1×10^{8} ions cm^{-2}. The irradiated films were developed directly in THF times from 5 min. The sizes and shapes of the nanostructures produced along particle trajectories were observed using an SPI-4000 atomic force microscope (AFM) from Seiko Instruments Inc and a JSM-7001F scanning electron microscope (SEM) from JEOL Ltd. The loss of kinetic energy of the ions due to penetration through the polymer films was estimated using the SRIM 2000 calculation code.

Synthesis. 11-Azido-3,6,9-trioxaundecan-1-amine (90%), bromotris(triphenylphosphine)copper (I) (98%), and *N*-*tert*-Butyl-*N*-(2-methyl-1-phenylpropyl)-*O*-(1-phenylethyl)hydroxylamine were used as-received from Sigma-Aldrich Chemical Co. Avidin from chicken egg white was purchased from Calzyme Lab, Inc. Poly(4-azidemethylstyrene)[45,46] and Biotin *N*-hydroxysuccinimide ester[47] were prepared by methods described in the literature. All other reagents

and solvents were purchased from Tokyo Kasei Kogyo Co. and Wako Chemical Co. and used without further purification.

Formation of multi-layer of polymer materials on the PSES nanowires

PSES nanowires with a length of 1100 nm were fabricated on Si substrates (0.5 × 0.5 cm^2). After development with THF for 24 h, the substrates were immersed in a THF solution of poly(4-azidemethylstyrene) (M_n: 5,600 g/mol, PDI: 1.15) (10 mM / based on azide unit), $CuBr(PPh_3)_4$ (1 mM), and DIPEA (10 mM) for 12 h. The substrates were washed with THF and immersed in the THF solution of PSES (M_n: 15,200 g/mol, PDI: 1.31) (10 mM / based on ethynyl unit), $CuBr(PPh_3)_4$ (1 mM), and DIPEA (10 mM) for 12 h. The radii of the nanowires were evaluated in each modification step by AFM cross-sectional measurements.

Fabrication of 1D-protein nanowires and 2D-protein sheets

PSES nanowires or "sheets" of nanowires were fabricated on Si substrates (0.5 × 0.5 cm^2). After development with THF or toluene for 24 h, the substrates were immersed in a mixture of 11-Azido-3,6,9-trioxaundecan-1-amine (10 mM), $CuBr(PPh_3)_4$ (1 mM) and DIPEA (1 mM) in 5 mL of THF for 12 h. In the next step, the substrates were washed with THF and DMF, and immersed in a DMF solution of NHS-biotin (10 mM) and NEt_3 (10 mM) for 2 h. After biotinylation, the substrate was carefully washed with water and a pH7.4 phosphate buffer solution (PBS). Finally, the substrates were immersed in an avidin solution (10 μM) in pH7.4 PBS for 2h. The radii of the nanowires were evaluated by AFM cross-sectional measurements. In the case of fabrication of 1D-protein nanowires, all the procedures and preservation of substrates were performed under solution in order to prevent the immobilization of nanowires by drying the surface of the substrates.

Surface modification of PSES macrogel with fluorescent porbe

In orfer to confirm the reactivity of the surface of PSES of nanowires, the surface modification of PSES macrogel with fluorescent probe was performed as shown in scheme 3-2-2. PSES macrogel was fabricated by using the 3 MeV H^+ particles. After the surface modification, the fluorescence image was confirmed by the confocal laser microscope measurement. The reactivity of the surface of PSES nanowires for the reaction was confirmed by the identical reaction scheme of Click chemistry using fluorescent probe molecules (5- and 6-carboxyfluorescein) applied to the PSES macrogel surface, suggesting enough high reactivity secured for the surface of the PSES nanowires as shown in figure 3-4-1.

Scheme 3-2-2. (a)Fabrication of PSES macro-gel by using proton beam writing technique (b)Surface modification of PSES macro-gel with fluorescence dye via click reaction

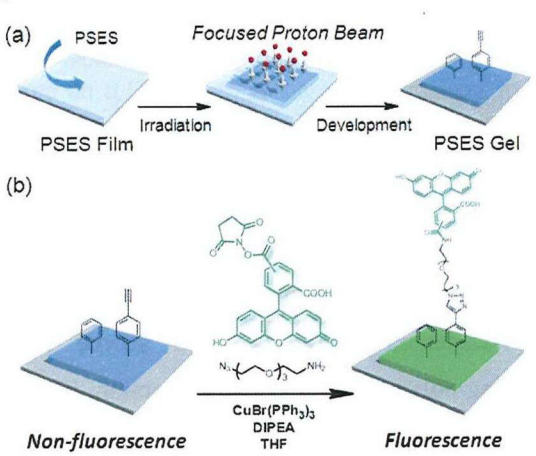

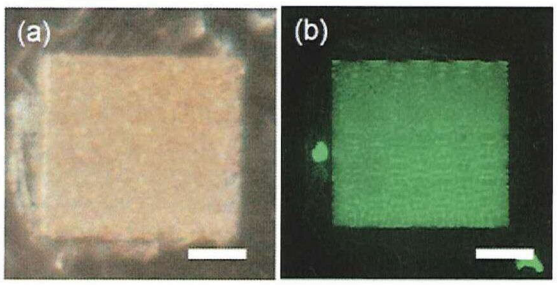

Figure 3-4-1. Optical and confocal laser microscope images of patterned gel structure based on PSES produced by patterned 3 MeV H^+ particles at the fluence of 2×10^{13} ions / cm^2 where the gel fraction of PSES solid film was higher than 0.95. After the pattern fabrication, the film was developed by THF for 24 h, and dried under vacuum. Surface modification via Click reaction by 5- and 6-carboxyfluorescein was performed. Scalebar: 100 μm.

Surface modification of PSES nanowires with synthetic polymers

The surface of a nanowire is to be found in the threshold region for the gelation of target materials where one crosslink is induced per a polymer chain in average. Polymer chains on the surfaces of nanowires have minimum amounts of cross-links. Therefore, it is expected that the surface of a nanowire preserves the physical and chemical functions of polymer materials. PSES contains alkyne groups in its backbone, and alkyne moieties quantitatively react with the azide group via copper (I)-catalyzed 1,3-dipolar cycloaddition called Click chemistry. PSES nanowire surfaces can be modified by various kinds of functional materials using Click chemistry.

Figure 3-4-2a shows the formation of multi-layers of polymer materials on PSES nanowires. After the formation of the PSES nanowires, the surfaces of nanowires were modified with azide (poly(4-azidemethylstyrene))[36] and alkyne (PSES) containing polymers by a stepwise reaction. Figure 4b shows AFM micrographs of the nanowires at each stage of modification.Fragmentation of nanowires caused by the modification conditions was not confirmed in Figures 3-4-2bii and iii. The height profiles of the nanowires at each step increased (Figure 3-4-2b-iv) and were evaluated to be (a) 10.5 nm, (b) 11.8 nm, and (c) 13.8 nm by cross-sectional measurements. When the catalysts, copper and base, were not added, the height profile hardly changed (*h* was 10.3 nm). These results indicate that the increasing height profile is not the result of physical absorption of polymer materials but rather chemical modifications by Click chemistry.

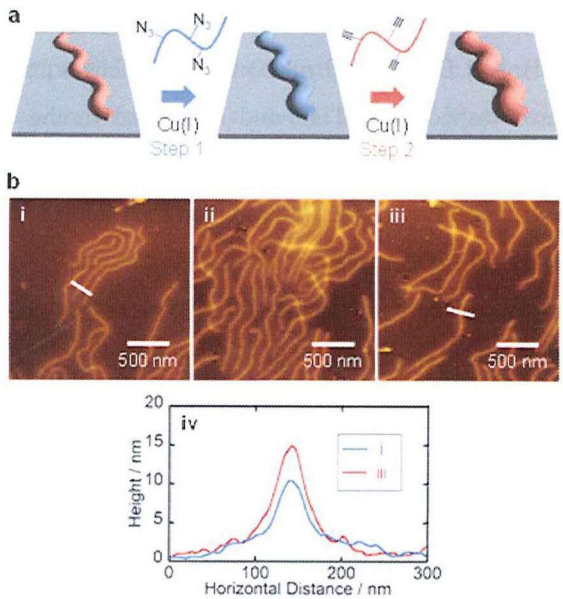

Figure 3-4-2. (a) Scheme for surface modification of PSES nanowires with azide and alkyne containg polymers by the Click reactions. (b-i) AFM micrograph of nanowires fabricated by exposing films of 1100 nm thickness to a 450 MeV $^{129}Xe^{25+}$ beam at 3.0×10^8 ions cm^{-2}. (b-ii, b-iii) AFM micrographs of nanowires modified with poly(4-azidestyrene) and PSES by the Click reaction, respectively. (b-iv) Cross-sectional profiles of nanowires based on PSES before and after modification.

Fabrication of 1D and 2D protein nanowires by surface modification of PSES nanowires

Fabrication of 1D-nanowires and 2D-arrays based on bio-macromolecules was demonstrated utilizing the Click reactions and avidin-biotin interactions. A

number of fabrication techniques of functional protein nanowires have been reported, utilizing the self-assembling ability of amyloid proteins[37,38] and metal–organic protein frameworks.[39] In contrast to these techniques indicating their many positive characteristics, control of the size and arrangement of nanowires is challenging. Avidin is a protein well-known for its extraordinary high affinity with biotin (K_d approximately 10^{-15} M).[40,41] In addition, the biotinylation of the synthetic and bio-macromolecules enables these materials to be immobilized through avidin-biotin interactions for developing functional biomaterials and their applications.[42,43] In order to fabricate the 1D-protein nanowires, avidin can be also introduced to the surface of PSES nanowires by using avidin-biotin affinity after the biotinylation reaction (Figure 3-4-3a-i). Figures 3-4-3ii and iii show the nanowires before and after modification of avidin, respectively. The radii of the nanowires were evaluated to be 16.4 nm and 27.1 nm respectively from the cross-sectional profiles in Figure 3-4-3iv. This value difference in the radii nearly corresponds to the size of avidin.[44] When the biotinylation process was not carried out, the radius of the nanowires hardly changed (r was 17.1 nm). These results indicate that a mono-layer of avidin is formed on the surface of the nanowire by the avidin-biotin interaction, as shown in Figure 3-4-3v.

The combination of the arrangement and modification techniques makes it feasible to design and fabricate highly controlled composites on a substrate (Figure 3-4-4i). After the arrangement of the nanowires, the assembly structure is fixed on the substrate. The PSES nanowires can thus produce not only 1D-protein nanowires, but also 2D-protein sheets by modifying the assembly structure of the nanowires (Figures 3-4-4ii and iii). After the modification, straggles of the nanowires were confirmed. Avidin, however, was modified and arranged in order of the array of nanowires. To the best of our knowledge, this is the first report of bio-macromolecular materials arranging a protein onto highly controlled structures composed of 1D-nanowires.

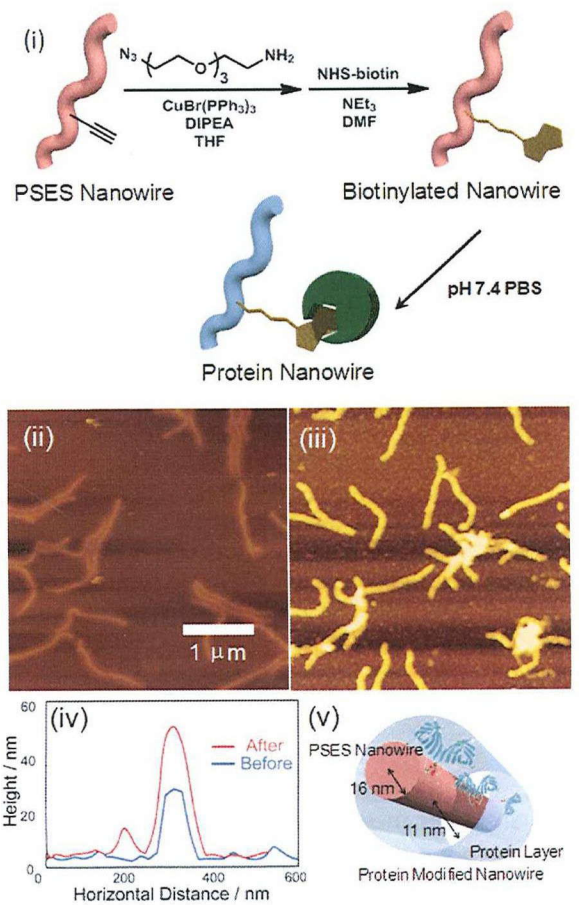

Figure 3-4-3. (i) Scheme for fabrication of the protein nanowires by using chemical modification and avidin-biotin system. (ii) AFM micrograph of nanowires based on a PSES film prepared by exposure to 490 MeV $^{192}Os^{30+}$ particles at 1.0×10^8 ions cm^{-2}. (iii) AFM micrograph of modified nanowires. The surfaces were modified with avidin. (iv) Cross-sectional profiles of nanowires based on PSES before and after modification. (v) A visualization of a bio-macromolecular nanowire covered with avidin.

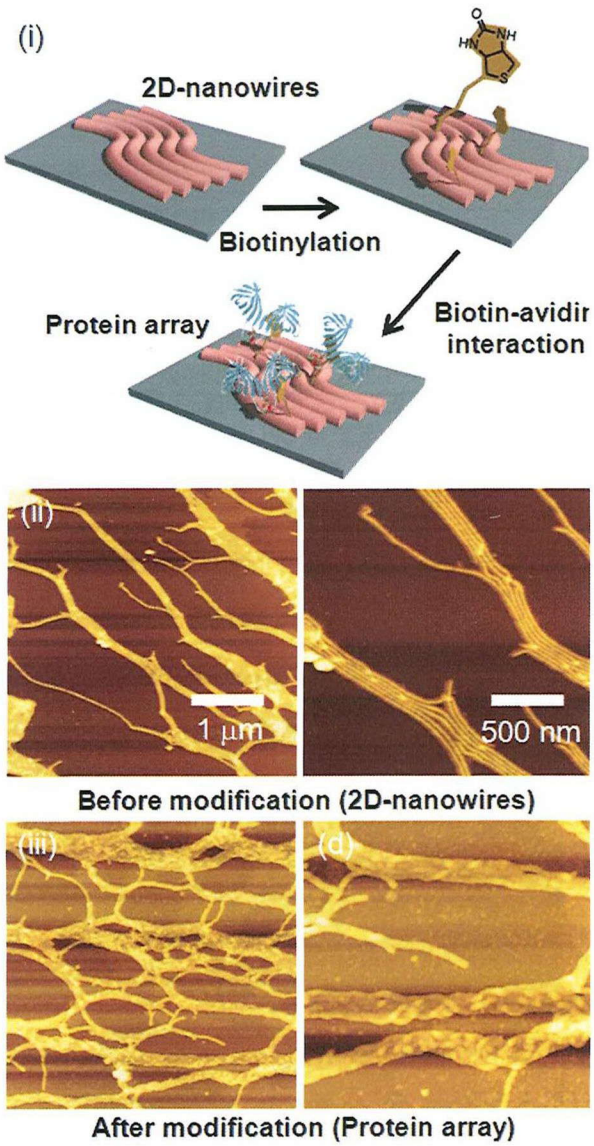

Figure 3-4-4. (i) Scheme for fabrication of the 2D-protein sheets by modifying the assembly structure of the nanowires. (ii) AFM micrograph of arrays of nanowires prepared by exposing PSES film to 490 MeV $^{192}Os^{30+}$ particles at 1.0×10^{8} ions cm^{-2}. Development was carried out in toluene for 5 min. (iii) AFM micrograph of arrays of protein-modified nanowires. The surface was modified with avidin.

3-5 Fabrication of nanowires based on π-conjugated molecules

Section 3-2 indicated PSES showed high cross-linking efficiency and gave the 'fine' nanowires with high mechanical strength. It is demonstrated phenyl acetylene unit in PSES has an important role to improve the cross-linking reactions. Pentacen is one of the most intensively studied organic materials about the charge transporting properties. Due to its low molecular weight, it is difficult to fabricate the nanowires based on pentacene. To improve the stability and solubility, silylethyne substituted pentacens are reported and indicate the excellent electronic performance. In this section, direct fabrication of the pentacene naowires were performed by using trialkylsilyl alkyne substituted pentacen derivatives. Nanowires based on trialkylsilyl alkyne substituted pentacens were confirmed by AFM measurement. Furthermore, fabrication of nanowires based on π-conjugated molecules, such as pyrene, anthracene, and tetraphenylethylene were demonstrated.

Experimental

General. Nuclear magnetic resonance (NMR) spectra were collected using an NM-EXSP instrument from JEOL Ltd. with chloroform-*d* as a solvent and tetramethylsilane as an internal standard. 6,13-Bis(triethylsilylethynyl)pentacene (≥99%), 6,13-bis(triisopropylsilylethynyl)pentacene (≥99%), and pentacene-*N*-sulfinyl-*tert*-butylcarbamate (99%) were used as received from Sigma and Aldrich Chemical Co. All other reagents and solvents were purchased from Tokyo kasei kogyo Co. and Wako Chemical Co. and used without further purification. Pentacene derivatives was dissolved 8wt% in chloroform, and spin-coated or drop-casted on Si substrate. Pentacene film was prepared by UV irradiation under acid generator and heating of pentacene-*N*-sulfinyl-*tert*-butylcarbamate following by the reported procedure. The thickness of the films

was confirmed by a Dektak 3st surface profiler. The films of pentacene derivatives irradiated by the MeV order charged particles from cyclotron accelerator at Japan Atomic Energy Agency, Takasaki Advanced Radiation Research Institute. The number of incident particles was controlled from $1\text{-}5\times10^{8}$ particles cm^{-2} to prevent overlapping of the particle trajectories. The irradiated films were developed directly in hexane for 10 to 30 s. The sizes and shapes of the nanostructures produced along particle trajectories were observed using a SPI-4000 atomic force microscope (AFM) from Seiko Instruments Inc. The loss of kinetic energy of ions due to penetration through the polymer films was estimated using the SRIM 2000 calculation code.

Synthesis.

4-(Propargyloxy)styrene. To a stirred mixture of 2.30 g (19 mmol) of 4-hydroxystyrene, 8.60 g (38 mmol) of potassium carbonate, and 0.62 g (3.3 mmol) of 18-crown-6 in 20 mL of acetone, a solution of 4.4 g (29 mmol) of propargyl bromide in 4 mL of acetone was slowly added. After the mixture was heated to reflux for 20h, 20 mL of water was added. The aqueous layer was extracted with dichloromethane (20.0 mL × 3). The combined organic layers were washed with brine, dried with anhydrous Na_2SO_4, and concentrated in vacuo. The residue was purified by column chromatography eluting with *n*-hexane and ethyl acetate (100:1) to yield 1.31 g (80%) of 4-(propargyloxy)styrene as colorless liquid. ^{1}H NMR (270 MHz, $CDCl_3$): δ 7.38 (d), 6.95 (d), 6.68 (dd), 5.65 (d), 5.17 (d), 4.70 (d), 2.54 (t)

4-(Trimethylsilylpropargyloxy)styrene. To a mixture of 5.4 mg (0.4 mmol) of silver chloride, 0.55 g (3.5 mmol) of 4-(propargyloxy)styrene and 0.65 g (4.3 mmol) DBU in 20 mL of dichloromethane, 0.49 g (4.5mmol) trimethylsilyl chloride were slowly dropped. After the mixture was heated to reflux for 28h, the reaction mixture was cooled to room temperature and passed the celite pad with 20 mL of *n*-hexane.water was added. The aqueous layer was extracted with dichloromethane (20.0 mL × 3). The combined organic layers were washed with brine, dried with anhydrous Na_2SO_4, and concentrated in vacuo. The residue was purified by column chromatography eluting with *n*-hexane and ethyl acetate (100:1) to yield 0.67 g (79%) of 4-(3′-Trimethylsilylpropargyloxy)styrene as colorless liquid. ^{1}H NMR (270 MHz, $CDCl_3$): δ 7.35 (d), 6.95 (d), 6.67 (dd), 5.62 (d), 5.14 (d), 4.69 (s), 0.18 (s)

Poly[styrene-*co*-4-(trimethylsilylpropargyloxy)ethynylstyrene]. A solution of *N*-*tert*-Butyl-*N*-(2-methyl-1-phenylpropyl)-*O*-(1-phenylethyl)hydroxylamine (40.3 mg, 0.075 mmol), styrene (2.56 g, 24.5 mmol) and 4-(trimethylsilylpropargyloxy)ethynylstyrene, (1.87 g, 8.2 mmol) was degassed and heated at 125 °C under N_2. After 20 h, the solution was dissolved in THF and precipitated twice in 2-propanol to yield Poly[styrene-*co*-4-(trimethylsilylpropargyloxy)ethynylstyrene] as a white powder (1.02 g, M_n = 14,200 g/mol, PDI = 1.52). ^{1}H NMR (270 MHz, $CDCl_3$): δ 6.2-6.8(m), 4.59(s), 1.1-2.1(m), 0.18(s)

Poly(styrene-*co*-4-ethynylstyrene).

Poly[styrene-*co*-4-(trimethylsilylpropargyloxy)ethynylstyrene] was dissolved in 20 mL anhydrous THF. To this suspension at 0 °C, tetrabutylammonium fluoride (1 M in THF, 10.5 mL) was slowly added over 20 min. The reaction mixture was stirred for 30 min at 0 °C. The solution was concentrated and precipitated twice in 2-propanol and methanol to give PSES as a white powder (0.82 g, M_n = 13,200 g/mol, PDI = 1.51). ^{1}H

NMR (270 MHz, $CDCl_3$): δ 6.2-7.0(m), 4.63(s), 2.5(bs) 1.1-2.1(m)

Scheme 3-2-3. Synthesis of poly(styrene-*co*-4-trimethyl- silylethynylstyrene)

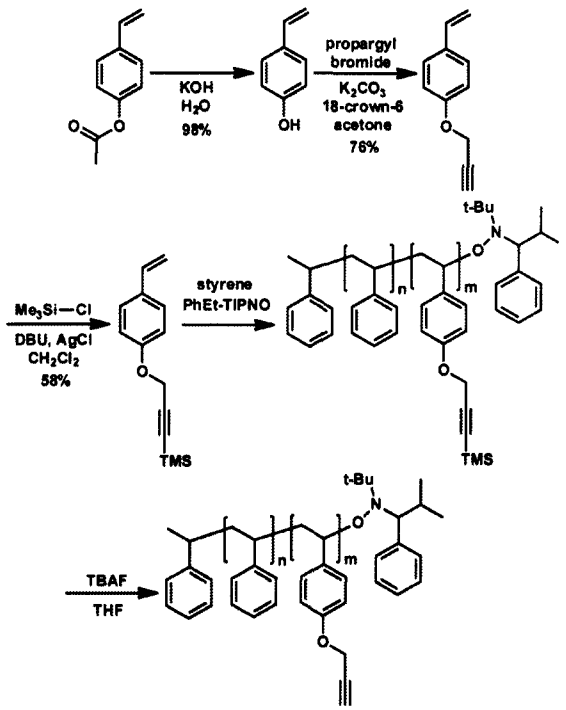

9,10-Di(trimethylsilanylethynyl)anthracene. To a stirred mixture of 111 mg (0.3 mmol) of 9,10-dibromoanthracene, 20 mg (0.1 mmol) of CuI, 72 mg (0.1 mmol) of bis(triphenylphosphine)palladium(II)chloride in 2 mL of THF, and 2 mL of *N,N*-diisopropylethylamine, a solution of 98 mg (1.0 mmol) of trimethylsilylacetylene in 2 mL of THF was added dropwise over 10 min. The mixture was refluxed for 8 hours and the solvent was evaporated. The obtained brown crude product was purified by column chromatography eluting with *n*-hexane to give a solid. The residue was purified by recrystallization with ethanol to yield 96 mg (78 %) of 9,10-di(trimethylsilanylethynyl)anthracene as yellow solid. ^{1}H NMR (400 MHz, $CDCl_3$): δ 8.59-8.57 (dd, *J*=3.35 Hz, 6.7, 4H), 7.63-7.60 (dd, *J*=3.35 Hz, 6.7, 4H), 0.43 (s, 18H)

9,10-Di(trimethylsilanylethynyl)anthracene. To a stirred mixture of 1.1 g (3 mmol) of 9,10-dibromoanthracene, 200 mg (1 mmol) of CuI, 720 mg (1 mmol) of bis(triphenylphosphine)palladium(II)chloride in 15 mL of THF, and 10 mL of *N,N*-diisopropylethylamine, a solution of 1.4 g (10 mmol) of triethylsilylacetylene in 3 mL of THF was added dropwise over 30 min. The mixture was refluxed for 12 hours and the solvent was evaporated. The obtained brown crude product was purified by column chromatography eluting with *n*-hexane to give a solid. The residue was purified by recrystallization with ethanol to yield 626 mg (42 %) of 9,10-di(trimethylsilanylethynyl)anthracene as yellow solid.

1,3,6,8-Tetrabromopyrene. To a stirred solution of pyrene (3 g, 14.8 mmol) in 20 mL of nitrobenzene at 0 °C, bromine (3.87 mL, 75 mmol) was added dropwise over 20 min. The solution was refluxed for 3 hours. The resulting solution was poured into water, and the precipitate was filtered and washed with ethanol. The obtained yellow crude product was purified by column chromatography eluting with *n*-hexane to give 1,3,6,8-tetrabromopyrene as a pale yellow solid of 6.96 g (90%). ^{1}H NMR (400 MHz, $CDCl_3$): δ 8.44 (s, 2H), 8.42 (s, 4H)

1,3,6,8-Tetrakis(trimethylsilanylethynyl)pyrene. To a stirred mixture of 500 mg (1.0 mmol) of 1,3,6,8-tetrabromopyrene, 60 mg (0.32 mmol) of CuI, 216 mg (0.32 mmol) of bis(triphenylphosphine)palladium(II)chloride in 8 mL of THF, and 4 mL of *N,N*-diisopropylethylamine, a solution of 588 mg (6.0 mmol) of trimethylsilylacetylene in 4 mL of THF was added dropwise over 30 min. The mixture was stirred for 8 hours at 50 °C and the solvent was evaporated. The obtained brown crude product was purified by column

chromatography eluting with *n*-hexane to give a red solid. The residue was purified by recrystallization with *n*-hexane/ethanol to yield 370 mg (65 %) of 1,3,6,8-tetrakis(trimethylsilanylethynyl)pyrene as red solid. ^{1}H NMR (400 MHz, $CDCl_3$): δ 8.58 (s, 4H), 8.30 (s, 2H), 0.39 (s, 36H)

1,3,6,8-tetrakis(triethylsilanylethynyl)pyrene. To a stirred mixture of 500 mg (1.0 mmol) of 1,3,6,8-tetrabromopyrene, 60 mg (0.32 mmol) of CuI, 216 mg (0.32 mmol) of bis(triphenylphosphine)palladium(II)chloride in 8 mL of THF, and 4 mL of *N,N*-diisopropylethylamine, a solution of 840 mg (6.0 mmol) of triethylsilylacetylene in 4 mL of THF was added dropwise over 30 min. The mixture was stirred for 8 hours at 50 °C and the solvent was evaporated. The obtained brown crude product was purified by column chromatography eluting with *n*-hexane to give a red solid. The residue was purified by recrystallization with *n*-hexane/ethanol to yield 426 mg (59 %) of 1,3,6,8-tetrakis(triethylsilanylethynyl)pyrene as red solid.

Scheme 3-2-4. Synthesis of ethynyl functionalized anthracene and pyrene.

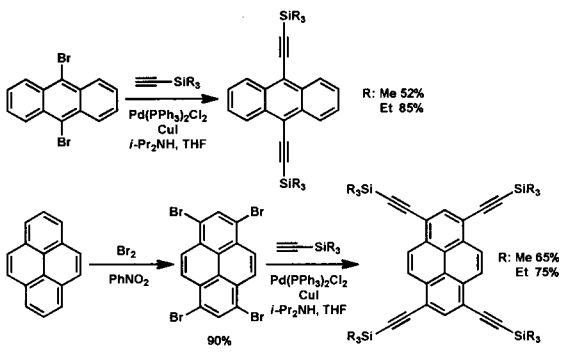

Tetrakis(4-bromophenyl)ethylene. To a tetraphenylethylene (5.1 g, 15.1 mmol) at 0 °C, bromine (7.64 mL, 143.32 mmol) was added dropwise over 20 min. The reaction mixture was stirred for 2 days at room temperature. The reaction was quenched with $Na_2S_2O_3$ and extracted with chloroform (20 mL × 3). The combined organic layers were washed with brine, dried with anhydrous Na_2SO_4, and concentrated in vacuo. The residue was purified by recrystallization with chloroform/methanol to yield 8.0 g (80 %) of tetrakis(4-bromophenyl)ethylene as white crystals. ^{1}H NMR (400 MHz, $CDCl_3$): δ 6.85 (d, J = 8.56 Hz, 8H), 7.26 (d, J = 8.56 Hz, 8H).

Tetrakis(4-trimethylsilanylethynylphenyl)ethylene. (procedure 1) To a stirred mixture of 500 mg (1.0 mmol) of tetrakis(4-bromophenyl)ethylene, 60 mg (0.32 mmol) of CuI, 216 mg (0.32 mmol) of bis(triphenylphosphine)palladium(II)chloride in 8 mL of THF, and 4 mL of *N,N*-diisopropylethylamine, a solution of 588 mg (6.0 mmol) of trimethylsilylacetylene in 4 mL of THF was added dropwise over 30 min. The mixture was stirred for 8 hours at 50 °C and the solvent was evaporated. The obtained brown crude product was purified by column chromatography eluting with *n*-hexane to give a red solid. The residue was purified by recrystallization with *n*-hexane/ethanol to yield 185 mg (33 %) of tetrakis(4-trimethylsilanylethynylphenyl)ethylene as red solid. ^{1}H NMR (400 MHz, $CDCl_3$): δ 7.18 (d, 8H), 6.86 (d, 8H), 0.22 (s, 36H)

4,4′-Bis(trimethylsilyl)benzophenone. To a stirred mixture of 1.7 g (10 mmol) of 4,4′-dibromobenzophenone, 60 mg (0.32 mmol) of CuI, 216 mg (0.32 mmol) of bis(triphenylphosphine)palladium(II)chloride in 20 mL of THF, and 4 mL of *N,N*-diisopropylethylamine, a solution of 3.3 g (24.0 mmol) of triethylsilylacetylene in 4 mL of THF was added dropwise over 30 min. The mixture was stirred for 8 hours at 50 °C and the solvent was evaporated. The crude product was purified by column chromatography using petroleum ether/ethyl acetate

mixture (100:1 by volume) as eluent. White solid of 2 was obtained to yield in 1.65 g (90%) ^{1}H NMR (400 MHz, $CDCl_3$): δ 7.69 (d, 4H), 7.54 (d, 4H), 0.27 (s, 18H).

Tetrakis(4-trimethylsilanylethynylphenyl)ethylene. (procedure 2) To a mixture of 0.59 g (0.04 mmol) of 4,4′-Bis(trimethylsilyl)benzophenone, 0.31 g (4.8 mmol) of zinc powder in 20 mL of dry THF, 0.45 g (2.4 mmol) of TiCl4 was slowly added at 0°C. The reaction mixture was refluxed for 23 h. The residue was washed with diethyl ether. After most of the solvent was evaporated, the filtrate was poured into 1 M HCl solution (50 mL) and extracted by dichloromethane (20 mL×3). The organic layer was combined and washed with brine and water and then dried over $MgSO_4$. After filtration and solvent evaporation, the crude product was purified by column chromatography using petroleum ether as eluent to yield 0.43 mg (75 %) of tetrakis(4-trimethylsilanylethynylphenyl)ethylene as red solid. ^{1}H NMR (400 MHz, $CDCl_3$): δ 7.18 (d, 8H), 6.86 (d, 8H), 0.22 (s, 36H)

Scheme 3-2-5. Synthesis of poly(styrene-*co*-4-trimethyl- silylethynylstyrene)

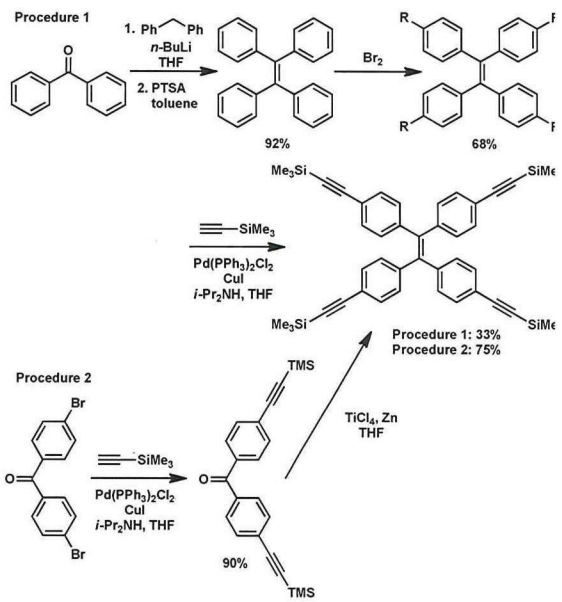

Cross-linking point of PSES

PSES showed high cross-linking efficiency and gave the 'fine' nanowires with high mechanical strength. In order to understand the cross-linking mechanism of PSES, the effects of chemical modification to the cross-linking efficiencies were evaluated by using polystyrene derivatives including the ethynyl group in polymer backbones. A drastic decrease in the cross-linking efficiency was confirmed when ethynyl groups were capped with silyl groups (poly[styrene-*co*-4-(trimethylsilyl)ethynylstyrene][18]; $G(x)$ >1.8) (Figure 3-5-1-a) and conjugation between phenyl and ethynyl groups was broken (poly[styrene-*co*-4-(trimethylsilylpropargyloxy)styrene][32]; $G(x)$ as > 0.5) (Figure 3-5-1-b).

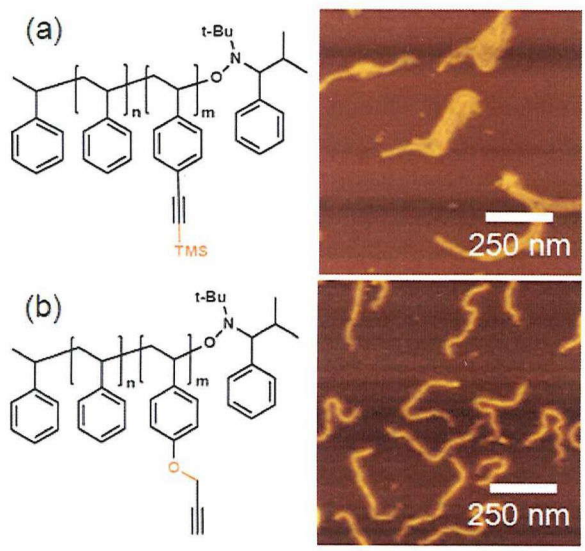

Figure 3-5-1. AFM micrographs of nanowires based on (a) poly(styrene-*co*-4-trimethyl- silylethynylstyrene) and (b) poly(styrene-*co*-4-trimethylsilylpropargyloxystyrene) films prepared by exposing films to 480 MeV $^{192}Os^{30+}$ particles at 4.0×10^8 ions cm^{-2}.

Especially, in the case of poly[styrene-*co*-4-(trimethylsilylpropargyloxy)styrene], the cross-linking efficiency was even equal in the case of polystyrene; $G(x)$ as > 0.4. These results indicate that terminal part of alkyne in PSES dominate

the cross-linking reactions in fabrication process of nanowires. Moreover, introduction of alkyne groups into the styrene backbone and expansion of conjugated systems significantly enhance the cross-linking efficiency and result in fabrication of nanowires with high mechanical strength.

Fabrication of pentacene nanowires

1-D nano-sized materials such as carbon nanotubes have attracted much attention as ideal quantum wires for future manufacturing techniques of nano-scaled optoelectronic devices. However, it is still difficult to control the sizes, spatial distribution, or position of nanotubes by conventional synthetic techniques to date. The films of pentacen and its derivatives (Figure 3-5-2) were irradiated and observed by AFM measurement. The nanowires based on TES and TIPS-pentacene (Figure 3-5-2-a, b) were confirmed as shown in figure 3-5-3. On the other hand, simple irradiation to pentacene (Figure 3-5-2-c) and photo-patternable pentacene derivatives: pentacene-*N*-sulfinyl-*tert*-butylcarbamate (Figure 3-5-2-d) films produced no nanostructures. This result indicates that alkyne moieties in the pentacene derivatives improve the cross-linking reactions and help the fabrication of nanowires. The terminal alkyne, especially, ethynylbenzene unit generates the radical intermediates under high pressure and temperature, or UV irradiation, and produces various adduct induced radical reactions. Therefore, irradiation of swift heavy ions was expected to promote the cross-linking reaction leading to fabrication of 1D-nanostructures based on TES and TIPS-pentacene.

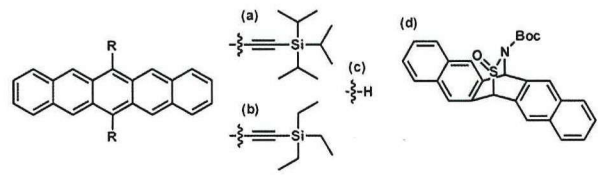

Figure 3-5-2. The chemical structures of the pentacene and functional pentacene derivatives investigated in this study: (a) 6,13-Bis(triisopropylsilylethynyl)pentacene: TIPS-pentacene, (b) 6,13-Bis(triethylsilylethynyl)pentacene: TES-pentacene, (c) pentacene, and (d) pentacene-*N*-sulfinyl-*tert*-butylcarbamate.

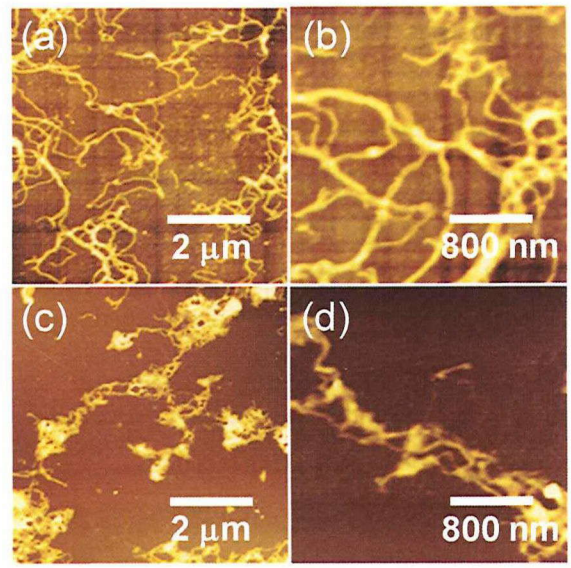

Figure 3-5-3. AFM micrographs of the nanowires based on (a, b) TES-pentacene and (c, d) TIPS-pentacene fabricated by irradiation of 490 MeV $^{192}Os^{30+}$ particles at 1.0×10^{9} ions cm^{-2}, respectively. Development was performed by hexane for 5 s.

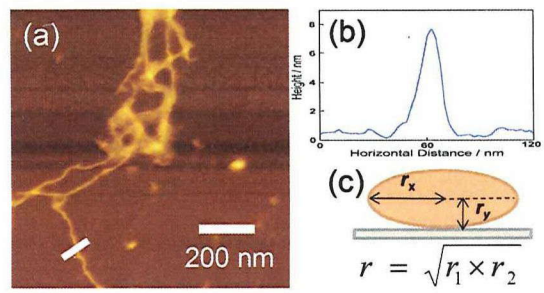

Figure 3-5-4. (a)An AFM micrograph of nanowires based on TES-pentacene. (b)Cross-sectional profiles of the nanowires on Si substrate based on TES-pentacene produced by SPNT. The profile was measured at the position indicated by lines in the corresponding AFM image.

Figure 3-5-3b shows the cross-sectional profile of

the nanowire based on TES-pentacene. The profile was measured on the line in figure 3-5-3a. After the development process, the cross-sections of nanowire on the substrate are elliptically deformed. Therefore, the radii of nanowires are calculated by applying the ellipse model to cross-sections of nanowires (figure 2(c)). The values of r_1 and r_2 are defined as the half-width and half-height of at half-maximum of the cross-sections of nanowires, respectively. The radius of the nanowires based on the TES pentacene and TIPS-pentacene were calculated as 4.5 and 4.2 nm, respectively.

In general, deprotection of trialkylsilyl groups are performed with acids, bases, or fluorides. The relative stability of trialkylsilyl protection can be controlled by changing the size of alkyl chains. TIPS group indicates higher resistance for these conditions than TES group. Therefore, it is expected TIPS group regulate the generation of radical intermediates and promotion of the cross-linking reactions.

In contrast to TES and TIPS-pentacene nanowires show the low mechanical strength. The length and number density of nanowires fabricated by the SPNT are completely controlled the initial film thickness and the number incident particles, respectively. The size control of TES and TIPS-pentacene nanowires was difficult because the fragmentation of nanowires was often confirmed.

Fabrication of ethynyl-functionalized π-molecules

Introduction of ethynyl group leaded to the formation of nanowires based on pentacene derivatives: TES and TIPS pentacenes. A numerous number of π-conjugated molecules with excellent properties have been synthesized and evaluated in organic electronics research[49,50]. Furthermore, 1D nanostructures (nanowires, nanobelts, and nanotubes) based on π-conjugated materials have been attracted in nano-science, organic field-effect transistors[51], organic photovoltaics[52], and biosensors[53]. Various methods for assembling the molecules or polymers into 1D nanostructures are reported. But, it is challenging to fabricate the 1D nanostructures based on π-conjugated small molecules. Sonogashira reaction is a well known cross-coupling reaction between a terminal alkyne and an aryl halide by using palladium catalyst[54]. This reaction can be carried out under mild conditions and proceed in high yields. Therefore, ethynyl functional π-conjugated molecules can be easily synthesized from trialkyl silyl protected acetylene. In this section, fabrication of nanowires based on π-conjugated molecules, such as pyrene, anthracene, and tetraphenylethylene were demonstrated.

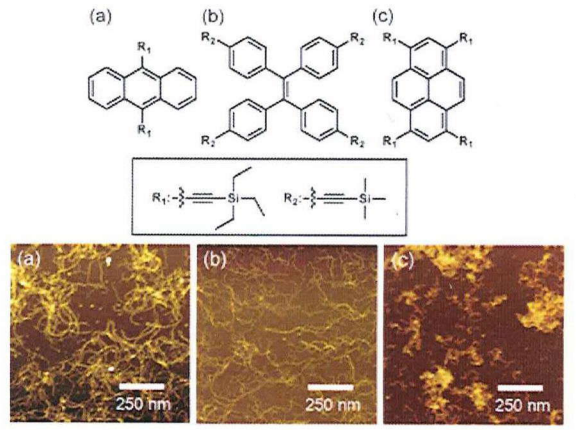

Figure 3-5-5. The chemical structures of ethynyl functionalized molecules: (a)9,10-Bis(triethylsilylethynyl)anthracene: TES-anthracene, (b)tetrakis((4-(trimethylsilyl)ethynyl)phenyl)ethylene: TMS-TPE, and (c)1,3,6,8-tetrakis(triethylsilylethynyl-)pyrene: TES-pyrene. AFM micrographs of nanowires based on ethynyl functionalized molecules (a-c) were prepared by exposing films to 480 MeV $^{192}Os^{30+}$ particles.

The size of trialkylsilyl groups affects not only the cross-linking efficiency but also the solubility of the ethynyl derivatives. Trimethylsilyl mediated tetraphenylethylene: TMS-TPE gave the uniform thin film from the chloroform solution by the spin-casted

method. On the other hand, both trimethylsilyl mediated anthracene and pyrene didn't form the amorphous film because of their high crystallinity. Therefore, fabrication of the nanostructures based on the anthracene and pyrene were performed by using triethylsilyl mediated derivatives. All the ethynyl functionalized molecules were successfully utilized in the fabrication of 1D-nanostructures by SPNT (figure 3-5-5). But, the length and number density control of nanostructures were difficult. The radii of nanowires were evaluated by the AFM measurements, and all the molecules gave the thin nanowires (table 3-5-1).

Table 3-5-1. The value of cross-sectional radius of nanowires based on ethynyl functionalized compounds fabricated by the SPNT.

	TES-anthracene	TMS-TPE	TES-pyrene
Radius *r* (nm)	2.4[a]	1.8[b]	1.7[a]

a: Development was carried out with cyclohexane. b: Development was carried out with hexane.

3-6 Summary

Acetylene functionalized polystyrene (poly(styrene-*co*-4-ethynylstyrene): PSES) was polymerized controlling the molecular weight and dispersity by nitroxide-mediated radical polymerization. PSES was successfully utilized in the fabrication of 1D-nanostructures by SPNT. Pendant alkyne moieties enhanced the cross-linking efficiency and mechanical strength, which is not comparable with those observed for other synthetic polymers. Due to high mechanical strength of PSES nanowires, the length, number density, and radius of PSES nanowires can be controlled by the initial film thickness, the number of incident particles, and linear energy transfer, respectively. Especially, in length control of nanowires, the maximum aspect ratio of the PSES nanowire reached ~750, which is a high value compared to the case of using the negative type photo-resist SU-8.

The PSES nanowires fabricated by SPNT have flexibility because they are in the form of nanosized gel induced by cross-linking reactions among the polymer chains. Thus, the arrangement of the nanowires is affected by the development conditions and length of the nanowires. The orientation of PSES nanowires can be controlled by the development procedure in the case of nanowires less than 8 μm in length. The development solvents used also affect the arrangement of nanowires. Three aggregation structures ("linear", "sheet", and "network") of the PSES nanowires with lengths of 8 μm could be controlled by changing the development solvents.

The functionality of alkyne groups on the surface of PSES nanowires was also preserved, and alkyne moieties quantitatively reacted with the azide compounds via copper (I)-catalyzed 1,3-dipolar cycloaddition called Click chemistry. PSES nanowire surfaces can be modified by various kinds of functional materials using Click chemistry. Fabrication of 1D-nanowires and 2D-arrays based on bio-macromolecules was demonstrated utilizing the Click reactions and avidin-biotin interactions. SPNT with the "top-down" technique was thus successfully used to fabricate the 1D-nanostructure, which

maintained the function of the base material. Furthermore, the surface of the nanowires can acquire any functionality using chemical and biological modifications. This overlap represents a step in fusing "top-down" and "bottom-up" approaches, providing the foundation for the development of a new strategy for the architectures of nanosized functional materials via radiation chemistry.

On the other hand, due to high cross-linking efficiency of phenyl acetylene group, direct formation of nanowires based on functional molecules was demonstrated without using self-assembling. The 1D-nanostructures based on pentacene was successfully fabricated by introducing the silyl protected ethynyl groups to pentacene backbone. Ethynyl groups improved and increased the cross-linking efficiency of pentacene.

References

1. Saito, O. *J. Phys. Soc. Jpn.* **1958**, *13*, 1451-1464.
2. Saito, O. *J. Phys. Soc. Jpn.* **1959**, *14*, 798-806.
3. Inokuti, M. *J. Chem. Phys.* **1960**, *33*, 1607-1615.
4. Inokuti, M. *J. Chem. Phys.* **1963**, *38*, 2999-3005.
5. Zhang, Y. F.; Ge, X. W.; Sun, J. Z. *Radiat. Phys. Chem.* **1990**, *35*, 163-166.
6. Olejniczak, K.; Rosiak, J.; Charlesby, A. *Radiat. Phys. Chem.* **1991**, *37*, 499-504.
7. Seki, S.; Maeda, K.; Tagawa, S.; Kudoh, H.; Sugimoto, M.; Morita, Y.; Shibata, H. *Adv. Mater.* **2001**, *13*, 1663-1665.
8. Tsukuda, S.; Seki, S.; Tagawa, S.; Sugimoto, M.; Idesaki, A.; Tanaka, S.; Ohshima, A. *J. Phys. Chem. B* **2004**, *108*, 3407-3409.
9. Seki, S.; Tsukuda, S.; Maeda, K.; Matsui, Y.; Saeki, A.; Tagawa, S. *Phys. Rev. B* **2004**, *70*, 144203-8.
10. Seki, S.; Tsukuda, S.; Maeda, K.; Tagawa, S.; Shibata, H.; Sugimoto, M.; Jimbo, K.; Hashitomi, I.; Kohyama, A. *Macromolecules* **2005**, *38*, 10164-10170.
11. Watanabe, S.; Asano, A.; Seki, S.; Sugimoto, M.; Yoshikawa, M.; Tagawa, S.; Tsukuda, S.; Tanaka, S. *Radiat. Phys. Chem.* **2009**, *78*, 1071-1075.
12. Price, P. B.; Walker, R. M. *Nature* **1962**, *196*, 732-734.
13. Spohr, R. *Ion Tracks and Microtechnology: Principle and Applications*; Vieweg: Braunschweig, 1990.
14. Peng, L.; Apel, P.; Maekawa, Y.; Yoshida, M. *Nucl. Instrum. Methods B* **2000**, *168*, 527-532.
15. Apel, P. *Radiat. Meas.* **2001**, *34*, 559-566.
16. Fink, D. *Fundamentals of Ion-Irradiated Polymers*; Springer: Berlin, 2004.
17. Wilson, R. R. *Radiology* **1946**, *47*, 487-491.
18. Malkoch, M.; Thibault, R. J.; Drockenmuller, E.; Messerschmidt, M.; Voit, B.; Russell, T. P.; Hawker, C. J. *J. Am. Chem. Soc.* **2005**, *127*, 14942-14949.
19. O'Reilly, R. K.; Joralemon, M. J.; Hawker, C. J.; Wooley, K. L. *Chem. Eur. J.* **2006**, *12*, 6776-6786.
20. Huisgen, R. *Angew. Chem. Int. Ed. Engl.* **1963**, *2*, 565-598.
21. Huisgen, R. *Angew. Chem. Int. Ed. Engl.* **1963**, *2*, 633-645.
22. Rostovtsev, V. V.; Green, L. G.; Fokin, V. V.; Sharpless, K. B. *Angew. Chem. Int. Ed.* **2002**, *41*, 2596-2599.
23. Tornoe, C. W.; Christensen, C.; Meldal, M. *J. Org. Chem.* **2002**, *67*, 3057-3064.
24. Kolb, H. C.; Finn, M. G.; Sharpless, K. B., *Angew. Chem. Int. Ed.* **2001**, *40*, 2004-2021.
25. van Steenis, D. J. V. C.; David, O. R. P.; van Strijdonck, G. P. F.; van Maarseveen, J. H.; Reek, J. N. H. *Chem. Commun.* **2005**, 4333-4335.
26. Zhu, Y.; Huang, Y.; Meng, W.-D.; Li, H.; Qing, F.-L., *Polymer* **2006**, *47*, 6272-6279.
27. Detz, R. J.; Heras, S. A.; de Gelder, R.; van Leeuwen, P. W. N. M.; Hiemstra, H.; Reek, J. N. H.; van Maarseveen, J. H. *Org. Lett.* **2006**, *8*, 3227-3230.
28. Whittaker, M. R.; Urbani, C. N.; Monteiro, M. J. *J. Am. Chem. Soc.* **2006**, *128*, 11360-11361.
29. Rozkiewicz, D. I.; Janacuteczewski, D.; Verboom, W.; Ravoo, B. J.; Reinhoudt, D. N. *Angew. Chem. Int. Ed.* **2006**, *45*, 5292-5296.
30. Li, H.; Cheng, F; Duft, A. M.; Adronov, A. *J. Am. Chem. Soc.* **2005**, *127*, 14518-14524
31. Seki, S.; Watanabe, S.; Sugimoto, M.; Tagawa, S.; Tsukuda, S. *J. Photopolym. Sci. Technol.* **2008**. *21*, 541-543.
32. Fleischmann, S.; Komber, H.; Voit, B. *Macromolecules* **2008**, *41*, 5255-5264.
33. Tang, C.; Bang, J.; Stein, G. E.; Fredrickson, G. H.; Hawker, C. J.; Kramer, E. J.; Sprung, M.; Wang, J. *Macromolecules* **2008**, *41*, 4328-4339.
34. Tercjak, A.; Gutierrez, J.; Peponi, L.; Rueda, L.; Mondragon, I. *Macromolecules* **2009**, *42*, 3386-3390.
35. Chan, T.-F.; Ha, C.; Phong, A.; Cai, D.; Wan, E.; Leung, L.; Kwok, P. -Y.; Xiao, M. A *Nucl. Acids Res.* **2006**. *34*. e113.
36. Li, Y.; Tsuboi, K.; Michinobu, T. *Macromolecules* **2010**, *43*, 5277-5286.

37. Burazerovic, S.; Gradinaru, J.; Pierron, J.; Ward, T. R. *Angew. Chem. Int. Ed.* **2007**, *46*, 5510-5514.
38. Men, D.; Guo, Y.-C.; Zhang, Z.-P.; Wei, H.P.; Zhou, Y.-F.; Cui, Z.-Q.; Liang, X.-S.; Li, K.; Leng, Y. You, X.-Y.; Zhang, X.-E. *Nano Lett.* **2009**, *9*, 2246-2250.
39. Scheibel, T.; Parthasarathy, R.; Sawicki, G.; Lin, X.-M.; Jaeger, H.; Lindquist, S. L. *Proc. Nat. Acad. Sci. USA* **2003**, *100*, 4527-4532.
40. Green, N. *Biochem. J.* **1963**, *89*, 585-591
41. Bayer, E. A.; de Meester, F.; Kulik, T.; Wilchek, M. *Appl. Biochem. Biotechnol.* **1995**, *53*, 1-9.
42. Rina, M.-L. L.; Lue, Y. P.; Chen, G. Y. J.; Zhu, Q.; Yao, S. Q. *J. Am. Chem. Soc.* **2002**, *124*, 8768-8769.
43. Reichel, A.; Schaible, D.; Furoukh, N. A.; Cohen, M.; Schreiber, G.; Piehler, J. *Anal. Chem.* **2007**, *79*, 8590-8600.
44. Pugliese, L.; Coda, A.; Malcovati, M.; Bolognesi, M. *J. Mol. Biol.* **1993**, *231*, 698-710.
45. Urbani, C. N.; Bell, C. A.; Lonsdale, D. E.; Whittaker, M. R.; Monteiro, M. J. *Macromolecules* **2007**, *40*, 7056-7059.
46. Ornelas, C.; Mery, D.; Cloutet, E.; Aranzaes, J. R.; Astruc, D. Cross *J. Am. Chem. Soc.* **2008**, *130*, 1495-1506.
47. Becker, J.M.; Wilchek, M.; Katchalski, E. *Proc. Nat. Acad. Sci. USA* **1971**, *68*, 2604-2607.
48. Tsuda, K.; Ishizone, T.; Hirao, A.; Nakahama, S. *Macromolecules* **1993**, *26*, 6985-6991.
49. Virkar, A. A; Stefan Mannsfeld, S; Bao, Z; Stingelin, N. *Adv. Mater.* **2010**, *22*, 3857-3875.
50. Mishra, A; Bäuerle, P. *Angew. Chem. Int. Ed.* **2012**, *51*, 2020-2067.
51. Briseno, A. L.; Mannsfeld, S. C. B.; Reese, C.; Hancock, J. M.; Xiong, Y.; Jenekhe, S. A.; Bao, Z.; Xia, Y. Nano Lett. **2007**, *7*, 2847–2853
52. Xin, H.; Reid, O. G.; Ren, G. Q.; Kim, F. S.; Ginger, D. S.; Jenekhe, S. A. *ACS Nano* **2010**, *4*, 1861–1872.
53. Liu, H.; Kameoka, J.; Czaplewski, D. A.; Craighead, H. G. Nano Lett. **2004**, *4*, 671–675.
54. Sonogashira, K.; Tohda, Y.; Hagiwara, N. *Tetrahedron Lett.* **1975**, *50*, 4467-4470.

Chapter 4 Conclusion

A high energy particle can deposit the extremely high energy and induce the non-homogeneous reaction in limited space along its trajectory. This energy deposition area called as 'ion track' gives high densely active intermediates in the target materials. These energy deposition events fundamentally differ from other low LET radiation, such as electron bean, γ ray. Nanowires formed in several kinds of polymers were successfully prepared for the first time under high LET ion beams. The formation of nanowires based on bio-macromolecules and synthetic polymer was performed, and functionalization of nanowires by using surface modification.

Human serum albumin (HSA) was successfully utilized in the fabrication of 1D-nanostructures by SPNT without using complicated chemically synthetic or biological procedures. Protein nanowires were confirmed from the film based on some proteins. Especially, HSA showed the high cross-linking efficiency, which is comparable with cross-linking type synthetic polymers for radiation. Due to high cross-linking efficiency of HSA, the length, number density, and radius of HSA nanowires can be controlled by the initial film thickness, the number of incident particles, and linear energy transfer, respectively. In length control of nanowires, the maximum length of nanowire reached 8 μm. The successful size control of protein nanowires was demonstrated that HSA was appropriate material for SPNT. On the other hand, hydrolysis of HSA nanowires by trypsin triggered the fragmentation of nanowires, and finally, nanowires were completely decomposed. These results revealed HSA nanowires retained the specific sequence of peptide structures. Moreover, preservation of the function of protein nanowires was demonstrated by surface modification of avidin-HSA nanowires with dibiotinyl linker and avidin. These results indicated that the proteins on the surface of nanowires have minimum amounts of cross-links. (Chapter 1)

Fabrication of functional nanowires was performed by using the mixture film based on functional materials (Au nanoparticles and cyclodextrin) and cross-linking type polymer for radiation. Especially, CD containing nanowires improved the sensitivity of QCM sensors for chemical compounds. Blended techniques indicated the feasibility of SPNT to direct formation of various functional nanowires with facile procedure. On the other hand, size control of nanowires and improvement of cross-linking efficiencies were succeeded by using chemical modification of polymer materials and γ ray irradiation. (Chapter 2)

Acetylene functionalized polystyrene (PSES) was successfully utilized in the fabrication of 1D-nanostructures by SPNT. Pendant alkyne moieties enhanced the cross-linking efficiency and mechanical strength, which is not comparable with those observed for other synthetic polymers. Due to high cross-linking efficiency, arrangement and aggregation structures of the PSES nanowires could be controlled. On the other hand, the functionality of alkyne groups on the surface of PSES nanowires was also preserved, and alkyne moieties quantitatively reacted with the azide compounds via Click chemistry leading to the fabrication of 1D-protein nanowires and

2D-protein arrays. Moreover, due to high cross-linking efficiency of phenyl acetylene group, direct formation of nanowires based on functional molecules was demonstrated without using self-assembling. The 1D-nanostructures based on pentacene was successfully fabricated by introducing the silyl protected ethynyl groups to pentacene backbone. (Chapter 3)

List of publication

1. Publications

(1) **Control of Radial Size of Crosslinked Polymer Nanowire by Ion Beam and γRay Irradiation**
Satoshi Tsukuda, Atsushi Asano, Masaki Sugimoto, Akira Idesaki, Shu Seki, Shun-Ichiro Tanaka
J. Photopolym. Sci. Technol., 23(2), 231-234 (2010).

(2) **Poly(vinylphenol) Nanowires Including Au Nanoparticles Formed by Single Particle Nanofabrication Technique**
Satoshi Tsukuda, Masaki Sugimoto, Akira Idesaki, Atsushi Asano, Shu Seki, Shun-Ichiro Tanaka
Radiat. Phys. Chem., DOI: 10.1016/j.radphyschem.2012.06.048.

(3) **Sugar Nanowires Based on Cyclodextrin on Quartz Crystal Microbalance for Gas Sensing with Ultra-High Sensitivity**
Atsushi Asano, Yuta Maeyoshi, Shogo Watanabe, Akinori Saeki, Masaki Sugimoto, Masahito Yoshikawa, Hidehito Nanto, Satoshi Tsukuda, Shun-Ichiro Tanaka, Shu Seki
Radiat. Phys. Chem., DOI: 10.1016/j.radphyschem.2012.06.018.

(4) **Fabrication of Nanowires Based on Polystyrene Derivatives by Single Particle Nano-Fabrication Technique**
Atsushi Asano, Yuta Maeyoshi, Katsuyoshi Takano, Masaaki Omichi, Masaki Sugimoto, Masahito Yoshikawa, Satoshi Tsukuda, Shun-Ichiro Tanaka, Aakinori Saeki, Shu Seki
J. Photopolym. Sci. Technol., 25(5), 685-688 (2012).

(5) **Fabrication and Arrangement of "Clickable" Nanowires by the Single-Particle Nanofabrication Technique**
Atsushi Asano, Masaaki Omichi, Satoshi Tsukuda, Katsuyoshi Takano, Masaki Sugimoto, Akinori Saeki, Shu Seki
J. Phys. Chem. C, 2012, 116 (32), 17274-17279 (2012).

(6) **Microprocessing of Arched Bridge Structures with Epoxy Resin by Proton Beam Writing**
Katsuyoshi Takano, Atsushi Asano, Yuta Maeyoshi, Hiromi Marui, Masaaki Omichi, Akinori Saeki, Shu Seki, Takahiro Satohb, Yasuyuki Ishii, Tomihiro Kamiya, Masashi Koka, Takeru Ohkubo, Masaki Sugimoto, Hiroyuki Nishikawa
J. Photopolym. Sci. Technol., 25(1), 43-46 (2012).

(7) **Fabrication of Nanowires Based on Pentacene Derivatives by Single Particle Nano-Fabrication Technique**
Atsushi Asano, Katsuyoshi Takano, Masaki Sugimoto, Shu Seki
In preparation

2. Supplementary publications

(1) Semiconducting Cross-Linked Polymer Nanowires Prepared by High-Energy Single-Particle Track Reactions
Shu Seki, Akinori Saeki, Wookjin Choi, Yuta Maeyoshi, Masaki Omichi, Atsushi Asano, Kazuyuki Enomoto, Chakkooth Vijayakumar, Masaki Sugimoto, Satoshi Tsukuda, Shun-ichiro Tanaka
J. Phys. Chem. B, 2012, 116 (32), 12857-12863 (2012).

(2) Fullerene Nanowires as a Versatile Platform for Organic Electronics
Yuta Maeyoshi, Akinori Saeki, Shotaro Suwa, Masaaki Omichi, Hiromi Marui, Atsushi Asano, Satoshi Tsukuda, Masaaki Sugimoto, Akihiro Kishimura, Kazunori Kataoka, Shu Seki
Scientific Reports, 2, 600 (2012).

(3) Highly Photoconducting π-Stacked Polymer Accommodated in Coordination Nanochannels
Takashi Uemura, Noriyuki Uchida, Atsushi Asano, Akinori Saeki, Shu Seki, Masahiko Tsujimoto, Seiji Isoda, Susumu Kitagawa
J. Am. Chem. Soc., 134(20), 8360-8363 (2012).

(4) Supramolecularly Engineered Perylene Bisimide Assemblies Exhibiting Thermal Transition from Columnar to Multilamellar Structures
Shiki Yagai, Mari Usui, Tomohiro Seki, Haruno Murayama, Yoshihiro Kikkawa, Shinobu Uemura, Takashi Karatsu, Akihide Kitamura, Atsushi Asano, Shu Seki
J. Am. Chem. Soc., 134(18), 7983-7994 (2012).

(5) π-Electron-System-Layered Polymer: Through-Space Conjugation and Properties as a Single Molecular Wire
Yasuhiro Morisaki, Shizue Ueno, Akinori Saeki, Atsushi Asano, Shu Seki, Yoshiki Chujo
Chem. Eur. J., 18(14), 4216-4224 (2012).

(6) Fabrication of Poly(9,9'-dioctylfluorene)-Based Nano- and Microstructures by Proton Beam Writing
Yuta Maeyoshi, Katsuyoshi Takano, Atsushi Asano, Hiromi Marui, Masaaki Omichi,

Takahiro Satoh, Tomihiro Kamiya, Yasuyuki Ishii, Takeru Ohkubo, Masashi Koka, Wataru Kada, Masaki Sugimoto, Hiroyuki Nishikawa, Akinori Saeki, Shu Seki
Jpn. J. Appl. Phys., 51(4-1), 045201/1-045201/4 (2012).

(7) Photoreversible Supramolecular Polymerisation and Hierarchical Organization of Hydrogen-Bonded Supramolecular Co-polymers Composed of Diarylethenes and Oligothiophenes
Shiki Yagai, Keisuke Ohta, Marina Gushiken, Kazunori Iwai, Atsushi Asano, Shu Seki, Yoshihiro Kikkawa, Masakazu Morimoto, Akihide Kitamura, Takashi Karatsu
Chem. Eur. J., 18(8), 2244-2253 (2012).

(8) Covalent Organic Frameworks with High Charge Carrier Mobility
Shun Wan, Felipe Gándara, Atsushi Asano, Hiroyasu Furukawa, Akinori Saeki, Sanjeev K. Dey, Lei Liao, Michael W. Ambrogio, Youssry Y. Botros, Xiangfeng Duan, Shu Seki, J. Fraser Stoddart, Omar M. Yaghi
Chem. Mater., 23(18), 4094-4097 (2011).

(9) Air-Stable n-Type Organic Field-Effect Transistors Based on Solution-Processable, Electronegative Oligomers Containing Dicyanomethylene-Substituted Cyclopenta[*b*]thiophene
Yutaka Ie, Kazufumi Nishida, Makoto Karakawa, Hirokazu Tada, Atsushi Asano, Akinori Saeki, Shu Seki, Yoshio Aso
Chem. Eur. J., 17(17), 4750-4758 (2011).

(10) Rational Construction of Perylene Bisimide Columnar Superstructures with a Biased Helical Sense
Tomohiro Seki, Atsushi Asano, Shu Seki, Yoshihiro Kikkawa, Haruno Murayama, Takashi Karatsu, Akihide Kitamura, Shiki Yagai
Chem. Eur. J., 17(13), 3598-3608 (2011).

(11) Electron Mobility in a Mercury-mediated Duplex of Triazole-linked DNA (^{TL}DNA)
Hiroyuki Isobe, Naomi Yamazaki, Atsushi Asano, Tomoko Fujino, Waka Nakanishi, Shu Seki
Chem. Lett., 40(3), 318-319 (2011).

(12) Hierarchical Polymer Assemblies Constructed by the Mutual Template Effect of Cationic Polymer Complex and Anionic Supramolecular Nanofiber
Kouta Sugikawa, Munenori Numata, Daiki Kinoshita, Kenji Kaneko, Kazuki Sada, Atsushi Asano, Shu Seki, Seiji Shinkai
Org. Biomol. Chem., 2011, 9(1), 146-153 (2011).

(13) Supramolecularly Engineered Aggregation of a Dipolar Dye: Vesicular and Ribbonlike Architectures
Shiki Yagai, Yujiro Nakano, Shu Seki, Atsushi Asano, Takashi Okubo, Takashi Isoshima, Takashi Karatsu, Akihide Kitamura, Yoshihiro Kikkawa
Angew. Chem. Int. Ed., 49(51), 9990-9994 (2010).

(14) Discotic Columnar Mesophases Derived from 'Rod-Like' π-Conjugated Anion-Responsive Acyclic Oligopyrroles
Hiromitsu Maeda, Yoshitaka Terashima, Yohei Haketa, Atsushi Asano, Yoshihito Honsho, Shu Seki, Masahiro Shimizu, Hidetomo Mukai, Kazuchika Ohta
Chem. Commun., 46, 4559-4561 (2010).

(15) Intra-molecular Mobility of Holes along Rod-like Helical Si backbones in Optically ActivePolysilanes
Yoshihito Honsho, Atsushi Asano, Shu Seki, Takeyoshi Sunagawa, Akinori Saeki
Synth. Met. 159(9-10), 843-846 (2009)

Acknowledgements

The author firstly acknowledges Prof. S. Seki for his guidance throughout this work, and Prof. M. Akashi, and Prof. T. Majima for their helpful comments.

The author is much indebted to Dr. K. Takano for his useful guidance and advice throughout this work. The author is much indebted to Dr. M. Sugimoto at JAEA, Takasaki for his kind help and advice about ion beam and equipment.

The author is much grateful to Aya Maitani, for her encouragement and thoughtfulness.

Finally, the author is deeply obliged to his parents for their generous understanding and support of his life.